Study of the Cysγ-nitrosation of Fetal Hemoglobin (HbF)

Georgia Kremmydiotis

A Thesis

in

The Department

of

Chemistry and Biochemistry

Presented in Partial Fulfillment of the Requirements
for the Degree of Master of Science (Chemistry) at
Concordia University
Montreal, Quebec, Canada

December 2004

Your file Votre référence
ISBN: 0-494-04345-8
Our file Notre référence
ISBN: 0-494-04345-8

ABSTRACT

Study of the Cysγ-nitrosation of Fetal Hemoglobin (HbF)

Georgia Kremmydiotis

Fetal hemoglobin (HbF) is a tetramer composed of two α- and two γ-chains. The γ-chains differ from the ß-chains of HbA at 39 residues, but a Cys residue at position 93, which is the residue that becomes S-nitrosated in HbA, is conserved.

As Cu,Zn-superoxide dismutase (CuZnSOD) has been suggested to participate in Hb-SNO formation, levels of the enzyme were measured in adult and newborn red blood cell (RBC) lysates by means of the pyrogallol assay. CuZnSOD levels were found to be higher in the newborn than in the adult lysates. Recently, it has been shown that HbF can be S-nitrosated in both its deoxy and oxy forms, but only oxyHbA is S-nitrosated. Also, our collaborators have shown an inverse correlation between the amount of Hb-SNO and HbF measured in chord blood samples collected from newborns, while no difference was detected in nitrosylHb ($HbFe^{II}NO$) levels. In an attempt to characterize differences between HbA and HbF, their S-nitrosation by GSNO was measured using the Saville assay. The observed levels of Hb-SNO are similar for HbA and HbF. An evaluation of the Saville assay for the determination of Hb-SNO levels was performed.

Since nitrite (NO_2^-) may provide a pool for NO in the vascular system if a catalyst for its reduction is present, NO_2^- binding to CuZnSOD was investigated spectrophotometrically. A decrease in the 680-nm d-d band of Cu^{II}ZnSOD was observed, which suggests that the enzyme was partially reduced in the presence of NO_2^- or that NO_2^- binds to Cu^{II}ZnSOD. Consistent with the latter is the observation of a possible

ligand-to-metal charge transfer (LTMCT) band at 360 nm (ε = 0.5 $mM^{-1}cm^{-1}$) for Cu^{II}ZnSOD in the presence of 10 mM NO_2^-.

Understanding differences in S-nitrosation of HbF and HbA and the mechanism involved in NO formation and delivery may impact the treatment of premature newborns, who continue to produce high levels of HbF until they reach their normal gestational age.

To my father and mother

Acknowledgements

I would like to thank my supervisor, Dr. Ann M. English, for giving me the opportunity to work on this very interesting project, as well as for her valuable insight and guidance throughout the completion of this study. I would also like to thank her for reading and editing this manuscript.

I would also like to thank our collaborator from Ste-Justine Children's hospital, Dr. Harry Bard, for his interest and support in this project. I thoroughly enjoyed every conversation and every visit. Thank you to Carmen Gagnon, for her help in this study and for preparing the HbA and HbF lysates and purified samples.

Thanks to Drs. J.P. Powlowski, R. Boushel and J. Pfaus, my committee members, for their helpful comments and suggestions.

Thanks to Dr. Limei Tao and Ernesto Moran for helping me run my samples on the Q-TOF2 ESI-MS, to Pascal Turcotte, Mengwei Ye for their helpful hints on the pyrogallol and the Saville assays, to David Yeung, Vicky Bablekis and to Dr. Louis Cuccia for all their help, and to all my friends and colleagues from Dr. English's lab. Thanks to the graduate students, faculty and staff in the department of Chemistry and Biochemistry who have been so helpful. Many thanks to my friends who have been so encouraging and supportive these past few years.

I would like to give a special thank you to my mother, who although is no longer here with us, has given me so much strength and courage.

A very special thank you to my father, my brother, and my sister for their constant love, support and encouragement.

And finally, thank you to Len, my fiance, for his love and encouragement and for giving me so much to look forward to.

Table of contents

1.0 GENERAL INTRODUCTION 1

1.1 S-NITROSATION OF HbA 1

1.2 S-NITROSATION OF FETAL HEMOGLOBIN 2

1.3 INVOLVEMENT OF Cu,Zn-SUPEROXIDE DISMUTASE IN THE FORMATION OF S-NITROSOHEMOGLOBIN 5

1.4 OUTLINE OF THESIS 8

2.0 ANALYSIS OF Cu,Zn-SUPEROXIDE DISMUTASE LEVELS IN HEMOGLOBIN SAMPLES 9

2.1 INTRODUCTION 9

2.1.1 Role of CuZnSOD in the formation of Hb-SNO 9

2.1.2 SOD activity assay 9

2.2 EXPERIMENTAL SECTION 10

2.2.1 Materials 10

2.2.2 Methods 11

2.2.2.1 Preparation of RBC lysates, HbF and HbA 11

2.2.2.2 Preparation of commercially obtained HbA 11

2.2.2.3 Removal of CuZnSOD from commercial metHbA 11

2.2.2.4 Determination of Hb concentration 12

2.2.2.5 SOD activity assay 12

(i) CuZnSOD determination by the direct method 13

(ii) CuZnSOD determination by the standard addition method 13

2.3 RESULTS 14

2.3.1 Determination of CuZnSOD by the direct method 14

2.3.2 Determination of CuZnSOD by the standard addition method 17

2.4 DISCUSSION 22

3.0 DETERMINATION OF HEMOGLOBIN S-NITROSATION BY THE SAVILLE ASSAY 27

3.1 INTRODUCTION 27

3.1.1 Levels of Hb-SNO in adult and newborn RBC lysates 27

3.1.2 Saville assay 30

3.1.3 Determination of RSNO and NO by ozone chemiluminescence 31

3.2 EXPERIMENTAL SECTION 33

3.2.1 Materials 33

3.2.2 Methods 33

3.2.2.1 Saville assay reagents 33

3.2.2.2 NO_2^- calibration curve 34

3.2.2.3 Sample analysis 34

3.3 RESULTS 35

3.3.1 NO_2^- calibration curve 35

3.3.2 Sample analysis 39

3.3.3 Effects of metHb on the Saville assay 42

3.3.4 Effects of order of addition of metHb, $XArNH_2$ and $HgCl_2$ on NO_2^- determination 45
3.3.5 Effects of metHb on the competition between $XArNH_2$ and $NH_2SO_3^-$ for NO_2^- 46
3.3.6 Effects of CuZnSOD and GSH on the Saville assay 50
3.4 DISCUSSION 53
3.4.1 Evaluation of the Saville assay 53
3.4.2 Relative reactivities of HbA and HbF with GSNO 57

4.0 PRELIMINARY INVESTIGATION OF NITRITE REDUCTION BY Cu,Zn-SUPEROXIDE DISMUTASE 59
4.1 INTRODUCTION 59
4.1.1 Role of NO_2^- in the human circulation 59
4.1.2 Role of NO_2^- in fetal circulation 60
4.1.3 CuZnSOD as a catalyst of nitrite reduction 60
4.2 EXPERIMENTAL SECTION 61
4.2.1 Materials 61
4.2.2 Absorption spectra of $Cu^{II}ZnSOD/NO_2^-$ incubates 61
4.3 RESULTS 62
4.3.1 Effects of added NO_2^- on the 680-nm d-d absorption of $Cu^{II}ZnSOD$ 62
4.3.2 Absorption of NO_2^- 63
4.3.3 Absorption of $Cu^{II}ZnSOD$ incubates in the LTMCT Region 66
4.4 DISCUSSION 70
4.4.1 Effects of added NO_2^- on the 680-nm d-d absorption of $Cu^{II}ZnSOD$ 70
4.4.2 Absorption of $Cu^{II}ZnSOD/NO_2^-$ incubates in the LTMCT region 71

5.0 SUMMARY AND SUGGESTIONS FOR FURTHER STUDY 72

6.0 APPENDIX A – Method of HbA preparation provided by Sigma 76

7.0 APPENDIX B – Calibration curves obtained using the standard addition method for CuZnSOD monomer determination in Hb-containing samples 77

8.0 APPENDIX C – Plots of A_{320nm} *vs* time used for the determination of relative SOD activities in newborn and adult RBC lysates from Ste-Justine Hospital 86

9.0 BIBLIOGRAPHY 88

List of Figures

Figure 1.1	Diagram of umbilical-placental circulation	**4**
Figure 1.2	S-Nitroso-L-glutathione (GSNO)	**6**
Figure 2.1	UV absorption of a pyrogallol solution	**14**
Figure 2.2	Pyrogallol autoxidation in the presence and absence of 3xDEAE-Hb and CuZnSOD	**18**
Figure 2.3	Rates of pyrogallol autoxidation in 50 mM Tris-cacodylate buffer (pH 8.2) containing increasing amounts of CuZnSOD	**19**
Figure 2.4	Determination by standard addition of CuZnSOD monomer in 0.375 μM Sigma metHbA	**20**
Figure 3.1	Griess reagents	**30**
Figure 3.2	Absorption spectrum of NO_2^- standards from Saville assay and NO_2^- calibration curve	**36**
Figure 3.3	Effects of $HgCl_2$ on NO_2^- calibration curve	**37**
Figure 3.4	Visible spectra and analysis of S-nitrosation of Hb samples	**38**
Figure 3.5	Deconvolved electrospray mass spectrum of HbF	**40**
Figure 3.6	Deconvolved electrospray mass spectrum of S-nitrosated HbF	**41**
Figure 3.7	Effects of metHb on the NO_2^- calibration curve	**43**
Figure 3.8	Effects of sequence of addition of metHb, $XArNH_2$ and $HgCl_2$ on NO_2^- determination	**44**
Figure 3.9	Competition between $NH_2SO_3^-$ and $XArNH_2$ for NO_2^-	**47**
Figure 3.10	Effects of metHb on competition between $NH_2SO_3^-$ and $XArNH_2$ for NO_2^-	**49**
Figure 3.11	Effects of CuZnSOD and GSH addition on NO_2^- determination	**51**
Figure 3.12	Competition between GSH and $XArNH_2$ for NO_2^-	**52**
Figure 4.1	d-d Absorption spectra of $Cu^{II}ZnSOD/NO_2^-$ incubates in Na*Pi* buffer	**64**
Figure 4.2	d-d Absorption spectra of $Cu^{II}ZnSOD/NO_2^-$ incubates in 50 mM HEPES buffer (pH 7.4)	**65**

Figure 4.3 d-d Absorption spectra of $Cu^{II}ZnSOD/NO_2^-$ incubates in 50 mM HEPES buffer (pH 7.4) **67**

Figure 4.4 Absorption spectra of NO_2^- in buffer **68**

Figure 4.5 Absorbance spectra in LTMCT region of $Cu^{II}ZnSOD/NO_2^-$ incubates in 50 mM HEPES buffer (pH 7.4) at room temperature **69**

List of Tables

Table 2.1 Relative SOD activities and CuZnSOD monomer concentrations in Hb solutions from the direct method **16**

Table 2.2 CuZnSOD monomer concentrations in Hb solutions from the standard addition method **21**

Table 2.3 Cu and Zn measurements by ICP-MS **23**

Table 2.4 Hb-SNO, $HbFe^{II}NO$ and CuZnSOD monomer levels in preterm newborn RBC lysates **25**

Table 3.1 Literature levels of HbA-SNO in adult RBC lysates **28**

Table 3.2 Literature levels of Hb-SNO in newborn RBC lysates **29**

Table 3.3 Percent Hb S-nitrosation in Hb samples **37**

Table 3.4 pH values of reagent mixtures used **46**

Table 3.5 Summary of effects of varying order of addition of Saville reagents on NO_2^- determination in absence of metHb **54**

Table 3.6 Summary of effects of varying order of addition of Saville reagents on NO_2^- determination in presence of metHb **54**

Table 3.7 Summary of effects of varying order of addition of Saville reagents on NO_2^- determination in presence of GSH and CuZnSOD **54**

Table 4.1 Time dependent loss of d-d absorption band of $Cu^{II}ZnSOD$ on addition of NO_2^- **66**

LIST OF ABBREVIATIONS

3xDEAE-Hb	RBC supernatant passed through DEAE column for CuZnSOD removal
CA	carbonic anhydrase
CuZnSOD	Cu,Zn-superoxide dismutase (erythrocuprein)
NOS	nitric oxide synthase
GSH	glutathione
GSNO	S-nitrosoglutathione
Hb	hemoglobin
HbA	adult hemoglobin
HbA-SNO	S-nitrosated adult hemoglobin
HbF	fetal hemoglobin
$HbFe^{III}$	oxidized hemoglobin (metHb)
$HbFe^{II}O_2$	oxyhemoglobin (oxyHb)
$HbFe^{II}SH$	deoxyhemoglobin
$HbFe^{II}NO$	nitrosylated hemoglobin
HbF-SNO	S-nitrosated fetal hemoglobin
Hb-SNO	S-nitrosated hemoglobin
ICP-MS	inductively coupled plasma mass spectrometry
Na*Pi*	phosphate buffer (200 mM, pH 7.2)
NED	N-(1-naphtyl-)ethylenediamine
$NH_2SO_3^-$	sulfamate
NiR	nitrite reductase
NO_x	$NO_2^- + NO_3^-$
PBS-EDTA	phosphate buffered saline with ethylenediaminetetraacetic acid
P_{50}	oxygen tension at which Hb is 50% saturated with O_2
pO_2	oxygen tension
RBC	red blood cell
RSNO	S-nitrosothiol
$XArNH_2$	sulfanilamide ($X = NH_2SO_2$)

1.0 GENERAL INTRODUCTION

1.1 S-NITROSATION OF HbA

Adult hemoglobin (HbA), the oxygen (O_2) transporter in the adult human body, is a protein whose structure and function have been extensively studied over many years. HbA is a tetrameric protein, composed of two α-chains and two β-chains, which are held together by noncovalent interactions. Each chain contains a heme center (1,2). Over the past eight years, the study of the interactions between HbA and nitric oxide (NO) has generated a lot of interest (3-12).

NO has been shown to be produced in the endothelium by nitric oxide synthase (NOS) catalyzed oxidation of arginine (13). Among the many functions attributed to NO, is its critical role in maintaining stable vasomotor tone in the circulation (14). NO is unstable and its action is brief. Within seconds of its formation, it can undergo oxidation to nitrite (NO_2^-) or nitrate (NO_3^-) by reactions with O_2 and oxyhemoglobin (oxyHb; $HbFe^{II}O_2$), which is converted to metHb ($HbFe^{III}$).

In recent years, HbA has been shown to undergo S-nitrosation (HbA-SNO) at the reactive thiol group of Cysβ93. HbA-SNO formation has been shown to be favored in the oxy form and has been suggested to provide a means of maintaining the bioavailability of NO in the vasculature (3,4,6,7,15,16). An interesting mechanism was proposed whereby HbA-SNO formation occurs following conversion of HbA to its relaxed (R) state upon O_2 binding. Under hypoxic conditions, with the release of O_2, HbA adopts a tense (T) state and NO is released from Cysβ93 (3,17). There is a lot of controversy over the mechanism of formation of HbA-SNO and its biological function. The levels of HbA-SNO that exist *in vivo* have also been hotly debated (18,19). Recently,

it has been suggested that the levels of HbA-SNO found *in vivo* (< 50 nM) are too low to provide a useful system of NO conservation in the vasculature. It was proposed instead that NO_2^-, with measured levels in the micromolar range, provides the necessary pool of NO required to maintain vascular homeostasis and that HbA catalyzes NO_2^- reduction to NO (12,20).

The mechanisms of Hb-SNO formation and breakdown, as well as its role in the delivery of the vasodilator action conferred by NO, certainly require further study and interpretation.

1.2 S-NITROSATION OF FETAL HEMOGLOBIN

Human fetal hemoglobin (HbF), like HbA, is a tetramer, composed of two α-chains and two γ-chains. While the α-subunits are identical, the γ-chains differ from the β-chains of HbA at 39 residues. These differences confer a slightly more charged character to the γ-chain (21). Interestingly, the Cys93 residue, which has been shown to become S-nitrosated in HbA, is conserved in the γ-chains of HbF.

Expression of the γ-gene in the fetus is approximately 50 times higher than the β-gene. However, at 30 weeks of gestation, a switchover takes place, which increases β-chain expression and decreases γ-chain expression (22). At birth, HbF comprises 60 to 80% of the total hemoglobin (Hb) and in the 16 to 18 week infant, the HbF content is reduced to 3% (23). Interestingly, the proportion of HbF in newborns is related to their age from conception and not to the birth itself (24). In premature newborns, where levels of HbF are very high, the switch to HbA production occurs at the time corresponding to the end of the normal gestational period of 40-42 weeks (25).

HbF and HbA likely have different roles in the vasculature. HbF has a higher affinity for O_2 than HbA. In adult red blood cells (RBCs) this has been shown to be modulated by interaction of the heme protein with 2,3-diphosphoglycerate (2,3-DPG), an intermediate in the glycolytic pathway, and by changes in RBC pH (26). HbF binds 2,3-DPG weakly due to the presence of Ser21 in its γ-chain in place of His21 found in the β-chain (26,27). While the higher O_2 affinity of HbF (P_{50} = 21 mm Hg; P_{50} = oxygen tension at which Hb is 50% saturated with O_2) *vs* HbA (P_{50} = 30 mm Hg) (28) has been interpreted to facilitate O_2 transport from the mother to the fetus, examination of cases where maternal (P_{50} = 27 mm Hg) and fetal (P_{50} = 32 mm Hg) oxygen affinities were reversed (due to Aspα94→His mutation in HbF) did not reveal any effects on fetal development (29). All infants with the mutant Hb(Dα94H) were born at term with appropriate weight for gestational age and without any evidence of hypoxic erythropoietic stress. It has thus been suggested that the high O_2 affinity of HbF may provide a protective role against O_2 toxicity instead of a facilitative transport role (29,30).

NO is a potent vasodilator in the human umbilical-placental circulation (31). It also plays a significant role in maintaining low basal tone by counteracting the vasoconstrictor actions of endothelin and thromboxane (32). The vasodilator properties of NO in the fetal circulation is further substantiated by evidence that the human placental circulation is maximally dilated under normal circumstances (33). There is evidence of NO synthesis in the placenta (34) as well as the presence of NOS in stem villous blood vessels, in the endothelium of arteries and veins of the umbilical cord, and in the chorionic plate (35). Therefore, a readily accessible supply of NO seems to be needed to maintain the basal tone required in fetal circulation.

It has been proposed that delivery of NO in the fetal circulation is assured by S-nitrosated HbF (HbF-SNO) by means of a similar allosterically controlled mechanism to that proposed for HbA in the adult circulation (36). There is evidence that Hb-SNO may be involved in the perinatal circulatory transition, with lower Hb-SNO levels detected in arterial cord blood samples from newborns who did not adjust normally to neonatal circulation (37).

It has been shown *in vitro* that release of NO from HbF-SNO occurs at pO_2 close to normal (*e.g.*, pO_2 = 20 mm Hg). For HbA-SNO, NO release occurs under hypoxic conditions (*e.g.*, pO_2 = 18 ± 2 mm Hg *vs* normal pO_2 = 30 mm Hg) (38). Also, S-nitrosation does not increase the O_2 affinity of HbF in contrast to HbA (38). In a comparative study of NO scavenging *in vitro*, HbF and HbA obtained from dialyzed fetal and adult RBC supernatants, respectively, were shown to scavenge NO at similar rates, but intact fetal RBCs exhibited a higher NO scavenging effect than adult RBCs. This indicates that there are possible differences in NO biochemistry in fetal *vs* adult RBCs (39).

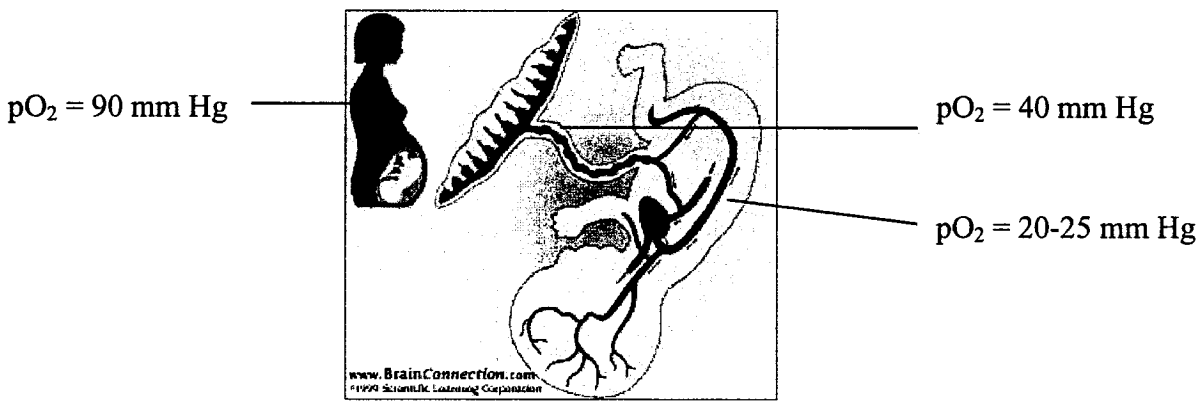

Figure 1.1 **Diagram of umbilical-placental circulation.**
(from www.brainconnection.com)

While adult arterial blood pO_2 is close to 90 mm Hg, the umbilical vein carries blood with a pO_2 of 40 mm Hg from the placenta to the fetus (Figure 1.1). This is reduced to 20-25 mm Hg in fetal venous blood (40). The maximal O_2 saturation of fetal blood is 70% (40) and this can decrease to 40-45% during labor (41). These data suggest that in the fetal circulation, HbF is approximately 50% deoxy. Recent studies have shown an inverse correlation between the amount of Hb-SNO and HbF measured in chord blood samples collected from newborns. Newborns with a higher percentage of HbF had lower levels of Hb-SNO. No difference was detected in nitrosylHb ($HbFe^{II}NO$) levels between newborns with high (~ 95%) and low (~ 75%) HbF (42).

From the published data, it would appear that there is strict control over NO and O_2 levels in the fetal circulation. Untimely release of NO or O_2 may lead to severe hypotension or O_2 toxicity. A higher affinity of HbF for NO (39) and O_2 may mediate less unbound O_2 in solution and a reservoir effect of HbF for NO. A reservoir of NO may be beneficial in the fetal circulation in cases such as ischemic hypoxia *in utero* (43,44). Conversely NO, which is used to improve oxygenation in premature infants and newborns suffering from pulmonary hypertension (44,45), may also play a role in the adaptation from fetal to newborn circulation. Understanding the reactions of NO and HbF will shed light on proper NO delivery with minimal NO oxidation in the fetus.

1.3 INVOLVEMENT OF Cu,Zn-SUPEROXIDE DISMUTASE IN THE FORMATION OF S-NITROSOHEMOGLOBIN

There is much controversy as to the exact role and the actual physiological levels of Hb-SNO formed *in vivo* (7,15,18,19). The elucidation of a mechanism for Hb-SNO formation has been under intense investigation as a means of shedding light on this matter. The transfer of NO to Cysβ93 of oxyHb has been suggested to occur by a direct

trans-S-nitrosation reaction, whereby NO^+ is delivered from endogenous low-molecular weight S-nitrosothiols (RSNOs), such as S-nitrosoglutathione (GSNO) (46), as shown in equation 1.1:

$$GSNO + oxyHb\text{-}SH \rightleftharpoons GSH + oxyHb\text{-}SNO \qquad 1.1$$

Levels of glutathione (GSH), the dominant low-molecular weight thiol in adult RBCs, are greater than 10 mM (4). Thus, it is considered that the S-nitrosated form of glutathione (GSNO), with concentrations estimated to be in the nanomolar range, is the major NO donor in the vasculature to Cysβ93 of oxyHb-SH (46).

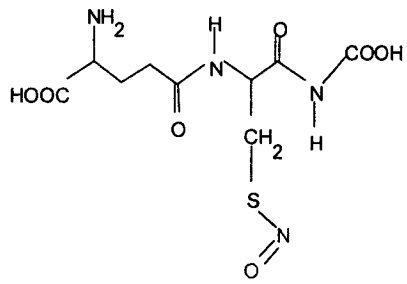

Figure 1.2 **S-Nitroso-L-glutathione (GSNO).**

However, evidence *in vitro* suggests that instead of the proposed direct *trans*-S-nitrosation reaction, the transfer of NO to Cysβ93 of oxyHb-SH is a metal-catalyzed reaction, which requires the presence of Cu^I as shown in the following equations (9):

$$GSNO + Cu^I \longrightarrow GS^- + NO + Cu^{II} \qquad 1.2$$

$$oxyHb\text{-}SH + NO + Cu^{II} \longrightarrow oxyHb\text{-}SNO + Cu^I \qquad 1.3$$

NO transfer was shown to occur with the addition of copper in the form of copper sulfate ($CuSO_4$), and was inhibited in the presence of neocuproine, a Cu^I-specific chelator (8). In

the RBC, copper is mostly present in the protein Cu,Zn-superoxide dismutase (CuZnSOD) (47). Interestingly, it has been shown *in vitro* using commercial human HbA at its physiological concentration (5 mM) that GSNO breakdown and oxyHb-SNO formation were catalyzed by CuZnSOD present at its physiological concentration (~ 20 μM) in the HbA solutions (11). The following mechanism has been proposed for CuZnSOD-catalyzed S-nitrosation of oxyHb at Cysβ93 (11):

$$\text{oxyHb-SH} + \text{Cu}^{\text{II}}\text{ZnSOD} \longrightarrow \text{oxyHb-S}\bullet + \text{Cu}^{\text{I}}\text{ZnSOD} + \text{H}^{+} \qquad 1.4$$

$$\text{GSNO} + \text{Cu}^{\text{I}}\text{ZnSOD} + \text{H}^{+} \longrightarrow \text{GSH} + \text{NO} + \text{Cu}^{\text{II}}\text{ZnSOD} \qquad 1.5$$

$$\text{NO} + \text{oxyHb-S}\bullet \longrightarrow \text{oxyHb-SNO} \qquad 1.6$$

NO transfer is thought to occur within an oxyHb-CuZnSOD encounter complex, with the two proteins oriented to target or channel the liberated NO to the thiyl radical on Cysβ93 (11). Such channeling would prevent NO scavenging by the $Fe^{II}O_2$ heme (5,11):

$$\text{oxyHb} + \text{NO} \longrightarrow \text{metHb} + \text{NO}_3^{-} \qquad 1.7$$

Thus, CuZnSOD was shown to play a critical role *in vitro* in the transfer of NO from GSNO to Cysβ93 rather than to the oxyheme of oxyHbA. As the Cys93 residue is conserved in the γ-chains of HbF (21), and there is evidence of S-nitrosation of HbF (36-38), CuZnSOD may have an important role in fetal and newborn RBCs as suggested for adult RBCs.

1.4 OUTLINE OF THESIS

In Chapter 2, levels of CuZnSOD measured by means of the pyrogallol assay in newborn and adult RBCs are reported and compared. The CuZnSOD levels are correlated to Cu levels previously measured in the samples by inductively coupled plasma mass spectrometry (ICP-MS) and to levels of Hb-SNO measured by ozone chemiluminescence at Ste-Justine Hospital.

In Chapter 3, S-nitrosation of newborn and adult RBC lysates following incubation with GSNO was measured by means of the Saville assay for RSNOs. An investigation of the Saville assay ensued to establish the effects of Hb on RSNO determination.

In Chapter 4, the potential of CuZnSOD to act as a catalyst for nitrite reduction was investigated by examining the effects of NO_2^- on the spectrum of the enzyme. Catalysis of nitrite reduction is of importance since NO_2^- is proposed to be a major source of NO in the vascular system (6).

Chapter 5 provides an overall discussion of the results and suggestions for future studies.

2.0 ANALYSIS OF Cu,Zn-SUPEROXIDE DISMUTASE LEVELS IN HEMOGLOBIN SAMPLES

2.1 INTRODUCTION

2.1.1 Role of CuZnSOD in the formation of Hb-SNO

CuZnSOD was shown to catalyze the transfer of NO from GSNO to Cysβ93 of oxyHbA *in vitro* (11). As the Cys93 residue is conserved in the γ-chains of HbF (21), and S-nitrosation of HbF has been shown to occur (36,38), the levels of CuZnSOD in RBC lysates of newborns were investigated. In these samples, the main form of Hb is HbF (23). A comparison of the levels of CuZnSOD and HbF might provide some insight into the role and mechanism of S-nitrosation of HbF. Measurement of SOD activities was performed by means of the pyrogallol oxidation assay (48) and activities were correlated to CuZnSOD levels.

2.1.2 SOD activity assay

Pyrogallol autoxidation produces superoxide ions, which further react with pyrogallol. The pyrogallol radicals formed dimerize to yield a product that can be monitored spectrophotometrically at 320 nm (48). Addition of CuZnSOD decreases the rate of pyrogallol dimerization by competing for the superoxide anion, thus resulting in a decreased rate of absorbance growth at 320 nm (48).

It was reported previously by our group that HbA catalyzes pyrogallol oxidation (11). Thus, CuZnSOD activities were measured in samples containing HbA and converted to active CuZnSOD concentrations (11). Due to large variability in the measured levels of CuZnSOD, a standard addition method based on the pyrogallol assay was explored for CuZnSOD determination. Both direct and standard addition methods

were used to measure and compare levels of CuZnSOD in newborn and adult RBC lysates.

2.2 EXPERIMENTAL SECTION

2.2.1 Materials

Human adult and newborn RBC lysates prepared as described in Section 2.2.2.1 were provided by Ste-Justine Children's Hospital, Montreal. Human lyophilized HbA was obtained from Sigma. Batches of Sigma human HbA have been shown to contain physiological levels of CuZnSOD (11). The method of Sigma human HbA preparation (Appendix A), which was obtained from the company (49), did not include any purification steps following RBC lysis by addition of ether and collection of the supernatant. Thus, HbA from Sigma should be considered as a RBC supernatant. Hb in the Sigma preparations is mainly in the metHb form, that is, its heme iron is oxidized (Fe^{III}).

Bovine RBC CuZnSOD was obtained from Roche; pyrogallol, and monobasic and dibasic sodium phosphate salts were obtained from Fisher; Tris was obtained from BioShop; cacodylic acid (dimethylarsenic acid) was obtained from Aldrich; trace-metal grade HCl and DEAE Sephacel anion-exchange gel were obtained from Sigma; Hi-Trap (5 mL; 16 x 2.5 cm) Sephadex G-25 columns were obtained from Amersham Pharmacia Biotech; Nanopure water (MilliQ; specific resistance of 18 mΩcm) from a Millipore Simplicity water purification system and treated with Chelex-100 (Sigma) to remove trace metal ions was used to prepare all solutions.

2.2.2 Methods

2.2.2.1 Preparation of RBC lysates, HbF and HbA

Preparations of RBC lysates, HbF and HbA were performed by Carmen Gagnon in Dr. Bard's research lab at Ste-Justine Hospital. Blood samples were collected from the umbilical cord veins of normal (appropriate weight for gestational age) newborns without medical or obstetrical complications delivering between 25 to 41 weeks of gestation. Samples from newborns delivered between 25 and 34 weeks of gestation are considered preterm, while samples from newborns delivered at 35 weeks of gestation and onwards are considered term. Adult blood samples were collected from healthy adult individuals. All blood samples were drawn into pre-chilled EDTA collection tubes and centrifuged. The residual RBC pellet was washed three times in 10 mL of phosphate buffered saline with 0.5 mM ethylenediaminetetraacetic acid (PBS-EDTA), and frozen at -80°C. RBC hemolysates were obtained by thawing, and when applicable, diluting 1:2 in 0.5 mM EDTA (42). Samples thus prepared are termed RBC lysates. HbF and HbA were separated by HPLC (50). Samples were stored at -20°C and thawed on ice on the day of use.

2.2.2.2 Preparation of commercially obtained HbA

Lyophilized HbA (mainly the met form, Appendix A) from Sigma was dissolved in 200 mM sodium phosphate buffer, pH 7.2 (Na*Pi*), centrifuged at 13400 g for 4 min, and the supernatant maintained on ice until use.

2.2.2.3 Removal of CuZnSOD from commercial metHbA

Removal of CuZnSOD from commercial metHbA samples was attempted by applying 0.5 mL of Sigma HbA at a concentration of ~ 30 mM heme to a DEAE-

Sephacel column (0.9 cm x 2.8 cm) equilibrated with Na*Pi*. The Hb sample was eluted with ~ 1 mL of 100 mM NaCl in Na*Pi* (11), and reapplied twice to the column. The final eluate (1-2 mL) was desalted on a Sephadex G-25 Hi-Trap column equilibrated with Na*Pi*, and eluted with the same buffer. Use of the Hi-Trap column ensured that sample dilution was minimal. The HbA sample treated in this manner is referred to as 3xDEAE-Hb.

2.2.2.4 Determination of Hb concentration

Hb in all samples was determined by monitoring the absorbance at 500 nm (ε = 10 $mM^{-1}cm^{-1}$ per heme) and 630 nm (ε = 4.4 $mM^{-1}cm^{-1}$ per heme) for metHb ($HbFe^{III}$); and at 541 nm (ε = 13.8 $mM^{-1}cm^{-1}$ per heme) and 577 nm (ε = 14.6 $mM^{-1}cm^{-1}$ per heme) for oxyHb ($HbFe^{II}O_2$) (2) on a Agilent 8453 UV-visible spectrophotometer.

2.2.2.5 SOD activity assay

Lyophilized CuZnSOD (10 mg) was reconstituted in 1 mL of Na*Pi* to give a stock solution of ~ 600 µM monomer (note: CuZnSOD is a homodimer and all concentrations here are given in terms of the monomer. Its concentration was verified by monitoring the absorbance at 258 nm (ε = 5.15 $mM^{-1}cm^{-1}$ per monomer) (51) and diluted in Na*Pi* to the desired concentration of 300 nM monomer.

Pyrogallol stock solution (40 mM) was prepared in 10 mM HCl. Tris-cacodylate buffer was prepared by adjusting the pH of 0.05 M Tris to 8.2 with 0.5 M cacodylic acid. The pyrogallol stock and buffer were considered stable for one week at 4°C.

For the assay, 10 µL of 37.5 µM Sigma metHbA tetramer was added to 990 µL of Tris-cacodylate buffer, with or without CuZnSOD, in a 1.5-mL quartz cuvette with a 1-cm pathlength. Pyrogallol (5 µL) was added to a final concentration of 200 µM and the

absorbance at 320 nm was read every 15 s over 3 min to monitor the rate of pyrogallol oxidation. Oxidized pyrogallol exhibits a maximum at 320 nm with little interference from metHb absorption.

(i) CuZnSOD determination by the direct method

A blank (0% SOD activity) containing 0.375 μM 3xDEAE-Hb tetramer and a standard (200% SOD activity) containing 0.375 μM 3xDEAE-Hb tetramer and 3.0 nM CuZnSOD monomer were prepared. At these concentrations, the ratio of CuZnSOD monomer to Hb tetramer (1:125) is twice that present in human RBCs (20 μM CuZnSOD:5 mM Hb = 1:250) (11). The unknowns (X) were diluted to 0.375 μM Hb tetramer and the relative SOD activities, and thus active CuZnSOD concentrations, were determined from the initial slopes (0-60 s) of plots of A_{320nm} *vs* time with the application of the following equation (11):

$$\% \text{ relative SOD activity} = \frac{\text{(blank slope} - \text{X slope)}}{\text{(blank slope} - \text{standard slope)}} \times 200 \qquad 2.1$$

The concentration of CuZnSOD monomer thus obtained was adjusted to 5 mM Hb tetramer, which is the HbA concentration in adult RBCs (52).

(ii) CuZnSOD determination by the standard addition method

Standard addition is a method of quantitation that is often employed for the analysis of unknowns containing interferences (53). Samples (10 μL) containing Hb were diluted to 0.375 μM tetramer in 990 μL of 50 mM Tris-cacodylate buffer, pH 8.2, in a 1.5-mL quartz cuvette with a 1-cm pathlength. CuZnSOD was added to final concentrations of 1.5 to 27.2 nM monomer followed by 5 μL of pyrogallol to a final concentration of 200 μM, and the SOD activity measured from the initial slopes (0-60 s) of absorbance at 320 nm over time ($\Delta A_{320nm}/s$). A calibration curve of

$1/(\Delta A_{320nm}/s)$ *vs* [CuZnSOD] monomer was constructed, and the concentration of CuZnSOD in the unknown was determined by extrapolation to $1/(\Delta A_{320nm}/s) = 0$, following correction for pyrogallol oxidation in buffer alone. It is not possible to obtain blanks with zero CuZnSOD analyte present that are identical to the samples since chromatography will likely remove other RBC components as well as the analyte. It was therefore assumed that $1/(\Delta A_{320nm}/s)$ in the absence of added CuZnSOD is the same as that determined in the buffer alone. Since this method is based on extrapolation, measurements were not considered accurate if the coefficient of linearity (r^2 value) of the calibration curve fell outside the range of 0.9 to 1.0.

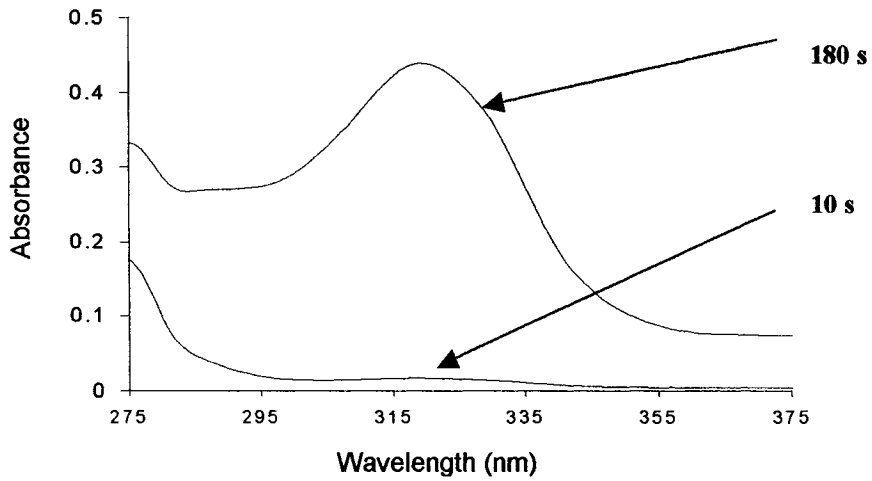

Figure 2.1 **UV absorption of a pyrogallol solution.** These spectra of a 200-μM pyrogallol solution were taken at 10 and 180 s following pyrogallol addition to 50 mM Tris-cacodylate buffer, pH 8.2. Spectra were recorded in a 1.5-mL quartz cuvette with a 1-cm pathlength at 25°C with a scan rate of 1200 nm/min.

2.3 RESULTS

2.3.1 Determination of CuZnSOD by the direct method

Spectra of 3xDEAE-Hb and CuZnSOD alone in the assay buffer confirmed that there is no change in absorption at 320 nm over time (data not shown). The spectrum of pyrogallol exposed to the alkaline buffer (pH 8.2) showed, as expected, that it undergoes

oxidation in a time-dependent manner to give a product that absorbs at 320 nm (Figure 2.1).

Rates of pyrogallol oxidation were determined from the initial (60 s) linear portion of the plots of A_{320nm} *vs* time. Addition of 0.375 μM 3xDEAE-Hb tetramer, prepared as described in Section 2.2.2.3, slightly decreased the rate of pyrogallol autoxidation compared to that in buffer alone (Figure 2.2a). Thus, for all activity measurements, the blank contained pyrogallol and 0.375 μM 3xDEAE-Hb tetramer. Addition of 3.0 nM CuZnSOD monomer to the blank decreased the rate of pyrogallol oxidation further (Figure 2.2b) due to competition for superoxide.

Analysis of samples containing 0.375 μM untreated Sigma metHb tetramer revealed 60 ± 24 % relative SOD activity (n=5), which corresponds to 0.90 ± 0.40 nM CuZnSOD monomer in the sample (Figure 2.2c, Table 2.1). The values obtained from these analyses are lower than the previously reported value of 1.5 nM CuZnSOD monomer per 0.375 μM metHb tetramer (11). This could be attributed in part to the difference in lot numbers of the lyophilized Sigma HbA samples that were used and/or to incomplete removal of CuZnSOD from the 3xDEAE-Hb sample. In this context it is important to note that our lab has previously reported that HbA catalyzed pyrogallol oxidation (11).

Analysis of newborn and adult RBC lysates from Ste-Justine Hospital revealed 296 ± 176 % and 224 ± 138 % relative SOD activity, which correspond to 4.6 ± 2.4 nM and 3.4 ± 2.0 nM CuZnSOD monomer, respectively (Table 2.1; Appendix C).

Table 2.1 **Relative SOD activities and CuZnSOD monomer concentrations in Hb solutions from the direct method** [a]

Sample	n [b]	% relative SOD activity [c]	Observed [CuZnSOD] (nM) [d]	Normalized [CuZnSOD] (μM) [e]
Sigma HbA [f]	5	60 ± 24 %	0.90 ± 0.40	12 ± 5.4
Newborn RBC lysate [g]	3	296 ± 176 %	4.6 ± 2.4	61 ± 32
Adult RBC lysate [h]	2	224 ± 138 %	3.4 ± 2.0	45 ± 27

[a] Samples contained 0.375 μM HbA tetramer in 50 mM Tris-cacodylate buffer, pH 8.2. The assay was initiated with the addition of 200 μM pyrogallol and the change in absorbance at 320 nm due to pyrogallol oxidation *vs* time was recorded (Section 2.2.2.5).

[b] Number of occasions of analysis.

[c] Percent relative SOD activity (as per equation 1 in text).

[d] Calculated concentration of active CuZnSOD monomer in solutions containing 0.375 μM HbA tetramer.

[e] CuZnSOD monomer concentration normalized to 5 mM Hb tetramer.

[f] Untreated commercial human HbA from Sigma from lot A.

[g, h] Samples from Ste-Justine Hospital.

Within experimental error, the CuZnSOD values are similar in newborn and adult RBCs. In addition, the CuZnSOD levels obtained for the adult RBC lysate are within the previously reported value of 1.5 nM CuZnSOD monomer in 0.375 μM Sigma metHbA (11).

Results from these direct analyses show large variability. The 3xDEAE-Hb sample was prepared fresh before each set of analyses and it is likely that the method used (Section 2.2.2.3) resulted in elution of variable amounts of CuZnSOD and RBC components from the DEAE column. A standard addition method was therefore explored to determine CuZnSOD levels in the Hb samples.

2.3.2 Determination of CuZnSOD by the standard addition method

Addition of increasing amounts of CuZnSOD to 50 mM Tris-cacodylate buffer, pH 8.2, resulted in a proportional decrease in the rate of pyrogallol oxidation (Figure 2.3a,b). The linear range was found to be between 0 – 7.2 nM monomer (Figure 2.3c), consistent with results found previously in our lab (54) where the inhibition of pyrogallol oxidation was linear up to 100 ng/mL CuZnSOD (6.67 nM CuZnSOD monomer). A plot of the inverse rates of pyrogallol oxidation *vs* the concentration of CuZnSOD monomer added is shown in the Figure 2.3d.

An example of the determination of CuZnSOD monomer in 0.375 μM Sigma HbA tetramer (lot A) by means of the standard addition method is shown in Figure 2.4. The amount of CuZnSOD monomer determined was 1.7 nM following extrapolation of the inverse rate of pyrogallol oxidation in buffer alone. The average CuZnSOD monomer concentration in Sigma metHbA from two occasions of analysis was 1.6 ± 0.1 nM CuZnSOD monomer (Table 2.2, Appendix B). This value is higher than the CuZnSOD monomer range (0.90 ± 0.40 nM) obtained here using the direct method (Table 2.1) but agrees with the previously reported value of 1.5 nM CuZnSOD monomer per 0.375 μM metHb tetramer in Sigma human HbA (11). Analysis of a second lot of Sigma HbA (lot B) resulted in significantly lower levels of CuZnSOD monomer (0.8 ± 0.1 nM in 0.375 μM HbA tetramer; Table 2.2), indicating that there are lot-to-lot differences in the CuZnSOD content or more specifically in the SOD activity in commercially available Sigma HbA.

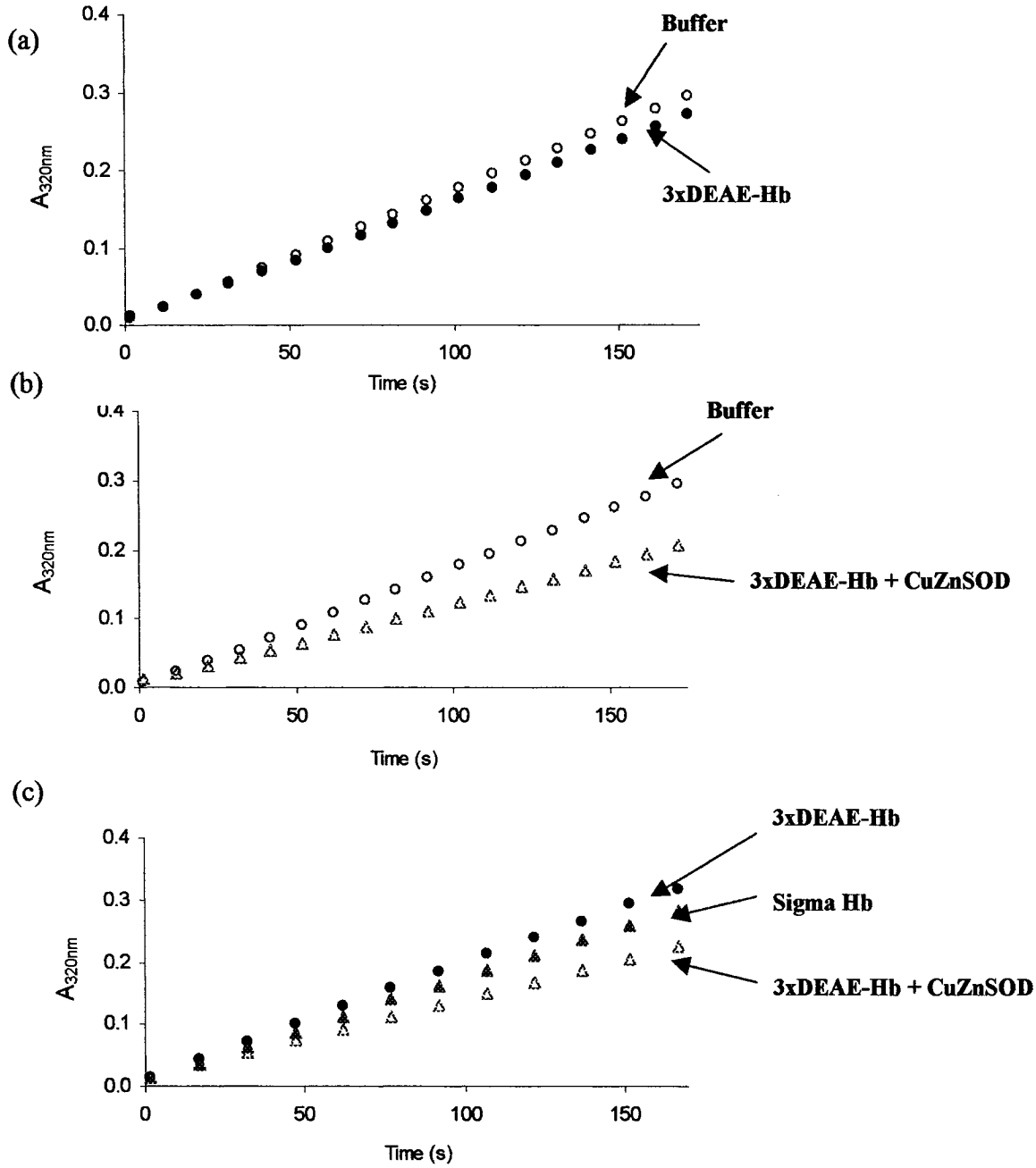

Figure 2.2 **Pyrogallol autoxidation in the presence and absence of 3xDEAE-Hb and CuZnSOD.** Time course of absorbance change at 320 nm following addition of 200 μM pyrogallol to (a) buffer only (○) and 0.375 μM 3xDEAE-Hb tetramer (●); (b) buffer only (○) and 0.375 μM 3xDEAE-Hb tetramer + 3.0 nM CuZnSOD monomer (△); (c) 0.375 μM 3xDEAE-Hb tetramer (●), 0.375 μM 3xDEAE-Hb tetramer + 3.0 nM CuZnSOD monomer (△), and 0.375 μM Sigma metHbA (▲). Absorbances were measured in 50 mM Tris-cacodylate buffer, pH 8.2, at 25°C in a 1.5-mL quartz cuvette with a 1-cm pathlength.

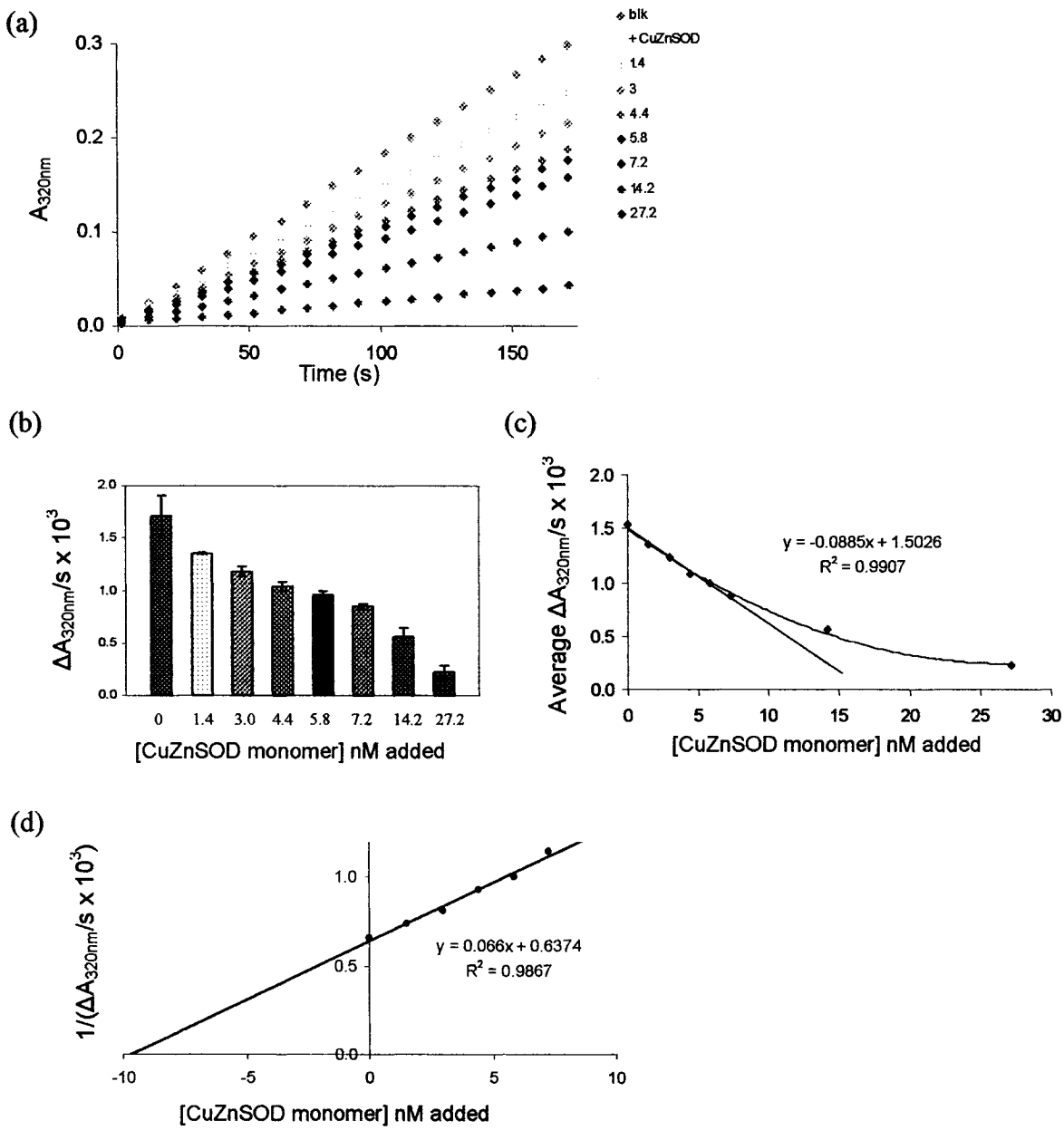

Figure 2.3 **Rates of pyrogallol autoxidation in 50 mM Tris-cacodylate buffer (pH 8.2) containing increasing amounts of CuZnSOD.** (a) Time course of absorbance change at 320 nm following addition of increasing amounts of CuZnSOD monomer and 200 μM pyrogallol. (b) Average rates and standard deviations (n=2, except for blank where n=5) of pyrogallol oxidation expressed as $\Delta A_{320nm}/s$ at each concentration of CuZnSOD monomer. (c) Plot of mean $\Delta A_{320nm}/s$ *vs* concentration of CuZnSOD monomer added to 200 μM pyrogallol. (d) Plot of mean $1/(A_{320nm}/s)$ *vs* concentration of CuZnSOD monomer added. Absorbance changes per second, which are multiplied by 10^3 in this figure, were recorded in a 1.5-mL quartz cuvette with a 1-cm pathlength at 25°C.

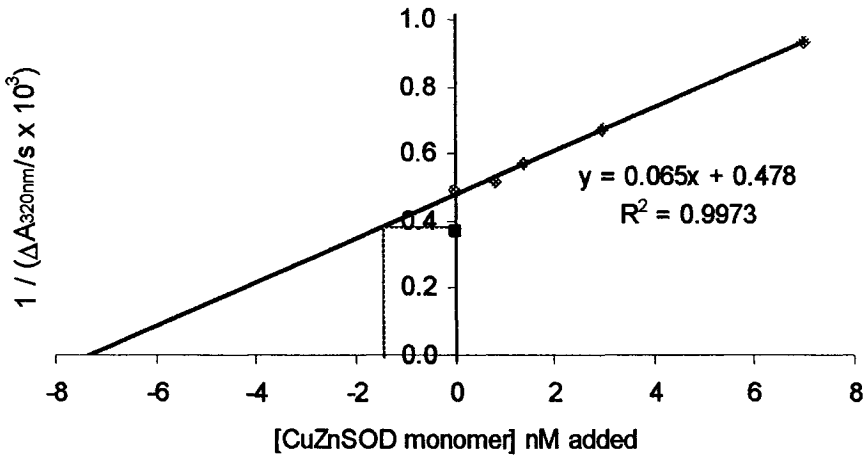

Figure 2.4 **Determination by standard addition of CuZnSOD monomer in 0.375 μM Sigma metHbA.** Plot of the inverse rate of pyrogallol oxidation, $1/(\Delta A_{320nm}/s)$ *vs* concentration of CuZnSOD monomer added to Sigma HbA and 200 μM pyrogallol in 50 mM Tris-cacodylate buffer, pH 8.2. The amount of CuZnSOD monomer present was determined to be 1.7 nM by extrapolation of the inverse rate ($\Delta A_{320nm}/s$) of pyrogallol oxidation in buffer alone (blank, ■). Absorbances were recorded in a 1.5-mL quartz cuvette with a 1-cm pathlength at 25°C. The $\Delta A_{320nm}/s$ values were multiplied by 10^3.

Analysis by the standard addition method of the different preparations of 3xDEAE-Hb used in Section 2.3.1 revealed the presence of 1.6 ± 0.4 nM CuZnSOD monomer in Sigma HbA from lot A and 0.2 nM CuZnSOD monomer in Sigma HbA from lot B following DEAE purification (Table 2.2). This confirms that CuZnSOD remained in the Sigma HbA samples following DEAE anion-exchange chromatography (Section 2.2.2.3).

Results from the single analysis of two RBC lysates collected at birth and 3.5 days following birth from preterm newborns indicated the presence of 11 and 16 μM CuZnSOD monomer, respectively, per 5 mM Hb tetramer (Table 2.2). The standard addition calibration curves for these samples are given in Appendix B. Thus, the CuZnSOD monomer content measured in the lysate of RBCs collected from a single

preterm newborn at 3.5 days following birth is higher than that measured in the lysate of RBCs collected from a single preterm newborn at birth. These RBC lysates, which are different from the samples analyzed in Section 2.3.1 (Table 2.1), were shown by chemiluminescence analysis performed at Ste-Justine Hospital to have different levels of Hb-SNO (Table 2.4).

Table 2.2 **CuZnSOD monomer concentrations in Hb solutions from the standard addition method** [a]

Sample	n [b]	Observed [CuZnSOD] (nM) [c]	Normalized [CuZnSOD] (μM) [d]	Linearity coefficient (r^2)	Data [i]
3xDEAE-Hb [j]	3	1.6 ± 0.4	21 ± 5	> 0.96	Fig. B.5-B7
3xDEAE-Hb [k]	1	0.2	3	1.00	B.8
Sigma HbA [e,j]	2	1.6 ± 0.1	21 ± 1	> 0.90	Fig. B.1-B.2
Sigma HbA [e,k]	2	0.8 ± 0.1	11 ± 1	> 0.96	Fig. B.3-B.4
Newborn RBC lysate [f]	1	0.8	11	0.99	Fig. B.9
Newborn RBC lysate [g]	1	1.2	16	0.93	Fig B.10
Adult RBC lysate [h]	1	0.6	8	0.98	Fig. B.11

[a] Samples contained 0.375 μM Hb tetramer in 50 mM Tris-cacodylate buffer, pH 8.2, and increasing amounts of CuZnSOD monomer. The assay was initiated with the addition of 200 μM pyrogallol and the change in absorbance at 320 nm due to pyrogallol oxidation *vs* time was recorded (Section 2.2.2.5).

[b] Number of occasions of analysis.

[c] Concentration of CuZnSOD monomer in solutions containing 0.375 μM Hb tetramer.

[d] CuZnSOD monomer concentration normalized to 5 mM Hb tetramer.

[e] Untreated commercial human HbA from Sigma.

[f] Cord blood collected at birth from a preterm newborn at Ste-Justine Hospital.

[g] Blood collected from a different preterm newborn 3.5 days following birth at Ste-Justine Hospital.

[h] Adult male RBC lysate from fresh blood collected at Ste-Justine Hospital.

[i] Standard addition plots are given in Appendix B in the figures indicated here.

[j] Sigma HbA from lot A.

[k] Sigma HbA from lot B.

Results from the single analysis of an adult RBC lysate, prepared the same way as the newborn lysates (Section 2.2.2.1), showed a concentration of 8 μM CuZnSOD monomer (Table 2.2; calibration curve in Figure B.11 of Appendix B). This value is lower than that measured above for the newborn RBC lysates, and is also lower than the reported value of 20 μM CuZnSOD monomer in adult RBCs (11). The three lysate samples in Table 2.2 were analyzed concurrently using the same blank (see data, page 85) to decrease errors in the analysis.

2.4 DISCUSSION

The standard addition method was shown to be more reproducible than the direct method for CuZnSOD monomer determination in Hb-containing samples. For example, analysis of an untreated Sigma HbA sample (lot A) on 5 separate occasions by the direct method gave 12 ± 5.4 μM CuZnSOD monomer per 5 mM Hb tetramer (Table 2.1), whereas analysis of the same sample on 2 separate occasions by the standard addition method gave 21 ± 1 μM CuZnSOD monomer per 5 mM Hb tetramer (Table 2.2).

Complete removal of CuZnSOD from Sigma HbA is a critical factor in the determination of CuZnSOD monomer by the direct method. However, by standard addition, it was shown that the 3xDEAE-Hb samples contained variable levels of CuZnSOD monomer (Table 2.2). Removal of CuZnSOD from Sigma HbA was attempted using a DEAE-Sephacel anion exchange column. Sigma HbA (7.5 mM tetramer) was passed three times through the DEAE column equilibrated with Na*Pi* and eluted with 100 mM NaCl in Na*Pi* (11). Since the isoelectric point of Hb (pI = 7.0) (55) is higher than that of CuZnSOD (pI = 4.7) (56), the latter was expected to remain on the column. However, as there was no reconditioning of the column following elution of HbA, co-

elution of CuZnSOD occurred, as seen in Table 2.2. Since the standard addition method gave reproducible results, removal of CuZnSOD from the Hb samples was not attempted again. The CuZnSOD concentration (21 ± 1 nM monomer per 5 mM Hb tetramer) found by the standard addition method is close to the previously reported value for Sigma HbA from lot A (11). However, the CuZnSOD monomer level from lot B was significantly different (11 ± 1 nM monomer per 5 mM Hb tetramer). Thus, there may be lot-to-lot variability in the CuZnSOD content or activity of Sigma human HbA.

Table 2.3 **Cu and Zn measurements by ICP-MS** [a]

Sample	Treatment	Cu (μM) [a]	Zn (μM) [a]
HbA Sigma [d]	-	19.7 ± 0.8	20.7 ± 0.9
	G25 [b]	16.6 ± 0.8	17.7 ± 0.6
	DEAE [c]	3.8 ± 0.7	4.0 ± 0.8
Newborn RBC lysate [e]	G25 [b]	13.6 ± 1.3	9.6 ± 0.7
	DEAE [c]	1.2 ± 0.2	4.3 ± 0.7
Adult RBC lysate [f]	G25 [b]	5.0 ± 0.3	5.8 ± 0.1
	DEAE [c]	1.8 ± 0.7	2.1 ± 0.9

[a] The ICP-MS measurements were recorded by A. Romeo on a PE Sciex Elan 6000 inductively coupled plasma mass spectrometer (ICP-MS) with a cross-flow nebulizer and Scott-type spray chamber. All reported values were normalized to the physiological concentration of Hb tetramer (5 mM) (11).

[b] Samples passed through a 1.3 x 2.6-cm G25 column to remove low molecular weight species.

[c] Purified Hb samples separated into HbF and HbA at Ste-Justine Hospital by HPLC using a Protein-Pak DEAE 5PW 8x75 mm column (Waters).

[d] Commercial human HbA from lot A Sigma.

[e] Cord blood RBCs from a term newborn at Ste-Justine Hospital.

[f] Adult RBCs collected at Ste-Justine Hospital.

The average level of CuZnSOD monomer found by both the direct (Table 2.1) and standard addition (Table 2.2) methods is higher in newborn than in adult RBC lysates

prepared in a similar way. Copper analyses carried out by our lab by ICP-MS show that Cu levels are also higher in a newborn *vs* an adult RBC lysate (Table 2.3).

As expected in all DEAE-treated Hb samples analyzed by ICP-MS, levels of Cu and Zn are lower than those measured for Hb samples passed through a 1.3 x 2.6-cm Sephadex G25 NAP-10 (fractionation range of 0.1 to 5 kD) gel filtration column (Table 2.3). This indicates that CuZnSOD is removed from the Hb sample by the action of anion exchange but not by G25 gel filtration. Furthermore, the values measured by ICP-MS for Zn appear to be only slightly higher than the Cu values in both Sigma HbA and the adult RBC lysate. This would suggest that Cu and Zn in the RBC are found mainly in CuZnSOD. The values for Zn in the newborn RBC lysate do not correlate with those measured for Cu. Zn levels measured for the G25-treated newborn RBC lysate (9.6 ± 0.7 μM) are lower than the Cu levels (13.6 ± 1.3 μM), whereas the same sample after DEAE-purification exhibited Zn levels (4.3 ± 0.7 μM) higher than Cu levels (1.2 ± 0.2 μM). This indicates that there is error in ICP-MS analyses and/or other proteins such as carbonic anhydrase, may contribute to the Zn levels.

The two newborn RBC lysates contained 11 and 16 nM CuZnSOD monomer per 5 mM Hb tetramer as analyzed by the standard addition method (Table 2.2). Measurements of RSNO levels in these two samples, performed at Ste-Justine Hospital by ozone chemiluminescence (Section 3.1.3), showed the presence of 24 and 146 nM Hb-SNO, respectively, per 5 mM Hb tetramer (Table 2.4). This increase in Hb-SNO level with expression of CuZnSOD is consistent with a role for CuZnSOD in the S-nitrosation of Hb, as discussed in Section 1.3. Since ~ 90% of Hb in the newborn samples (Table

2.4) was HbF, it can be assumed that CuZnSOD catalyzes NO transfer to Cysγ93 in a fashion similar to that described for Cysβ93 (equations 1.4-1.6) (11).

Table 2.4 **Hb-SNO, $HbFe^{II}NO$ and CuZnSOD monomer levels in preterm newborn RBC lysates**

Sample	% HbF [a]	[Hb-SNO] (nM) [b]	[HbFeNO] (nM) [b]	[CuZnSOD] (μM) [c]
Newborn RBC lysate [d]	91.3 %	24	38	11
Newborn RBC lysate [e]	92.6 %	146	73	16

[a] Estimated % HbF values based on gestational age (42).

[b] Values measured at Ste-Justine Hospital and normalized to 5 mM Hb tetramer.

[c] CuZnSOD monomer concentrations normalized to 5 mM Hb tetramer (from Table 2.2).

[d] RBC lysate from cord blood collected at birth from a preterm newborn.

[e] RBCs from a different preterm newborn collected 3.5 days following birth.

While the standard addition method was shown to provide data with less error, there is still some variability in the method. To decrease variability, data with r^2 values less than 0.9 were not considered linear and were rejected. Data points were sometimes removed with a minimum of three points per reported standard addition graph (Appendix B, plot B2). In order to decrease variability, in future analyses using the pyrogallol oxidation method the temperature should be controlled. Also, continuous stirring, which was not done here, during recording of the absorbance at 320 nm would ensure oxygen saturation. This has been shown to be critical (48), since a decrease in the oxygen level lowers the rate of pyrogallol oxidation. Thus, maintaining constant oxygen saturation would decrease variability.

Use of the standard addition method requires that a blank without the analyte be prepared. Here the blanks contained buffer and pyrogallol only. Thus, the implicit assumption is that Hb and RBC components present in the samples did not interfere with the pyrogallol autoxidation. This assumption needs to be further investigated. For example, we have previously reported that Hb can catalyze pyrogallol autoxidation (11), whereas GSH should compete with pyrogallol for superoxide. To establish the effects of RBC components on the SOD assay, Hb free of CuZnSOD and GSH should be prepared and its ability to catalyze pyrogallol autoxidation analyzed in detail. The reactive free thiols of Hb (Cysβ93, see Chapter 1) should be modified with a thiol-specific reagent to prevent interference. Such studies will reveal if it is necessary to use a blank containing Hb and/or GSH, and if thiol modification is required. Repeat analyses should then be performed in order to confirm the results reported here and the results corroborated by ICP-MS where possible.

In summary, CuZnSOD levels in newborn RBC lysates were found to be higher than in an adult RBC lysate. In addition, higher levels of CuZnSOD were correlated to higher levels of Hb-SNO in the RBC lysate of a preterm newborn 3.5 days following birth *vs* the RBC lysate of a preterm newborn at birth. This correlation is consistent with a role for CuZnSOD in Hb-SNO formation. It will be interesting to compare concentrations of CuZnSOD in a large number of newborn *vs* adult RBC lysates to establish if CuZnSOD does play a role in Hb-SNO formation.

3.0 DETERMINATION OF HEMOGLOBIN S-NITROSATION BY THE SAVILLE ASSAY

3.1 INTRODUCTION

3.1.1 Levels of Hb-SNO in adult and newborn RBC lysates

As stated previously (Section 1.3) there is much controversy in the literature as to the Hb-SNO levels found *in vivo*. Measured values in adult RBC lysates reported from two research groups, who have been studying the S-nitrosation of Hb extensively, were collected and normalized to molar concentrations of Hb-SNO per 5 mM Hb (Table 3.1). Values determined by different means by the two groups were in the same range initially (300 to 500 nM Hb-SNO per 5 mM Hb) (6,17). However, Gladwin and coworkers went on to show that their values were erroneous due to nitrites, which were also present (15). Following nitrite subtraction, their corrected Hb-SNO values are in the range of 20-35 nM Hb-SNO per 5 mM Hb. These SNO concentrations are assumed by this group to be too low to support NO conservation *in vivo* (20).

Hb-SNO values in newborn RBC lysates were also normalized to 5 mM Hb (Table 3.2). Values in either newborn or adult RBC lysates reported by Funai *et al.* (36) are more than 100-fold higher than those reported by most groups and in the same range as those reported by James and coworkers for adult lysates (57). Funai *et al.* are also the only group that used the Saville assay to measure Hb-SNO levels. Values measured by our collaborators Bard *et al.* (~40 nM Hb-SNO per 5 mM Hb) for term newborns (42) are in the same range as the adult values corrected for nitrite reported by Gladwin and coworkers (15). Interestingly, Hb-SNO values were shown to be lower in preterm than in term newborns (~25 nM *vs* 40 nM Hb-SNO per 5 mM Hb) (42).

Table 3.1 **Literature levels of HbA-SNO in adult RBC lysates**

Blood	Hb-SNO [a]	[Hb-SNO] / 5 mM Hb [b]	Analysis method [c]	Year / Ref.
Arterial	16 ± 4 µmol / mol heme	320 ± 80 nM	CN^-,EDTA / G25 / I_3^- / chemilum [d]	2000 / (6)
Veinous	14 ± 3 µmol / mol heme	280 ± 60 nM		
Veinous [e]	0.00125 mol / mol Hb	6.25 µM	ultrafiltration / G25 / photolysis / chemilum [e,f]	2002 / (17)
Veinous [f]	0.0001 mol / mol Hb	~ 0.5 µM		
Arterial	0.00046 ± 0.0001 / [Hb] (mol %)	23 ± 9 nM	CN^-,DTPA,NEM,P-40 / G25 / ± $HgCl_2$ / sulfanilamide / I_3^- / chemilum [g]	2002 / (15)
Veinous	0.00069 ± 0.00011 / [Hb] (mol %)	35 ± 6 nM		
Veinous	2.93 ± 0.89 mmol / mol Hb	14.7 ± 4.5 µM	CN^- / EDTA G25 I_3^- / NO meter [h]	2004 / (57)
Arterial	5.85 ± 1.09 mmol / mol Hb	29.3 ± 5.5 µM		

[a] Hb-SNO concentrations in the units reported in the literature.

[b] Hb-SNO values normalized to 5 mM Hb tetramer (*i.e.*, 20 mM heme).

[c] Method of analysis used for Hb-SNO determination.

[d] Hb-SNO levels measured by ozone chemiluminescence (Section 3.1.3) following incubation of the RBC lysates with CN^- and EDTA, G25 gel filtration and treatment with I_3^-.

[e] Hb-SNO levels measured by ozone chemiluminescence following ultrafiltration of the RBC lysates, G25 gel filtration and photolysis with a 200-W mercury-vapor lamp (58). Prior to lysis, the veinous blood was exposed to room air (pO_2 68 mm Hg).

[f] Hb-SNO levels measured as in footnote e but the veinous blood was exposed to normoxic conditions (pO_2 37 mm Hg).

[g] Hb-SNO levels measured by ozone chemiluminescence after incubation of RBC lysates with CN^-, NEM, DTPA and Nonidet P-40, followed by G25 gel filtration, incubation in $HgCl_2$ (where applicable) and sulfanilamide, and treatment with I_3^-.

[h] Hb-SNO levels determined by measuring released NO with an NO meter, following incubation of RBC lysates with CN^- and EDTA, G25 gel filtration and treatment with I_3^-. Blood was obtained from patients with congestive heart failure.

The Saville assay has been used to measure physiological levels of Hb-SNO and NO-derived species (NO_2^-, NO_3^-) (36). In the present study, the Saville assay was employed to determine the extent of S-nitrosation of HbF and HbA by S-nitrosoglutathione (GSNO) *in vitro* to compare the reactivities of HbF *vs* HbA toward S-nitrosation. In addition, a series of experiments were performed to evaluate the effects of Hb, CuZnSOD and GSH on the Saville assay to establish the reliability of Hb-SNO determination. Results from this investigation shed light on the variability of the reported Hb-SNO levels, as well as the effectiveness of various methods used (Tables 3.1 and 3.2), which in some cases utilize a number of reagents in common with the Saville assay.

Table 3.2 **Literature levels of Hb-SNO in newborn RBC lysates**

Blood	Hb-SNO [a]	[Hb-SNO] / 5 mM Hb [b]	Analysis method [c]	Year / Ref.
umbilical vein [d]	2.19 ± 1.22 mmol / mol Hb	10.95 ± 6.10 μM	Saville assay [f]	1997 / (36)
umbilical artery [d]	1.45 ± 0.66 mmol / mol Hb	7.25 ± 3.30 μM		
umbilical vein [d]	8 μmol / mol Hb	40 nM	CN^-,EDTA / G25 / I_3^- / chemilum [g]	2004 / (42)
umbilical vein [e]	5 μmol / mol Hb	25 nM		

[a] Hb-SNO concentrations in the units reported in the literature.

[b] Hb-SNO values normalized to 5 mM Hb tetramer.

[c] Method of analysis used for Hb-SNO determination.

[d] Blood from the umbilical vein and artery of a term newborn collected at Ste-Justine Hospital.

[e] Blood from the umbilical vein of a pre-term newborn collected at Ste-Justine Hospital.

[f] Hb-SNO levels measured in RBC supernatants by the Saville assay as described in Section 3.1.2, with the exception that following $HgCl_2$ addition, Hb was purified by centrifugation and ultrafiltration and treated to cadmium mesh to reduce any oxidized NO_2^-.

[g] see footnote d, Table 3.1.

3.1.2 Saville assay

S-nitroso derivatives of thiols, such as cysteine, can be measured by means of the Saville assay. S-Nitrosothiols (RSNOs) undergo hydrolysis to yield nitrous acid in the presence of mercuric salts. *In vitro*, RSNOs are frequently prepared using acidified sodium nitrite as a nitrosating agent. Following thiol S-nitrosation, ammonium sulfamate is added to eliminate nitrite (NO_2^-) from the sample. Addition of a solution containing both mercuric chloride ($HgCl_2$) and sulfanilamide ($XArNH_2$) to a RSNO liberates nitrogen in the form of nitrous acid, which is converted to a diazonium ion. The presence of $XArNH_2$ provides an aromatic amine, which competes favourably with sulfamate ($NH_2SO_3^-$) for the nitrous acid equivalent to the RSNO initially present.

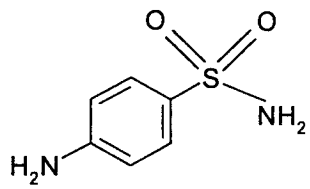

sulfanilamide
($XArNH_2$)

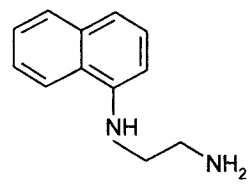

N-(1-naphtyl-) ethylenediamine
(NED)

Figure 3.1 **Griess reagents**

For colorimetric analysis, an amine such as NED is added to convert the diazonium ion into an azo dye, which can be monitored spectrophotometrically at 540 nm. The key reactions in the Saville assay are summarized as follows:

$$RSNO + H_2O + Hg^{2+} \longrightarrow HONO + RSHg^+ + H^+ \qquad 3.1$$

$$HONO + XArNH_2 + H^+ \longrightarrow XArN{\equiv}N^+ + 2H_2O \qquad (X{=}SO_2NH_2) \qquad 3.2$$

$$XArN{\equiv}N^+ + NED \longrightarrow ArN{=}N{-}NED \qquad 3.3$$

$XArNH_2$ and NED (Figure 3.1) are known as the Griess reagents for the colorimetric determination of RSNOs. Omission of $XArNH_2$ from the $HgCl_2$ solution results in the rapid conversion of the released nitrous acid to nitrogen gas by sulfamate as follows (59,60):

$$HONO + NH_2SO_3^- \longrightarrow HSO_4^- + N_2 + H_2O \qquad 3.4$$

3.1.3 Determination of RSNO and NO by ozone chemiluminescence

Among the most widely used methods for the detection of NO are ozone chemiluminescence (6,15,17,42) and potentiometry with an NO-selective electrode (57). In ozone chemiluminescence, NO is oxidized to NO_2 on reaction with excess O_3. The electronically excited NO_2 emits light, which is captured by a chemiluminescence detector. Various chemical methods are used for the treatment of RBC samples and the release of NO from Hb-SNO.

In the Hb-SNO determinations initially reported by Gladwin *et al.* (6), RBC lysates in PBS solution were pretreated with excess KCN and $K_3Fe(CN)_6$, which converted the NO present as $HbFe^{II}NO$ to a species not detectable by chemiluminescence while preserving Hb-SNO. Samples were then passed through a G25 gel filtration column (fractionation range of 0.1 to 5 kD) for removal of low-molecular weight species including nitrites, small RSNOs, KCN and $K_3Fe(CN)_6$. Release of NO from Hb-SNO was achieved by reaction with I_3 in glacial acetic acid, followed by chemiluminescence detection (6). James and coworkers (57) employed a similar sample preparation method, but used an electrode for NO detection following its release from Hb-SNO.

In the methodology currently used by Gladwin *et al.* (15), RBCs are lysed in PBS containing 1% Nonidet P-40, 4 mM KCN, 4 mM $K_3Fe(CN)_6$, 10 mM NEM and 100

μM DTPA; Nonidet P-40 is used to solubilize the membrane, which is thought to contain S-nitrosated anion exchange protein 1, NEM is used to block any free thiols and DTPA to chelate free copper. Samples are then passed through a G25 column and reacted, with or without, 5 mM $HgCl_2$ and 5% $XArNH_2$ in 1 N HCl prior to reaction with I_3, and subsequent chemiluminescent detection. $HgCl_2$ is used for NO release from Hb-SNO, which in the presence of acidified $XArNH_2$ forms a diazonium ion (reactions 3.1 and 3.2). It was shown that the diazonium ion does not produce a signal in I_3^--based ozone chemiluminescence. Hb-SNO values corrected for background NO_2^- are obtained by subtraction of the NO values measured in the absence of $HgCl_2$ from the values in the presence of $HgCl_2$. The Hb-SNO values thus obtained are comparable to levels measured by the Saville assay corrected for background nitrites (15).

Stamler *et al.* (17) also use ozone chemiluminescence for Hb-SNO detection. Their method of preparation involves RBC lysis in aqueous 0.5 mM EDTA, G25 gel filtration followed by NO release by photolysis and measurement by ozone chemiluminescence. Samples photolyzed with or without $HgCl_2$ were analyzed to determine $HbFe^{II}NO$ only and $HbFe^{II}NO$ plus Hb-SNO levels, respectively (58). Specificity for their method was verified with the analysis of samples from mice deficient in SNO-metabolizing activity and from yeast deficient in enzymes that control levels of FeNO and SNO, respectively. Hb-SNO values thus obtained are shown to be comparable to those measured by 4,5-diaminofluorescein (DAF-2) fluorescence. In this assay, the RBC lysate is incubated in PBS containing DAF-2 with and without $HgCl_2$. Hb is removed by ultrafiltration and the filtrate is treated with 0.4 N HCl to generate S-

nitrosating equivalents and with excess NaOH to maximize fluorescence of S-nitrosated DAF-2 (λ_{ex} = 485 nm, λ_{em} = 520 nm) (17).

3.2 EXPERIMENTAL SECTION

3.2.1 Materials

Purified HbA and HbF from adult and newborn RBC lysates, respectively, prepared as described in Section 2.2.2.1, were provided by Ste-Justine Children's Hospital, Montreal. Lyophilized human HbA was purchased from Sigma. The method of preparation used by the supplier does not include any purification steps following washing, lysis of the RBCs and collection of the supernatant (Appendix A). Thus, Sigma HbA can be considered equivalent to lyophilized RBC supernatant (Section 2.2.1). Bovine CuZnSOD was purchased from Roche; pyrogallol, monobasic and dibasic sodium phosphate salts were purchased from Fisher; trace-metal grade HCl, ammonium sulfamate, $XArNH_2$, $HgCl_2$ and NED were purchased from Sigma; NAP-5 (0.5 mL; 0.9 x 2.8 cm) Sephadex G-25 columns were purchased from Amersham Pharmacia Biotech; sodium nitrite was purchased from Aldrich; sulfuric acid was purchased from Baker; GSNO was purchased from Cayman. Nanopure water (MilliQ; specific resistance of 18 mΩ-cm), from a Millipore Simplicity water purification system and treated with Chelex-100 (Sigma) to remove trace metal ions, was used to prepare all solutions.

3.2.2 Methods

3.2.2.1 Saville assay reagents

A 100 mM sodium nitrite standard stock solution was prepared in water and stored at 4°C for up to one month. $XArNH_2$ (0.22 M) and 10 mM ammonium sulfamate

were prepared in 0.4 N HCl and stored at 4°C for up to one month. $HgCl_2$ (46 mM) was prepared in water and stored at room temperature for up to one month. NED (5 mM) was prepared fresh in 0.4 N HCl on each occasion of analysis. A stock solution containing both 9 mM $HgCl_2$ and 180 mM $XArNH_2$ was prepared fresh from the stored stock solutions on each occasion.

3.2.2.2 NO_2^- calibration curve

Sodium nitrite stock calibration standards (10, 20, 40, 100, 200 and 400 μM) were prepared in water from the standard stock solution and stored at 4°C for up to one month. On each occasion of analysis, a calibration curve was generated by taking a 125 μL aliquot from each aqueous stock calibration standard, and adding 375 μL of 0.4 N HCl followed by 500 μL of 180 mM $XArNH_2$ in 0.4 N HCl and 500 μL of 5 mM NED in 0.4 N HCl. The final reagent concentrations were 0.8 to 33 μM NO_2^-, 60 mM $XArNH_2$, 3 mM $HgCl_2$ and 2 mM NED in 0.4 N HCl. The standards were incubated at room temperature for 30 min and the absorbance read at 540 nm.

3.2.2.3 Sample analysis

HbF, HbA and Sigma HbA were analyzed following S-nitrosation of Hb with GSNO. S-nitrosation was achieved by incubating Hb diluted to 300 μM Hb with a 10-fold molar excess of GSNO to Hb in 200 mM sodium phosphate buffer, pH 7.2 (Na*Pi*) for 30 min at room temperature in the dark. Following S-nitrosation, samples were passed through a NAP-5 G25 column to remove excess GSNO and GSH, and the Hb was eluted with Na*Pi*.

A 250 μL aliquot of the G25 eluate from each sample was transferred to a 1.5 mL Eppendorf tube, to which 250 μL of ammonium sulfamate was added, followed by

500 μL of $XArNH_2$ and 500 μL of NED. A second 250 μL aliquot of the eluate was taken from each sample, to which the same reagents plus $HgCl_2$ were added. The samples were incubated at room temperature for 30 min and the absorbance at 540 nm read. The final concentrations in the incubates were 15-22 μM Hb tetramer, 1.5 mM $NH_2SO_3^-$, 60 mM $XArNH_2$, 3 mM $HgCl_2$ and 2 mM NED. The extent of S-nitrosation was determined by measuring the amount of NO_2^- released by the Saville assay. The values of NO_2^- measured without $HgCl_2$ (background nitrites) were subtracted from the values of NO_2^- measured with $HgCl_2$ (background nitrites + RSNOs). All values obtained were read against a calibration curve in 0.8 to 17 μM NO_2^-.

Mass spectral analysis was performed on an HbF sample incubated with GSNO. The protein was diluted into acetonitrile:water (50:50 v/v)/0.2% formic acid and directly infused into the ESI source of a Waters Micromass Q-TOF2 mass spectrometer by flow injection at 50 μL/min. The instrument parameters are given in the figure captions.

3.3 RESULTS

3.3.1 NO_2^- calibration curve

The NO_2^- calibration curve was shown to be linear in the assayed range (0.8 to 33 μM) and a linearity coefficient greater than 0.99 was obtained on every occasion of analysis (Figure 3.2). As all NO_2^- was free in solution, $HgCl_2$ was not added to the standards. However, since $HgCl_2$ was used in the sample analysis, as well as in most of the other methods used for Hb-SNO quantitation, its effects on the NO_2^- calibration curve were examined by addition of $HgCl_2$ to the $XArNH_2$ solution. At a final concentration of 3 mM, $HgCl_2$ had little effect on the calibration curve except that in the samples containing 33 μM NO_2^- precipitation occurred 40 min after the addition of NED (Figure

3.3). Thus, the Saville assay may not yield reliable results for RSNO concentrations above 15 μM due to precipitation.

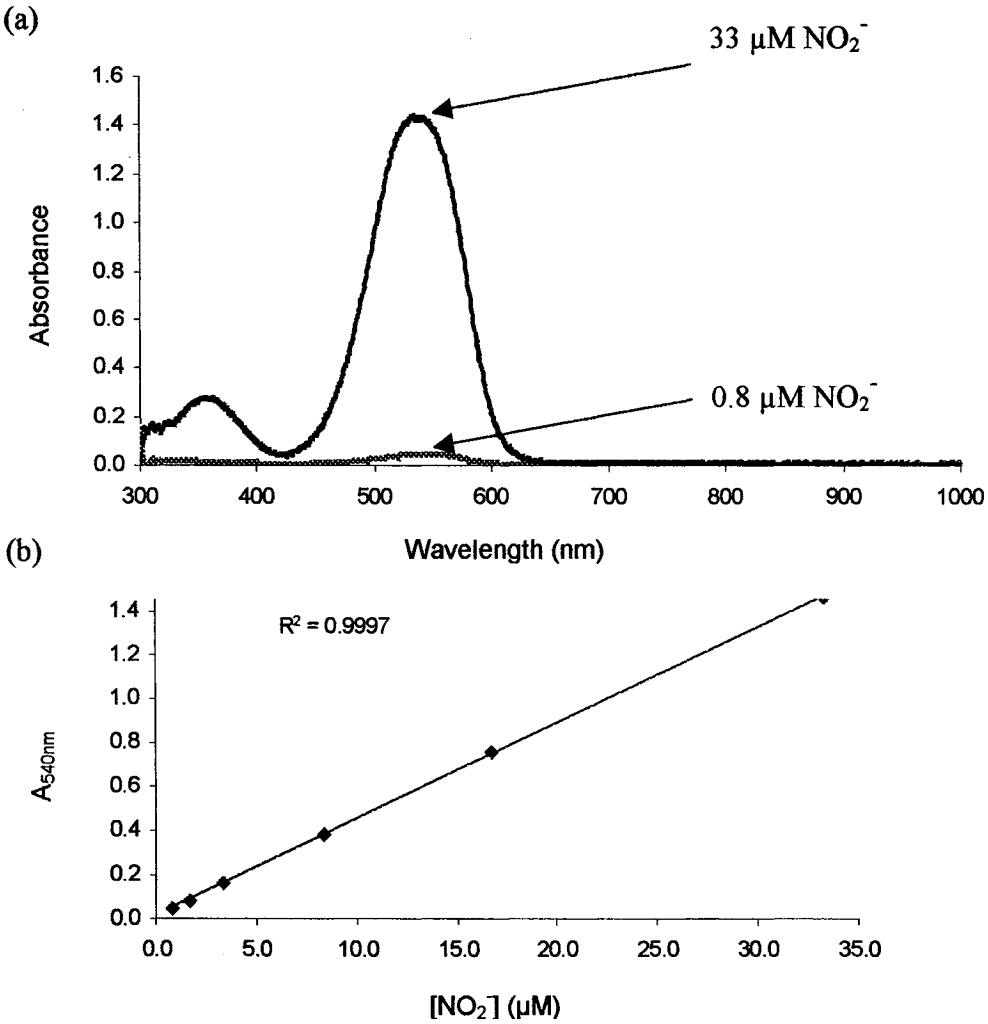

Figure 3.2 **Absorption spectrum of NO_2^- standards from Saville assay and NO_2^- calibration curve.** (a) Spectra of 0.8 μM and 33 μM NO_2^- calibration standards. (b) Calibration curve from 0.3 to 33 μM NO_2^-. Absorbances were recorded in 1.5-mL cuvettes with a 1-cm pathlength at 25°C following 10 min incubation after addition of 60 mM $XArNH_2$ and 2 mM NED in 0.4 N HCl.

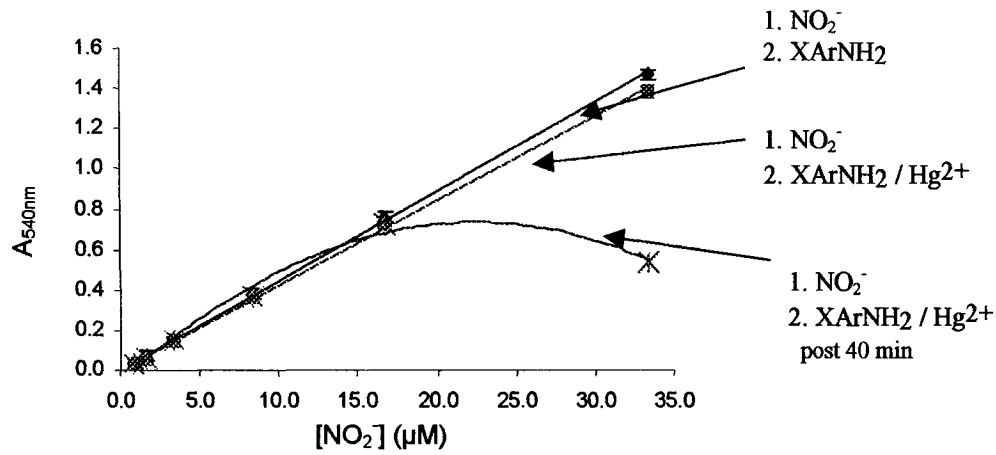

Figure 3.3 **Effects of $HgCl_2$ on NO_2^- calibration curve.** NO_2^- standards (0.8 to 33 μM) with 60 mM $XArNH_2$ only (◆); with 60 mM $XArNH_2$ + 3 mM $HgCl_2$ 10 min (■), and 40 min post immediate 2 mM NED addition (*). Absorbances at 540 nm were recorded in 1.5-mL cuvettes with a 1-cm pathlength at 25°C. Note that precipitation was observed in the sample containing 33 μM NO_2^- post 40 min but the sample was not filtered prior to reading A_{540nm}.

Table 3.3 **Percent Hb S-nitrosation in Hb samples**[a]

Sample	Hb (μM) [b]	NO_2^- (μM) [c]	% S-nitrosation of Cys93 [d]
HbF[a]	22	11	25
HbA[a]	15	7.5	25
Sigma Hb[a]	14.5	7.0	24

[a] Samples (15-22 μM Hb) were S-nitrosated by GSNO (GSNO:Hb = 10:1) and the SNO concentration determined by the Saville assay (Figure 3.4 c).

[b] Hb concentrations were determined spectrophotometrically with ε_{541nm} = 13.8 $mM^{-1}cm^{-1}$ per heme and ε_{577nm} = 14.6 $mM^{-1}cm^{-1}$ per heme for the Hb samples containing oxyHb (Figure 3.4 a), and with ε_{500nm} = 10 $mM^{-1}cm^{-1}$ per heme and ε_{630nm} = 4.4 $mM^{-1}cm^{-1}$ per heme for the Sigma metHbA sample (Figure 3.4 b).

[c] NO_2^- concentrations determined by the Saville assay.

[d] $[NO_2^-]$ / [Cys93] x 100, where [Cys93] = 2[Hb].

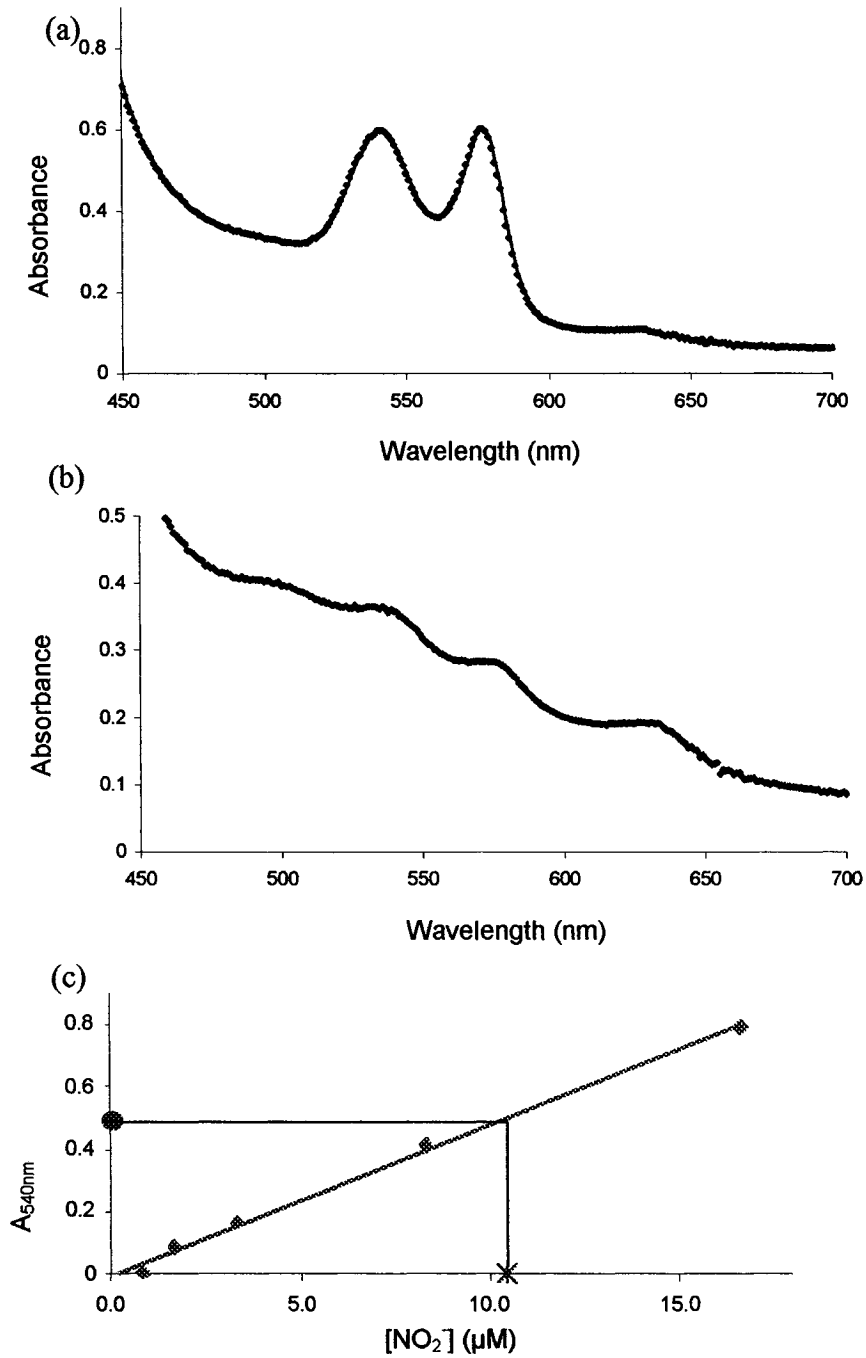

Figure 3.4 **Visible spectra and analysis of S-nitrosation of Hb samples.** Spectra of (a) newborn RBC lysate and (b) Sigma HbA containing 22 mM Hb in Na*Pi*. (c) Determination of SNO concentration in a newborn RBC lysate by the Saville assay. Spectra and single point absorbances at 540 nm were recorded in 1.5-mL quartz cuvettes with a 1-cm pathlength at 25°C.

3.3.2 Sample analysis

The visible absorption spectra of the HbF (Figure 3.4a) and HbA (data not shown) samples provided by Ste-Justine Hospital and of Sigma HbA (Figure 3.4b) reveal that Hb was mainly in the oxygenated form ($Fe^{II}O_2$) in the Ste-Justine samples, and in the met form (Fe^{III}) in the Sigma sample. OxyHb exhibits two bands at 540 and 576 nm, while metHb gives rise to bands at 500 and 630 nm (36). The variation in the state of the heme is presumably due to differences in sample preparation; Sigma HbA was likely oxidized to metHb during lyophilization.

Analysis of the RSNO concentration of HbF, HbA and Sigma HbA (Figure 3.4; Table 3.3) indicates that approximately 25% of the Cys93 residues were S-nitrosated. Only Cysβ93 has been shown to be reactive in HbA, the other Cys residues (Cysα104 and Cysβ112) being too buried for S-nitrosation to occur. S-nitrosation of the γ-chain of HbF has recently been shown by mass spectrometry (38), and Cys93 is the only Cys residue in the γ-chain. The extent of S-nitrosation measured in the samples (Table 3.3) suggests that oxyHbF has similar reactivity to GSNO as oxyHbA and metHbA under the conditions used here.

The mass spectrum of HbF contained free heme and α, γ_A and γ_G subunits (Figure 3.5). The γ subunits have either glycine (γ_G) or alanine (γ_A) at position 136 (50), and the β subunit has glycine at this position. It has been shown that HbF with a higher fraction of γ_G exhibits stronger surface hydrophobicity, is more soluble and less stable, but has the same oxygen affinity as HbF with higher fractions of γ_A (61). During fetal life, γ_G makes up 70% of the γ globins, while during the postconceptional-age switchover from HbF to HbA synthesis, γ_A and γ_G are expressed equally (50).

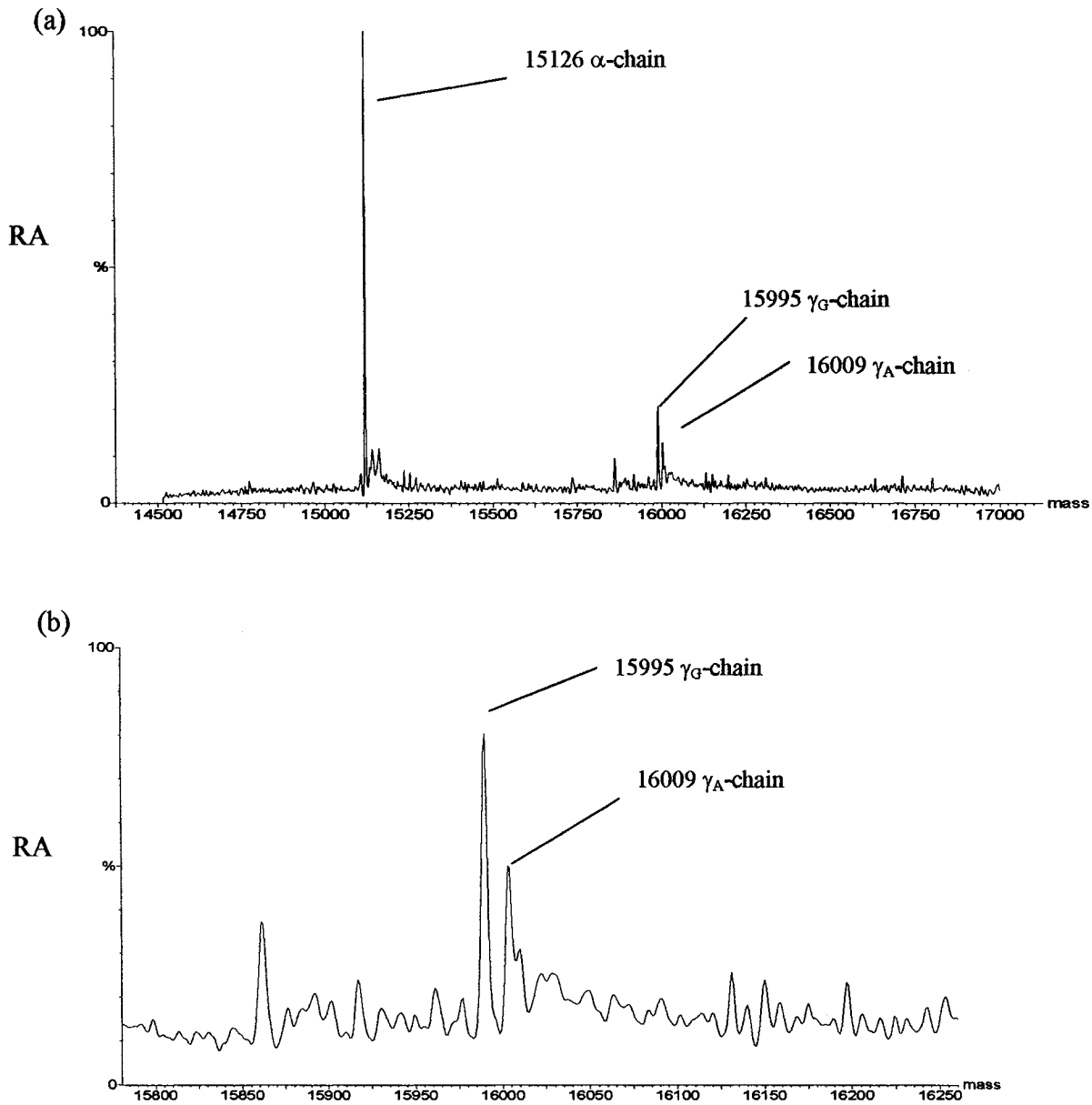

Figure 3.5 **Deconvolved electrospray mass spectrum of HbF.** A sample containing 300 μM G25-purified HbF tetramer in Na*Pi* was diluted 1000-fold into acetonitrile:water (50:50 v/v)/0.2% formic acid and infused into the ESI source of a Q-TOF2 mass spectrometer by flow injection at 50 μL/min. HbF dissociated into free heme and α, γ_A and γ_γ subunits under the MS conditions. (a) Spectrum of both subunits. (b) Spectrum of the γ-chains only. The observed masses of the subunits are given in the figures and RA is the relative abundance of the observed ions.

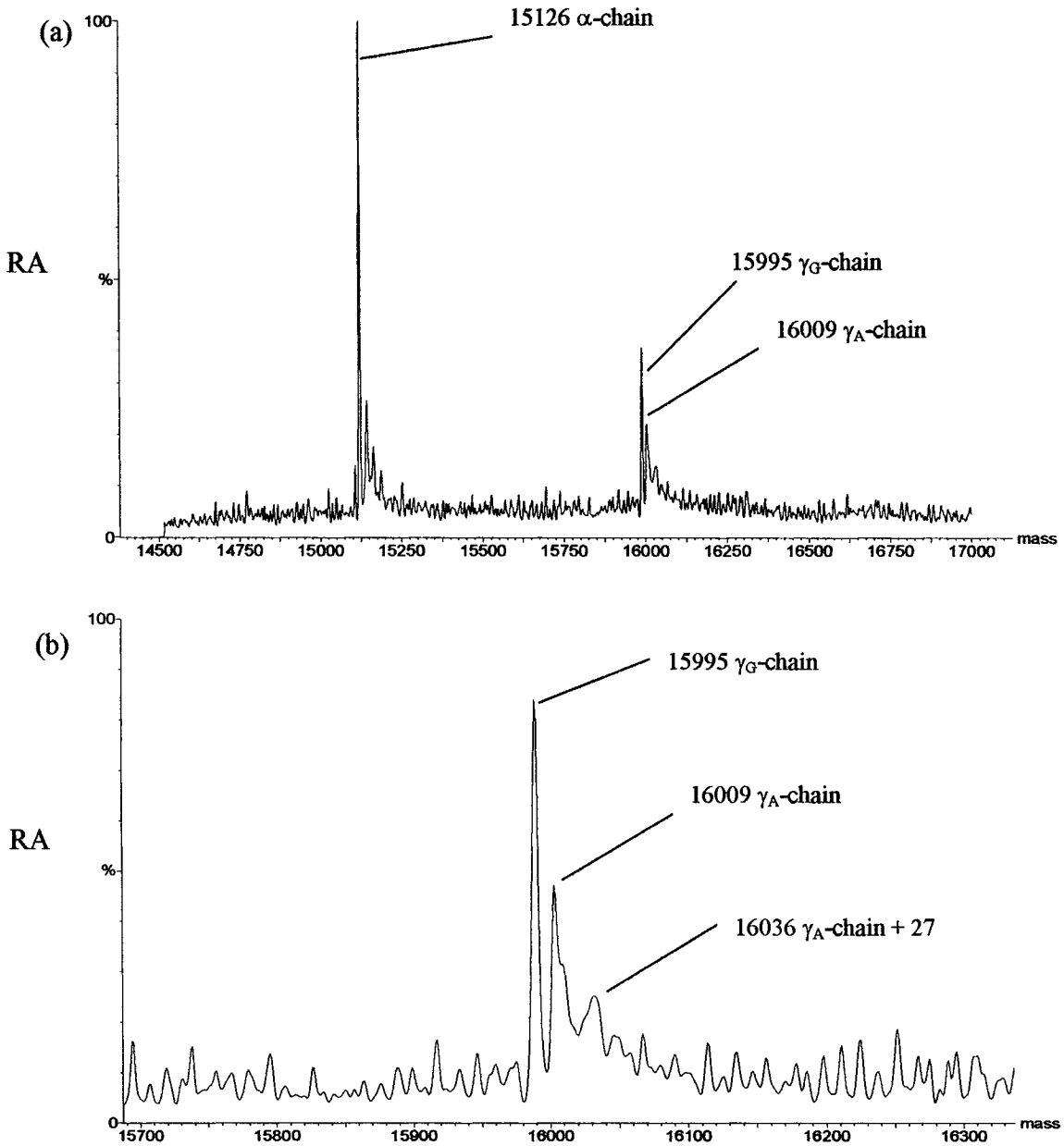

Figure 3.6 **Deconvolved electrospray mass spectrum of S-nitrosated HbF.** A sample containing 300 μM HbF tetramer in Na*Pi* was S-nitrosated by 30 min incubation with 3 mM GSNO in Na*Pi* at 25°C. See legend of Figure 3.5 for the experimental conditions. (a) Spectrum of both subunits. (b) Spectrum of the γ-chain region only. The weak peak at M + 27 in (b) may correspond to the γ_A-chain modified with NO, but this needs to be confirmed.

The deconvolved ESI mass spectrum of the HbF sample incubated with GSNO revealed a peak with a mass corresponding to the γ_A-subunit+27, which is likely due to S-nitrosation of the γ_A-chain (Figure 3.6b). Since no corresponding peak was observed for the other chains, the γ_A-chain may be preferentially S-nitrosated by GSNO. However, given the lability of RSNO groups in the mass spectrometer, further investigation is necessary to determine the site(s) of S-nitrosation of HbF.

3.3.3 Effects of metHb on the Saville assay

Since Hb absorbs at the working wavelength of 540 nm, its effects on the Saville assay were examined by adding a fixed amount (~ 3 μM) of metHb with A_{540} ~ 0.2 to the NO_2^- calibration standards. It was possible to cancel the metHb absorbance by reading the standards against a metHbA blank in 0.4 N HCl (Figure 3.7a), which indicates that there are no saturation or interference effects due to the absorption of metHb. However, a comparison of NO_2^- calibration curves obtained with and without ~3 μM metHbA reveals loss of free NO_2^- when the heme protein is present. Furthermore, addition of 13 μM metHb results in greater loss of NO_2^- (Figure 3.7b).

Since addition of an equal volume of NO_2^- in 0.4 N HCl to metHb in 100 mM Na*Pi* should result in a solution with a pH ~ 0.9 (Table 3.4), Cysβ93 and possibly other thiols (Cysα104, Cysβ112) in Hb were likely S-nitrosated (Section 3.3.3) thereby decreasing the available NO_2^-. Therefore, it was considered worthwhile to investigate NO_2^- quantitation in the presence of metHb and the effects, if any, of adding the Saville reagents in different sequences.

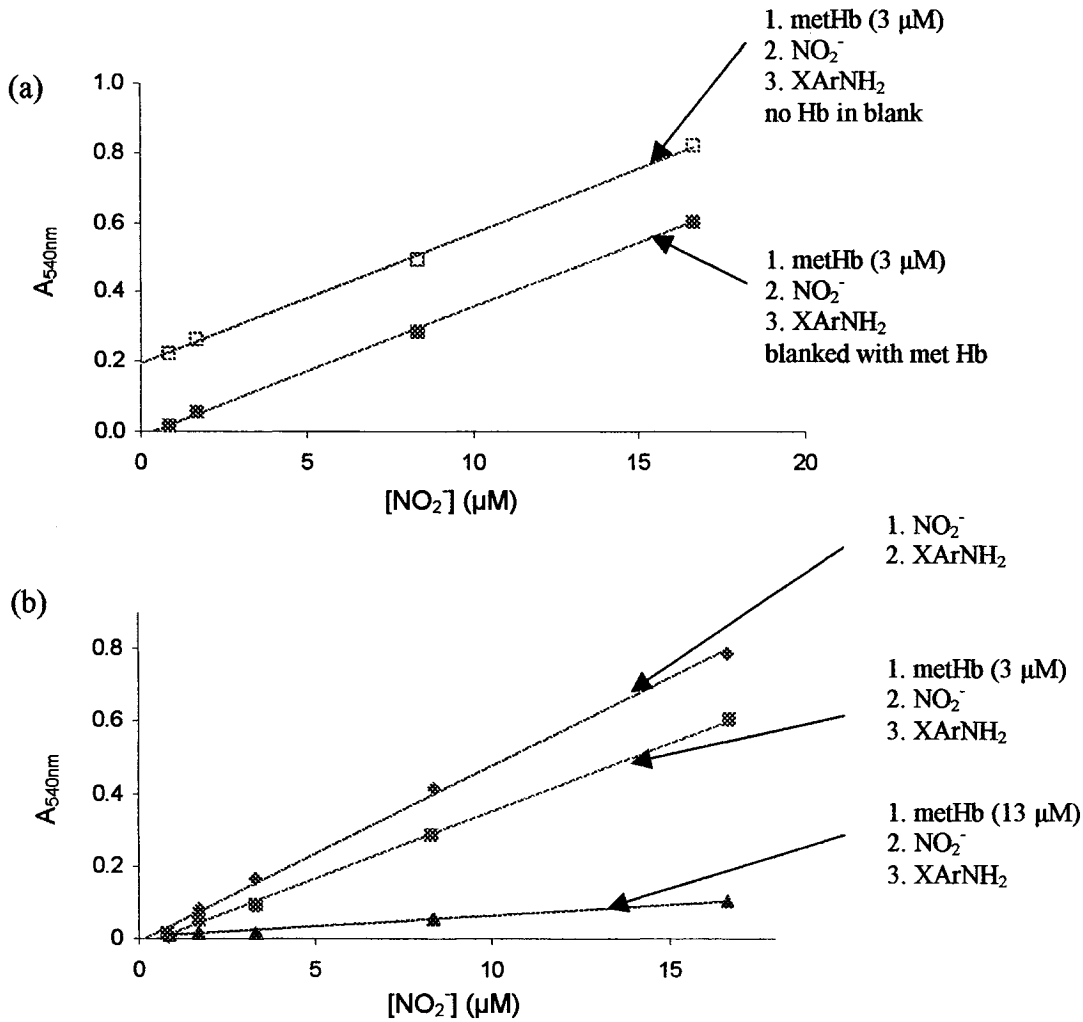

Figure 3.7 **Effects of metHb on the NO_2^- calibration curve.** (a) 3 μM metHb + 0.8-17 μM NO_2^- standard in 0.4 N HCl; top curve: no Hb in blank (□); bottom curve: blanked with metHb (■). (b) Top curve: 0.8-17 μM NO_2^- standard in 0.4 N HCl (◆); middle curve: 3 μM metHb + 0.8-17 μM NO_2^- standard in 0.4 N HCl (■); bottom curve: 3 μM metHb + 0.8-17 μM NO_2^- standard in 0.4 N HCl (▲). NED (2 mM) in 0.4 N HCl was immediately added to each sample, and absorbances at 540 nm were recorded in 1.5-mL cuvettes with a 1-cm pathlength at 25°C following 10 min incubation. The order of addition of the reagents is indicated on the graphs.

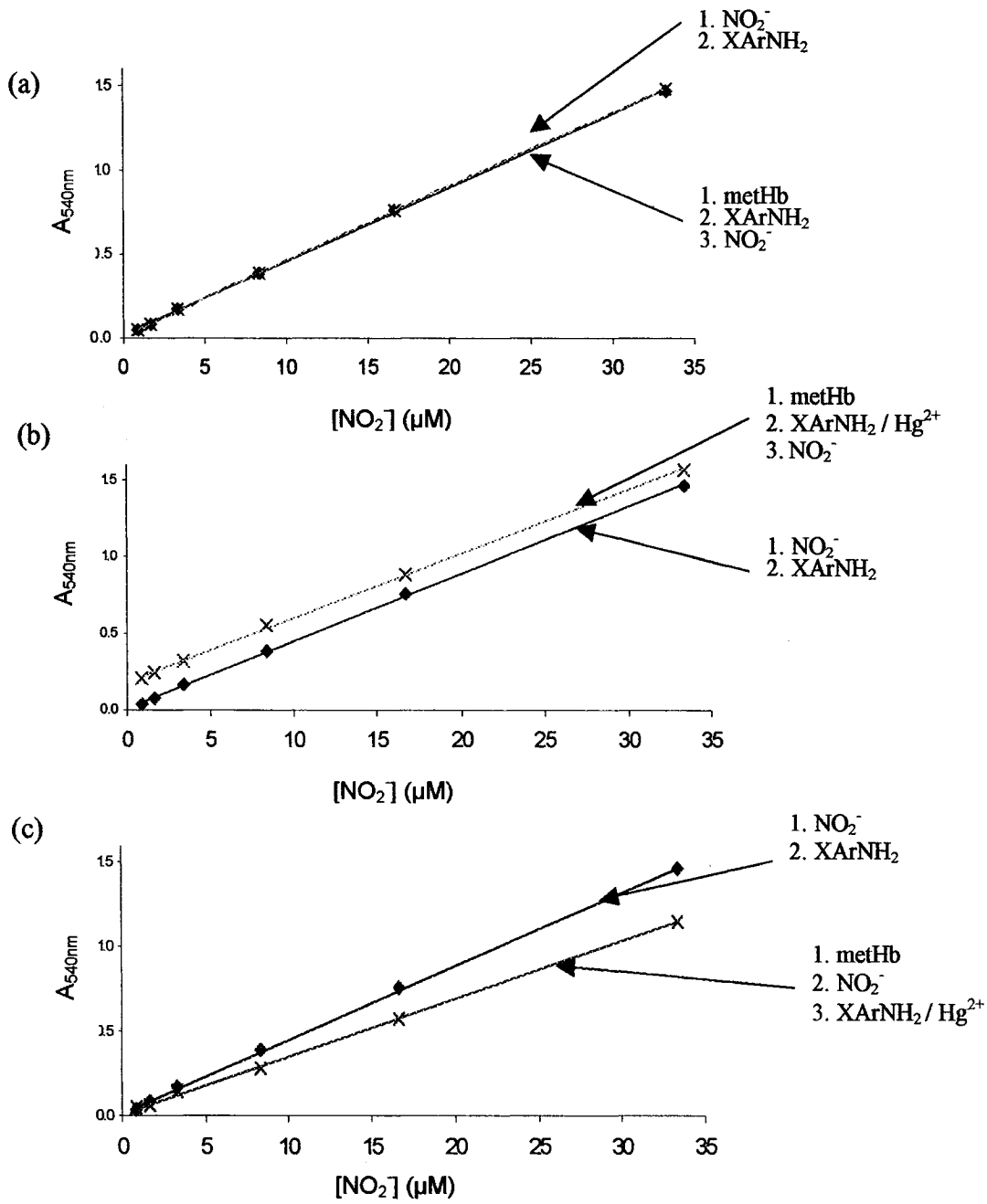

Figure 3.8 **Effects of sequence of addition of metHb, $XArNH_2$ and $HgCl_2$ on NO_2^- determination.** (a-c) 0.8-33 μM NO_2^- standard containing 60 mM $XArNH_2$ in 0.4 N HCl (◆). (a) 0.8-33 μM NO_2^- standard was added to 12 μM metHb + 60 mM $XArNH_2$ (×). (b) 0.8-33 μM NO_2^- standard was added to 12 μM metHb + 60 mM $XArNH_2$ + 3 mM $HgCl_2$ (×). (c) 60 mM $XArNH_2$ + 3 mM $HgCl_2$ was added to 12 μM metHb + 0.8-33 μM NO_2^- standard (×). Samples were blanked with a solution containing all of the reagents except NO_2^- and $HgCl_2$. NED (2 mM) in 0.4 N HCl was immediately added to each sample, and absorbances at 540 nm were recorded in 1.5-mL cuvettes with a 1-cm pathlength at 25°C following 10 min incubation. The order of addition of the reagents is indicated on the graphs.

3.3.4 Effects of order of addition of metHb, $XArNH_2$ and $HgCl_2$ on NO_2^- determination

The conversion of free NO_2^- to N_2 gas (reaction 3.4) is prevented by adding $XArNH_2$ and $HgCl_2$ to the RSNO samples at the same time as $NH_2SO_3^-$. This is because $XArNH_2$ reacts faster with NO_2^- than $NH_2SO_3^-$ (59). Therefore, it was questioned whether $XArNH_2$ would rescue the NO_2^- lost in the presence of metHb only (Figure 3.7b). As illustrated in Figure 3.8a, there was no loss of the NO_2^- standards when added to a 13 μM metHb + 60 mM $XArNH_2$ solution, indicating that $XArNH_2$ at 5,000-fold molar excess over Hb, effectively reacts with all the free NO_2^- present in the samples, leaving no NO_2^- available to react with metHb.

Addition of 3 mM $HgCl_2$ resulted in increased absorbance of the standards but no change in slope (Figure 3.8b). The absorbances plotted in Figure 3.8a were read against a blank containing metHb only; thus, the increased absorbance at 520 nm in all the samples in Figure 3.8b must be due to the presence of $HgCl_2$. However, blanking the sample against metHb + $HgCl_2$, resulted in a plot with negative values in the lower NO_2^- concentration range (data not shown).

Addition of a 3 mM $HgCl_2$ + 60 mM $XArNH_2$ solution to 11 μM metHb + NO_2^- solutions resulted in NO_2^- underdetermination (Figure 3.8c) albeit to a lesser extent than addition of $XArNH_2$ alone to 13 μM metHb + NO_2^- (Figure 3.7b). Thus, $HgCl_2$ may rescue some but not all NO_2^- from metHb, which can also bind NO_2^- at the heme (62), reduce nitrite to NO (12) and become nitrosated on its free lysine residues. These possibilities need to be investigated further under the conditions of the Saville assay.

Table 3.4 **pH values of reagent mixtures used**

Reagents [a] (v:v) [b]	pH
200 mM Na*Pi*	7.27
100 mM Na*Pi* + 0.4 N HCl (1:1)	0.92
50 mM Na*Pi* + 100 mM $XArNH_2$ [c] (1:1)	1.47
33 mM Na*Pi* + 60 mM $XArNH_2$ [c] + 0.4 N HCl + 2 mM NED[c] (1:2:1:2)	0.68
33 mM Na*Pi* + 60 mM $XArNH_2$/3 mM $HgCl_2$ [c,d] + 0.4 N HCl + 2 mM NED[c] (1:2:1:2)	0.66
12 μM metHb[f] + 60 mM $XarNH_2$ [c] + 0.4 N HCl + 2 mM NED[c] (1:2:1:2)	0.52
12 μM metHb[f] + 60 mM $XArNH_2$/3 mM $HgCl_2$ [c,d] + 0.4 N HCl + 2 mM NED [c] (1:2:1:2)	0.79
0.4 N HCl + 60 mM $XArNH_2$/3 mM $HgCl_2$ [c,d] + 2 mM NED [c] (1:1:1)	0.68

[a] Final concentrations in mixtures.

[b] Ratio of volumes added.

[c] Reagents in 0.4N HCl.

[d] Mixture of 60 mM $XarNH_2$ and 3 mM $HgCl_2$.

[f] In 200 mM Na*Pi*, pH 7.2.

From the experiments shown in Figure 3.8, we can see that addition of NO_2^- to metHb + $XArNH_2$ gives rise to accurate NO_2^- determination (Figure 3.8a), but addition of $XArNH_2/HgCl_2$ to metHb + NO_2^- results in underestimation of NO_2^- by ~ 25% (Figure 3.8c). Furthermore, Figure 3.8b reveals that all NO_2^- values will be overestimated by ~ 3.4 μM when NO_2^- is added to a solution of metHb + $XArNH_2/HgCl_2$ if the blank is missing $HgCl_2$. When $HgCl_2$ is added to the blank, the slope remains the same but NO_2^- is underestimated (data not shown).

3.3.5 Effects of metHb on the competition between $XArNH_2$ and $NH_2SO_3^-$ for NO_2^-

In the Saville method, $NH_2SO_3^-$ is added to remove contaminating NO_2^- before RSNO decomposition with $HgCl_2$. Competition between $XArNH_2$ and $NH_2SO_3^-$ for NO_2^- was examined first in the absence of metHb.

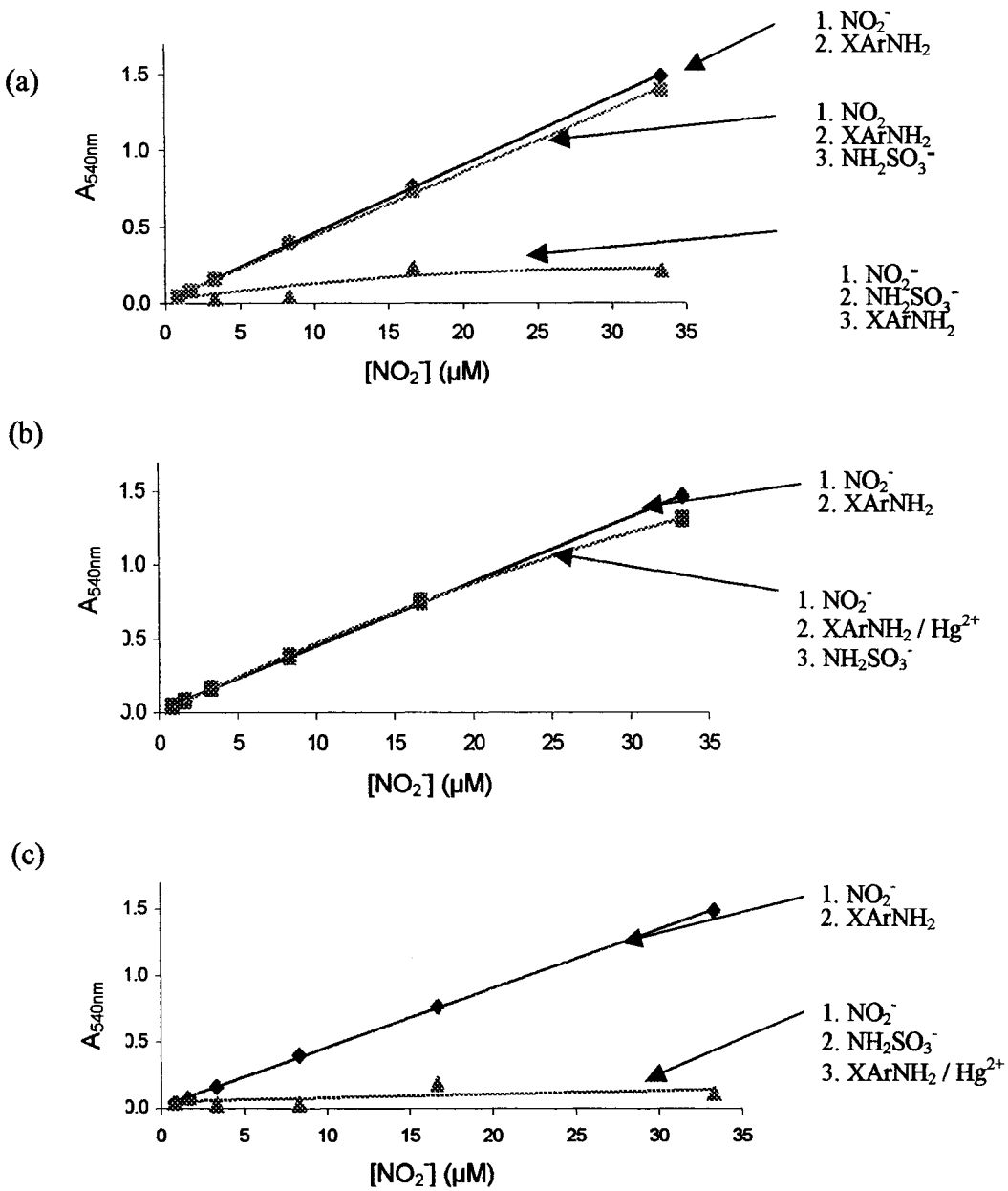

Figure 3.9 **Competition between $NH_2SO_3^-$ and $XArNH_2$ for NO_2^-.** (a-c) 0.8-33 μM NO_2^- standard containing 60 mM $XArNH_2$ in 0.4 N HCl (♦). (a) Top curve: 1.5 mM $NH_2SO_3^-$ was added to 60 mM $XArNH_2$ + 0.8-33 μM NO_2^- standard in 0.4 N HCl (■); bottom curve: 60 mM $XArNH_2$ was added to 1.5 mM $NH_2SO_3^-$ + 0.8-33 μM NO_2^- standard in 0.4 N HCl (▲). (b) 1.5 mM $NH_2SO_3^-$ was added to 60 mM $XArNH_2$ + 3 mM $HgCl_2$ + 0.8-3.3 μM NO_2^- standard in 0.4 N HCl (■). (c) 60 mM $XArNH_2$ + 3 mM $HgCl_2$ was added to 3 mM $NH_2SO_3^-$ + 0.8-33 μM NO_2^- standard in 0.4 N HCl (▲). NED (2 mM) in 0.4 N HCl was immediately added to each sample and absorbances at 540 nm were recorded in 1.5-mL cuvettes with a 1-cm pathlength at 25°C following 10 min incubation. The order of addition of the reagents is indicated on the graphs.

Addition of 1.5 mM $NH_2SO_3^-$ to NO_2^- + 60 mM $XArNH_2$ resulted in ~ 5% underestimation of the 16 and 33 μM NO_2^- standards (Figure 3.9a). $HgCl_2$ does not alter the competition for NO_2^- between $XArNH_2$ and $NH_2SO_3^-$ (Figure 3.9a *vs* b), but precipitation was observed at longer times (40 min) in the 33 μM NO_2^- standard (data not shown) as seen previously in the presence of $HgCl_2$ (Figure 3.3). These results demonstrate that $XArNH_2$ reacts rapidly with NO_2^-. Hence, $NH_2SO_3^-$ added to remove contaminating NO_2^- will interfere negligibly with the determination of NO_2^- generated *in situ* from RSNO by $HgCl_2$ in the presence of $XArNH_2$ as described by Saville (59). However, addition of 60 mM $XArNH_2$ to 1.5 mM $NH_2SO_3^-$ + NO_2^- reveals that $NH_2SO_3^-$ does not stoichiometrically remove NO_2^- (Figures 3.9a,c). This is especially apparent at 16 and 33 μM NO_2^-, but even with the less concentrated NO_2^- standards, absorbance at 540 nm is detected on $XArNH_2$ addition to $NH_2SO_3^-$ + NO_2^-.

The competition for NO_2^- between $NH_2SO_3^-$ and $XArNH_2$ was repeated in the presence of 12 μM metHb. Addition of NO_2^- to metHb + $XArNH_2$ + $NH_2SO_3^-$ led to drastic underestimation of NO_2^- (Figure 3.10a). This is surprising given that NO_2^- addition to metHb + $XArNH_2$ in the absence of $NH_2SO_3^-$ led to detection of all the NO_2^- present (Figure 3.8a). Since $HgCl_2$ rescues most of the NO_2^- (Figure 3.10a), S-nitrosation of Hb must have occurred in the absence of $HgCl_2$. Thus, S-nitrosation is more rapid than either diazotization (reaction 3.2) or N_2 formation (reaction 3.4) in the metHb solution containing both $XArNH_2$ and $NH_2SO_3^-$.

Since stocks of the latter reagents were prepared in 0.4 N HCl (Section 3.2.2.1), the pH would be higher in the presence of $XArNH_2$ only than in the presence of both reagents. Precipitation was also observed at high NO_2^- concentration in the presence of $HgCl_2$ (data not shown) as seen previously in the absence of $NH_2SO_3^-$ (Figure 3.3).

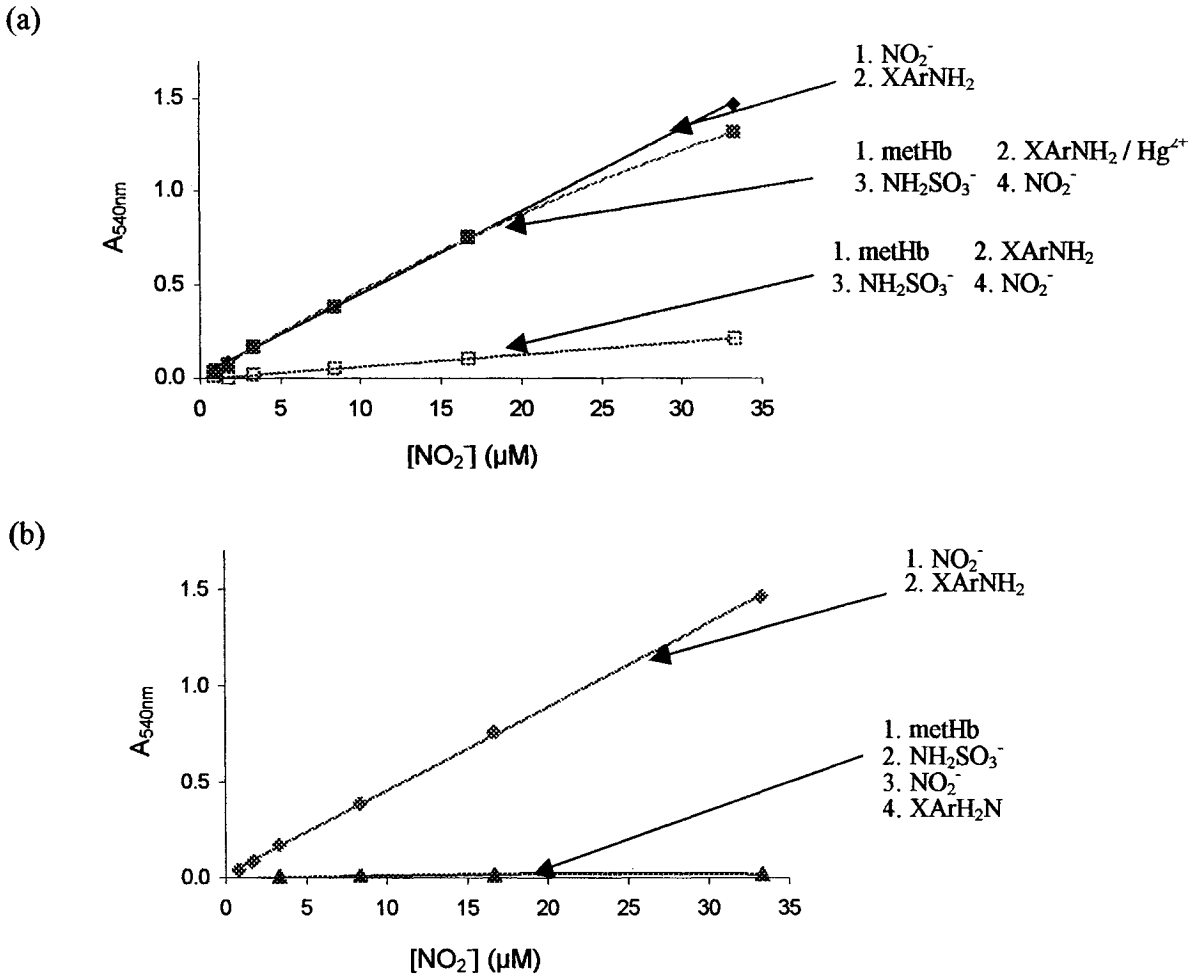

Figure 3.10 **Effects of metHb on competition between $NH_2SO_3^-$ and $XArNH_2$ for NO_2^-.** (a-b) 0.8-33 μM NO_2^- standard containing 60 mM $XArNH_2$ in 0.4 N HCl (◆). (a) Top curve: 0.8-33 μM NO_2^- standards added to 12 μM metHb tetramer + 60 mM $XArNH_2$ + 3 mM $HgCl_2$ + 1.5 mM $NH_2SO_3^-$ (■) bottom curve: 0.8-33 μM NO_2^- standard was added to 12 μM metHb tetramer + 60 mM $XArNH_2$ + 1.5 mM $NH_2SO_3^-$ (□). (b) 60 mM $XArNH_2$ was added to 12 μM metHb tetramer + 1.5 mM $NH_2SO_3^-$ + 0.8-33 μM NO_2^- standard (▲). NED (2 mM) in 0.4 N HCl was immediately added to each sample, and absorbances at 540 nm were recorded in 1.5-mL cuvettes with a 1-cm pathlength at 25°C following 10 min incubation. The order of addition of the reagents is indicated on the graphs.

The effects of metHb on NO_2^- elimination by $NH_2SO_3^-$ were also investigated. $NH_2SO_3^-$ was added to metHb prior to addition of NO_2^- and then $XArNH_2$. This resulted in no detection of NO_2^- (Figure 3.10b). Presumably through the combined effects of N_2 formation (reaction 3.4) and S-nitrosation of metHb all NO_2^- is consumed. Whether N_2 formation is favored over S-nitrosation of metHb may be verified by the addition of $HgCl_2$ with $XArNH_2$. However, this was not investigated.

3.3.6 Effects of CuZnSOD and GSH on the Saville assay

CuZnSOD and GSH are known to be present in human adult RBCs at concentrations of 10 μM (*i.e.*, 20 μM monomer) (11) and 10 mM (4), respectively. Hence, the effects on NO_2^- determination by the Saville assay of adding 60 nM CuZnSOD monomer and 30 μM GSH were investigated. These concentrations correspond to 25% excess over the RBC values normalized to 12 μM Hb tetramer, which was the concentration of Hb used in the experiments shown in Figure 3.10.

Addition of 60 nM CuZnSOD monomer to the NO_2^- standards followed by addition of $XArNH_2$ resulted in ~ 30% underestimation of NO_2^- (Figure 3.11a). However, in the presence of DTPA, which is a Cu^{II} chelator, there was no loss of NO_2^-.

The decrease in NO_2^- detected in the presence of CuZnSOD could be due in part to S-nitrosation of CuZnSOD, which has ten thiols. Since there is no loss of NO_2^- in the presence of DTPA, the active site and/or Cu released from the enzyme at low pH may have catalyzed the transformation of NO_2^- to NO or RSNO in the absence of chelator.

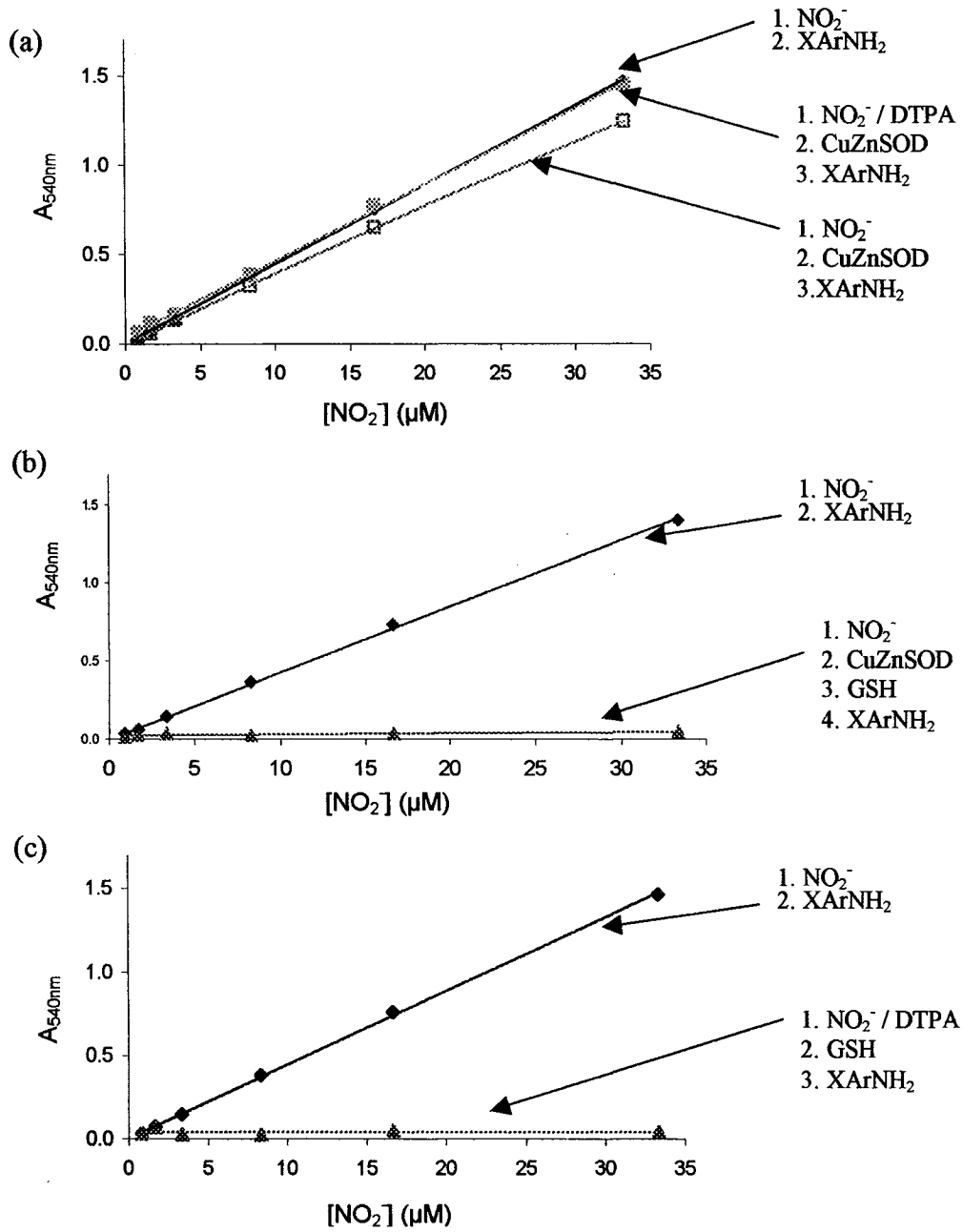

Figure 3.11 **Effects of CuZnSOD and GSH addition on NO_2^- determination.** (a-c) 0.8-33 μM NO_2^- standard containing 60 mM $XArNH_2$ in 0.4 N HCl (◆). (a) Top curve: 60 nM CuZnSOD monomer added to 0.8-33 μM NO_2^- standard + 1 mM DTPA (■); bottom curve: 60 nM CuZnSOD monomer added to 0.8-33 μM NO_2^- standard (□). (b) 30 μM GSH added to 0.8-33 μM NO_2^- standard + 60 nM CuZnSOD monomer (▲). (c) 30 μM GSH added to 0.8-33 μM NO_2^- standard + 1 mM DTPA (▲). NED (2 mM) in 0.4 N HCl was immediately added to each sample, and absorbances at 540 nm were recorded in 1.5-mL cuvettes with a 1-cm pathlength at 25°C following 10 min incubation. The order of addition of the reagents is indicated on the graphs.

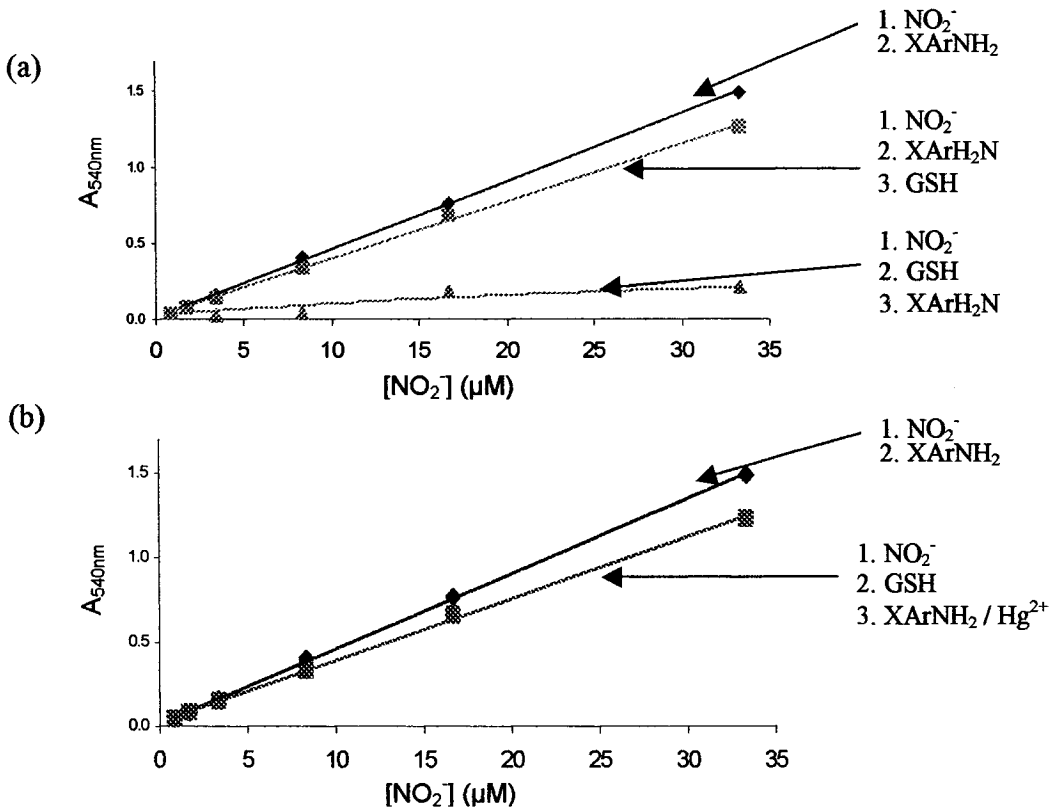

Figure 3.12 **Competition between GSH and $XArNH_2$ for NO_2^-.** (a-b) 0.8-33 μM NO_2^- standard in 0.4 N HCl with 60 mM $XArNH_2$ in 0.4 N HCl (◆). (a) Top curve: 30 μM GSH added to 0.8-33 μM NO_2^- standard + 60 mM $XArNH_2$ (■); bottom curve: 60 mM $XArNH_2$ added to 0.8-33 μM NO_2^- standard + 30 μM GSH (▲). (b) Top curve: 60 mM $XArNH_2$ added to 0.8-33 μM NO_2^- standard + 30 μM GSH (■); bottom curve: 60 mM $XArNH_2$ + 3 mM $HgCl_2$ added to 0.8-33 μM NO_2^- standard + 30 μM GSH (▲). NED (2 mM) in 0.4 N HCl was immediately added to each sample, and absorbances at 540 nm were recorded in 1.5-mL cuvettes with a 1-cm pathlength at 25°C following 10 min incubation. The order of addition of the reagents is indicated on the graphs.

Addition of 30 μM GSH to the NO_2^- standards resulted in total consumption of NO_2^- in the presence of CuZnSOD (Figure 3.11b) or DTPA (Figure 3.11c). This is due to GSNO formation by acidified nitrite. Addition of 60 mM $XArNH_2$ prior to GSH shows that diazotization (reaction 3.2) competes with 30 μM GSH for most but not all of the NO_2^- (Figure 3.12a). Addition of $HgCl_2$ rescues the nitrite from GSNO but, significantly, the amount of NO_2^- not released by $HgCl_2$ (Figure 3.12b) is comparable to that lost when

GSH is added to a stock solution of NO_2^- + $XArNH_2$ (Figure 3.12a). Thus, in the presence of GSH, NO_2^- may be consumed by a route other than GSNO formation such as N-nitrosation of the free amino group of GSH.

3.4 DISCUSSION

3.4.1 Evaluation of the Saville assay

Tables 3.5-3.7 summarize the effects of varying the order of addition of the Saville reagents on the determination of 0.8 - 33 μM NO_2^-. Addition of metHb at ~ pH 0.9 (Table 3.4) decreases the concentration of free NO_2^- (Figure 3.7b) but prior addition of 60 mM $XArNH_2$ rescues the NO_2^- from Hb (Figure 3.8a). Addition of 3 mM $HgCl_2$ + 60 mM $XArNH_2$ to metHb prior to NO_2^- resulted in overestimation of NO_2^- (Figure 3.8b) due to problems with blanking. When the blank contained all of the reagents except NO_2^-, the sample absorbance at 540 nm was below the NO_2^- + $XArNH_2$ line but above this line on omission of $HgCl_2$ from the blank. The slopes were the same for all the lines indicating higher but constant absorbance in the samples when $HgCl_2$ was added to metHb before NO_2^-. This reveals that $HgCl_2$ is causing interference, which should be further investigated.

Addition of $XArNH_2$ + $HgCl_2$ to metHb + NO_2^- at ~ pH 0.9 resulted in ~ 25% underestimation of NO_2^- (Figure 3.8c, Table 3.6). Thus, $HgCl_2$ did not rescue all the NO_2^- originally present. A fraction of NO_2^- may bind to the anion binding sites of metHb, or to the heme, or free amino groups may be N-nitrosated. Thus, RSNO levels may be underestimated in assays where $HgCl_2$ is used to hydrolyze the release of NO.

Table 3.5 **Summary of effects of varying order of addition of Saville reagents on NO_2^- determination in absence of metHb**

Order of reagent addition [a]	Effect on NO_2^- determination	Figure
1.NO_2^- 2.$XArNH_2$ / Hg^{2+}	no effect [b]	3.3
1.NO_2^- 2.$XArNH_2$ 3.$NH_2SO_3^-$	5% NO_2^- loss	3.9a top
1.NO_2^- 2.$NH_2SO_3^-$ 3.$XArNH_2$	95% NO_2^- loss	3.9a bottom
1.NO_2^- 2.$XArNH_2$ / Hg^{2+} 3.$NH_2SO_3^-$	~100% NO_2^- rescue	3.9b
1.NO_2^- 2.$NH_2SO_3^-$ 3.$XArNH_2$ / Hg^{2+}	95% NO_2^- loss	3.9c

Table 3.6 **Summary of effects of varying order of addition of Saville reagents on NO_2^- determination in presence of metHb**

Order of reagent addition [a]	Effect on NO_2^- determination	Figure
1.metHb 2.NO_2^- 3.$XArNH_2$	[metHb]-dependent loss of 60-90% NO_2^-	3.7b
1.metHb 2.$XArNH_2$ 3.NO_2^-	no effect	3.8a
1.metHb 2.$XArNH_2$ / Hg^{2+} 3.NO_2^-	12% NO_2^- overestimation	3.8b
1.metHb 2.NO_2^- 3.$XArNH_2$ / Hg^{2+}	75% NO_2^- rescue	3.8c
1.metHb 2.$NH_2SO_3^-$ 3.NO_2^- 4.$XArNH_2$	100% NO_2^- loss	3.10b
1.metHb 2.$XArNH_2$ / Hg^{2+} 3.$NH_2SO_3^-$ 4.NO_2^-	~100% NO_2^- rescue [b]	3.10a top
1.metHb 2.$XArNH_2$ 3.$NH_2SO_3^-$ 4.NO_2^-	90% NO_2^- loss	3.10a bottom

Table 3.7 **Summary of effects of varying order of addition of Saville reagents on NO_2^- determination in presence of GSH and CuZnSOD**

Order of reagent addition [a]	Effect on NO_2^- determination	Figure
1.NO_2^- 2.CuZnSOD 3.$XArNH_2$	15% NO_2^- loss	3.11a top
1.NO_2^- / DTPA 2.CuZnSOD 3. $XArNH_2$	100% NO_2^- rescue	3.11a bottom
1.NO_2^- 2.CuZnSOD 3.GSH 4. $XArNH_2$	100% NO_2^- loss	3.11b
1.NO_2^- 2.DTPA 3.GSH 4. $XArNH_2$	100% NO_2^- loss	3.11c
1.NO_2^- 2.$XArNH_2$ 3.GSH	85% NO_2^- rescue	3.12a top
1.NO_2^- 2.GSH 3.$XArNH_2$	100% NO_2^- loss	3.12a bottom
1.NO_2^- 2.GSH 3.$XArNH_2$ / Hg^{2+}	85% NO_2^- rescue	3.12b top

[a] Slash indicates reagents were added together.

[b] Precipitation at $\geq 15\mu$ M NO_2^-.

Stamler *et al.* used $HgCl_2$ in their photolysis-chemiluminescence (58) and DAF-2 Hb-SNO assays (Section 3.1.3) (17), as did Gladwin *et al.* in their experiments developed to correct for background nitrites (15).

The control experiments revealed that ~ 95% and ~ 5% of NO_2^- was converted to the diazonium ion (reaction 3.2) if $XArNH_2$ was added before and after $NH_2SO_3^-$, respectively (Figure 3.9a, Table 3.5). Therefore, $NH_2SO_3^-$ removes NO_2^- almost completely if added before $XArNH_2$ (Figures 3.9a,c; Table 3.5), and the presence of $HgCl_2$ does not affect the yield of NO_2^- (Figures 3.9b,c; Table 3.5).

Interestingly, $XArNH_2$ can compete with metHb for NO_2^- in the absence but not the presence of $NH_2SO_3^-$ (Figure 3.8a *vs* 3.10a; Table 3.6). Therefore, levels of RSNO measured in the presence of $NH_2SO_3^-$ may be underestimated. Addition of $HgCl_2$ reveals that metHb S-nitrosation was likely the dominant NO_2^- consumption pathway (Figure 3.10a, Table 3.6). NO_2^- in the 33 μM standard was underestimated in all cases where $NH_2SO_3^-$ was present with (Figures 3.9a-b) or without (Figure 3.10a) metHb.

From Table 3.7, we see that CuZnSOD and GSH, which are present in RBCs, affect Hb-SNO measurements by the Saville assay. Addition of CuZnSOD to the NO_2^- standards resulted in ~15% underestimation of NO_2^- in the absence but not in the presence of the Cu^{II} chelator, DTPA (Figure 3.11). In Section 3.3.6 it was mentioned that Cu from CuZnSOD may catalyze the transformation of NO_2^- to possibly NO or RSNO in the absence of the chelator. Another possibility is that Cu breaks down the diazonium ion (63):

$$XArN{\equiv}N^+ + Cu^+ + H^+ \longrightarrow XArH + N_2 + Cu^{2+} \qquad 3.5$$

The presence of GSH resulted in 90-100% NO_2^- loss (Figure 3.12a). Rescue of ~ 85% NO_2^- by $HgCl_2$ (Figure 3.12b) confirms that this was mainly due to S-nitrosation of GSNO. Rescue of ~ 85% NO_2^- also was observed when $XArNH_2$ was added prior to GSH (Figure 3.12b). Therefore, it seems that ~ 15% NO_2^- loss occurs through another route such as N-nitrosation of the primary amino group of GSH (64):

$$RNH_2 + HNO_2 \longrightarrow RNH\text{-}NO + H_2O \longrightarrow \longrightarrow RNH_2^+ \qquad 3.6$$

Reaction 3.6 may interfere in the methods used for the determination of Hb-SNO levels. MetHb contains 44 lysines, whose amino groups can provide a site of N-nitrosation under the acidic conditions used for the Saville assay.

The series of experiments reported here (Figures 3.7 to 3.12; Tables 3.5 to 3.7) demonstrate that RSNO determination by the Saville assay is susceptible to many interferences. In particular, the data presented in Figure 3.8c illustrate that accurate Hb-SNO quantification by the Saville assay might not be possible. For example, the 17 μM and 33 μM NO_2^- standards yielded absorbance readings corresponding to 12 and 25 μM NO_2^-, respectively. Thus, NO_2^- was underestimated by ~ 25%, which may be due in part to nitrosation of amino groups, as discussed above. This problem could be magnified in assays of RBC lysates where the concentration of Hb is high (5 mM) and Hb-SNO is low (20-1000 nM; Tables 3.1, 3.2).

Sample preparation is very crucial in RSNO determinations on partially purified hemolysates (6,15,17,57). While low-molecular-weight interferences, such as GSH, may be removed by G25 gel filtration, proteins such CuZnSOD and carbonic anhydrase at concentrations of ~ 20 μM (11) and ~150 μM (65), respectively, per 5 mM Hb, are likely

likely still present in the hemolysates analyzed. While NEM is sometimes used to block free thiols from becoming S-nitrosated (15), all proteins contain multiple lysine residues that can be N-nitrosated by NO_2^- under acidic conditions (64). CuZnSOD may also release copper at low pH, which could cause NO underestimation, as discussed above.

The large variability encountered in the reported Hb-SNO values (Tables 3.1, 3.2) illustrates the complexity of RSNO analysis (6,15,17,57). An accurate and highly sensitive method for Hb-SNO determination has yet to be found.

3.4.2 Relative reactivities of HbA and HbF with GSNO

Using the Saville assay, the Hb samples containing oxyHbF, oxyHbA and metHbA were found to be S-nitrosated to the same extent by GSNO (Table 3.3). Even if the level of S-nitrosation was underestimated, the results suggest that HbA and HbF exhibit similar reactivity toward GSNO as an NO donor. Hence, any differences in the levels of HbA and HbF S-nitrosation in cells may arise from the stabilities of their S-nitrosated forms. Interestingly, mass spectral analysis (Figure 3.6) revealed that the γ_A-chain of HbF may be preferentially S-nitrosated. The biological significance of such a result remains to be elucidated. As was discussed previously, it has been shown that HbF with higher fractions of γ_A has different physical properties than HbF containing higher fractions of γ_G, but no difference in oxygen affinity (61). During fetal life, γ_G makes up 70% of the γ globins, while during the postconceptional age switchover from HbF to HbA synthesis, the two chains are expressed equally (50). If γ_A is indeed preferentially S-nitrosated, it may be that HbF-SNO formation in the fetus is limited since there is little expression of this γ-chain in the fetus. This could explain the lower levels of Hb-SNO

measured at Ste-Justine Hospital for the RBC lysates from premature newborns *vs* term newborns following birth (Table 2.4) (42).

4.0 PRELIMINARY INVESTIGATION OF NITRITE REDUCTION BY Cu,Zn-SUPEROXIDE DISMUTASE

4.1 INTRODUCTION

4.1.1 Role of NO_2^- in the human circulation

NO_2^- is produced from the oxidation of NO (20), which has a half-life of 10 to 30 s under physiological conditions (66,67). NO_2^- has previously been shown to be reduced to NO enzymatically in many bacterial systems by the action of nitrite reductases (NiRs) (68) and in humans by xanthine oxidoreductase (69). From measurements of endogenous NO_2^- levels, it has been proposed that NO_2^- may provide an additional source of bioavailable NO (6). More recently, it has been suggested by the same group (6) that NO_2^- could comprise the largest vascular storage pool of NO provided that physiological mechanisms exist to reduce NO_2^- to NO. They propose that deoxyHb provides the necessary mechanism by functioning as a reductant of NO_2^- (20).

Reported levels of NO_2^- in the human vasculature vary extensively. Plasma levels between 150 nM (70) and 3 μM (66) have been measured. In a recent publication, basal plasma NO_2^- levels were found to be 305 ± 23 nM using three analytical techniques, flow-injection analysis, reductive gas phase luminescence, and sensitive HPLC (70). NO_2^- levels in RBCs have not been studied extensively. In one study, NO_2^- levels were reported to be between 200 and 300 nM in RBC lysates (18), which is within the range of the reported plasma values. The relatively high values in plasma and RBCs in the adult human vasculature, as well as its greater stability compared to NO, would allow NO_2^- to serve as a pool for NO on one-electron reduction:

$$NO_2^- + 1e^- + 2H^+ \longrightarrow NO + H_2O \qquad 4.1$$

4.1.2 Role of NO_2^- in fetal circulation

If NO_2^- provides a pool of bioavailable NO in the adult vasculature, a similar pool may exist in the fetal or newborn infant circulation. Total NO metabolite values ($NO_x = NO_2^- + NO_3^-$) in the range of 11 to 90 μM have been found in the serum prepared from veinous umbilical cord samples collected at birth (71-73). Interestingly, these values are comparable to adult serum NO_x values measured in the range of 15 to 80 μM (72). It has been presumed that NO_x play little role in the circulatory adaptation of the fetus at birth (73). However, an observed increase in NO_x on day 5 following birth, which decreases by day 30, along with a parallel decrease in the vasoconstrictor endothelin-1 (73), suggest a possible role for NO_x in the systemic and pulmonary adaptation of the newborn infant from fetal to neonatal life (72).

4.1.3 CuZnSOD as a catalyst of nitrite reduction

NO_2^- can serve as a pool for NO provided that reaction 4.1 is catalyzed in humans. There are two known classes of NiRs, one with heme prosthetic groups and the other with copper centers (74). It has been reported that deoxyHb reduces NO_2^- with a bimolecular rate constant of ~0.2 $M^{-1}s^{-1}$ in whole blood (20). It is possible, as shown for biomimetic copper centers (75), that CuZnSOD also may catalyze NO_2^- reduction.

Binding of NO_2^- to biomimetic Cu^{II} complexes gives rise to a ligand-to-metal charge transfer (LTMCT) transition in the near-UV region. This is of interest since the reduction of NO_2^- to NO by copper NiRs in the presence of a donor substrate likely occurs on binding of NO_2^- *via* one of its oxygen atoms to Cu^{II} (76). Recently, it has been reported that NO_2^- is reduced to NO by binding to copper centers with tridentate nitrogen donor ligands (75). This type of coordination is found in the copper center of Cu^{I}ZnSOD,

which is linked to three histidine (imidazole) ligands in an almost trigonal planar geometry (74). Thus, the spectrum of the oxidized form of CuZnSOD in the presence of NO_2^- was examined here to obtain evidence for binding of NO_2^- to the active-site Cu^{II}:

$$NO_2^- + Cu^{II}ZnSOD \longrightarrow Cu^{II}ZnSOD\text{-}NO_2^- \qquad 4.2$$

4.2 EXPERIMENTAL SECTION

4.2.1 Materials

Bovine CuZnSOD was purchased from Roche; sodium nitrite and 4-(2-hydroxyethyl)piperazine-1-ethanesulfonic acid (HEPES) were purchased from Aldrich; monobasic sodium phosphate and dibasic sodium phosphate salts were obtained from Fisher; cysteine and DTPA were purchased from Sigma; Sephadex G-25 columns were obtained from Amersham Pharmacia Biotech; Nanopure water (MilliQ; specific resistance of 18mΩ-cm) from a Millipore Simplicity water purification system and treated with Chelex-100 (Sigma) to remove trace metal ions was used to prepare all solutions.

4.2.2 Absorption spectra of $Cu^{II}ZnSOD/NO_2^-$ incubates

Lyophilized CuZnSOD (10 mg) was reconstituted in 1 mL of 200 mM sodium phosphate buffer, pH 7.2 (Na*Pi*), to give a stock solution of 600 μM monomer. The concentration of the prepared solution was verified by monitoring the absorbance at 258 nm (ε=10.3 $mM^{-1}cm^{-1}$ per dimer) (51) of the oxidized form, $Cu^{II}ZnSOD$ (74).

Aliquots of $Cu^{II}ZnSOD$ were mixed with sodium nitrite in water to obtain 500 μM $Cu^{II}ZnSOD$ monomer and NO_2^- at $Cu:NO_2^-$ molar ratios of 1:30 or 1:300 in Na*Pi*, and 233 μM $Cu^{II}ZnSOD$ monomer and NO_2^- at $Cu:NO_2^-$ molar ratios of 1:20, 1:220 or

1:2400 in 50 mM HEPES buffer, pH 7.4. Spectra of these samples were recorded to observe the visible d-d band at 680 nm (ε = 300 $M^{-1}cm^{-1}$ per monomer), which is characteristic of active site Cu^{II} (77).

More dilute Cu^{II}ZnSOD samples were prepared to examine the spectra for evidence of ligand-to-metal charge-transfer (LTMCT) bands (76). Aliquots of Cu^{II}ZnSOD were mixed with sodium nitrite in water to give 100 μM Cu^{II}ZnSOD monomer and NO_2^- at Cu:NO_2^- molar ratios of 1:5 or 1:500 in 100 mM Na*Pi* buffer, pH 7.2 (Na*Pi*), and 200 μM Cu^{II}ZnSOD monomer with NO_2^- at Cu:NO_2^- molar ratios of 1:10, 1:100 or 1:600 in 50 mM HEPES buffer, pH 7.4.

Experiments were performed in both Na*Pi* and HEPES since phosphate has been previously reported to bind close to the active site of CuZnSOD (78). Spectra were recorded on a Beckman model DU-650 or an Agilent model 8453 UV-vis spectrophotometer following 5 to 60 min incubation at room temperature after the addition of NO_2^-. All spectra were corrected for buffer absorption.

4.3 RESULTS

4.3.1 Effects of added NO_2^- on the 680-nm d-d absorption of Cu^{II}ZnSOD

A decrease in the Cu^{II} d-d band of 500 μM CuZnSOD monomer in Na*Pi* was detected in the presence of NO_2^-. The decrease in absorbance was greater for the sample with a Cu to NO_2^- ratio of 1:300 than the sample with a ratio of 1:30 (Figure 4.1a,b).

In 50 mM HEPES buffer, pH 7.4, a decrease in the Cu^{II} d-d band at 680 nm of 233 μM Cu^{II}ZnSOD monomer was observed for samples with Cu to NO_2^- ratios of 1:220 and 1:2400 (Figures 4.2a,b). For the sample with a Cu to NO_2^- ratio of 1:220, scans were taken every minute over 5 min (Figure 4.2a). For the sample with a Cu to NO_2^- ratio of

taken every minute over 5 min (Figure 4.2a). For the sample with a Cu to NO_2^- ratio of 1:2400, scans were taken every minute over 5 min and at 10, 20 and 30 min following addition of NO_2^- (Figure 4.2b). The decrease in absorbance of the 680-nm band observed for these samples was gradual over time. At 30 min following addition of NO_2^- the sample with a Cu to NO_2^- ratio of 1:2400 exhibited significant loss of 680-nm absorption. For the sample with a Cu to NO_2^- ratio of 1:20, spectra recorded following addition of NO_2^- revealed negligible changes in the Cu^{II} d-d band at 680 nm (data not shown). Also, superposition of the spectra of samples with Cu to NO_2^- ratios of 1:200 and 1:2400 obtained only 5 min after NO_2^- addition revealed negligible decrease in the 680-nm band (Figure 4.3).

In Table 4.1, the time dependent loss of 680-nm absorption of a Cu^{II}ZnSOD sample with a Cu to NO_2^- ratio of 1:2400 is summarized. A gradual decrease in A_{680} was observed for the spectra recorded at 10 (3%), 20 (7%) and 30 (10%) min. These results may be indicative of slow reduction of the enzyme to Cu^{I}ZnSOD with time or of NO_2^- binding to the Cu^{II} center.

4.3.2 Absorption of NO_2^-

In the literature, absorption bands for NO_2^- have been assigned at 210 nm (ε = 5500 $M^{-1}cm^{-1}$), 300 nm (ε = 15 $M^{-1}cm^{-1}$) and 350 nm (ε= 25 $M^{-1}cm^{-1}$) due to the following electronic transitions: $\pi_2 \rightarrow \pi_3$, $n_o \rightarrow \pi_3$ and $n_N \rightarrow \pi_3$ (79). The spectra obtained of 2 mM, 20 mM and 100 mM NO_2^- in 50 mM HEPES buffer, pH 7.4 are shown in Figure 4.4a.

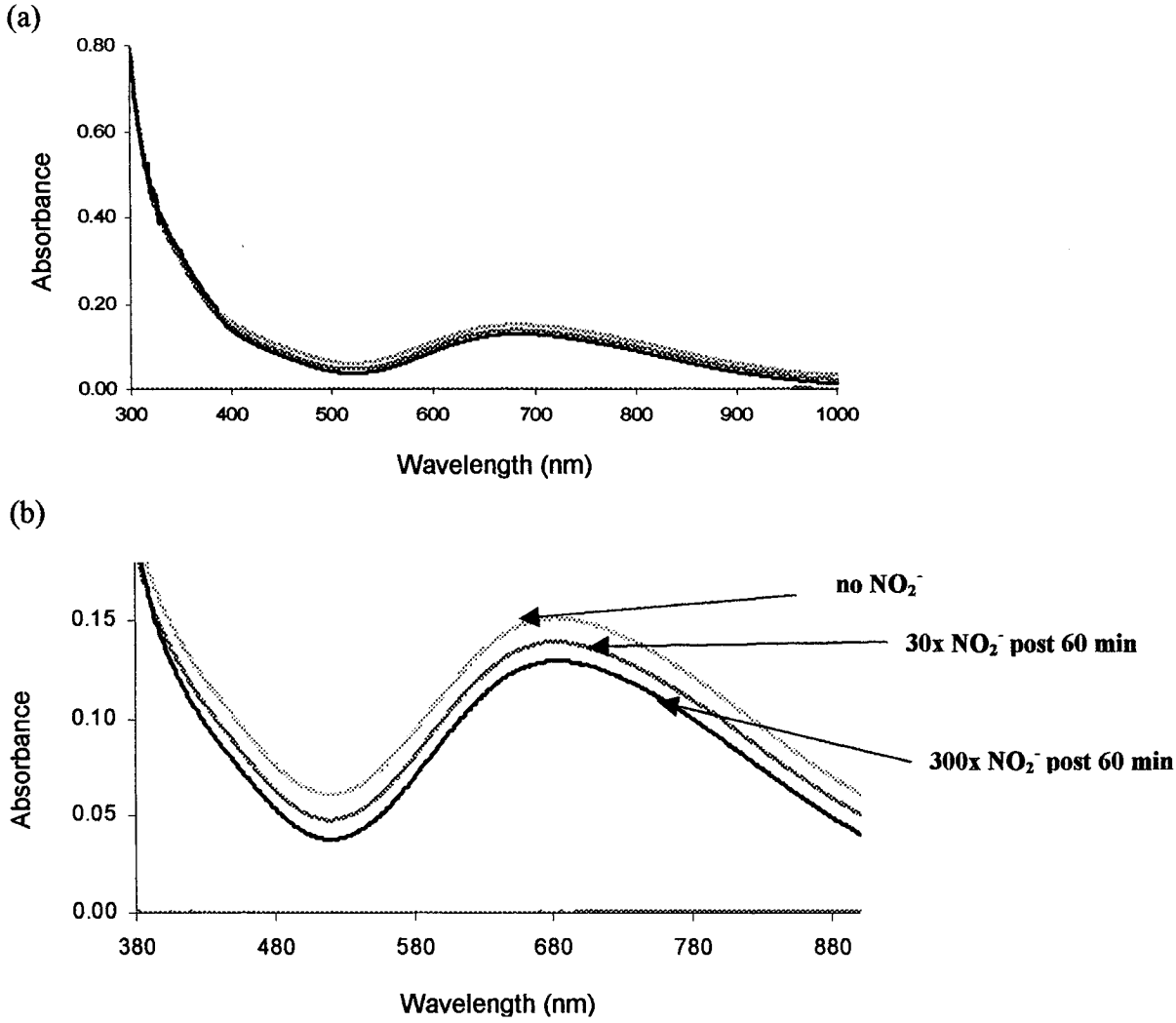

Figure 4.1 **d-d Absorption spectra of Cu^{II}ZnSOD/NO_2^- incubates in Na*Pi* buffer.** (a) Spectra of 500 μM Cu^{II}ZnSOD monomer without and with 15 or 150 mM NO_2^- (1:30 and 1:300 Cu:NO_2^- molar ratios) following 60 min incubation at room temperature. (b) Expansion (4x) of the spectra in a. The incubates were in 100 mM sodium phosphate buffer, pH 7.2 (Na*Pi*). Spectra were recorded on an Agilent 8453 UV-vis spectrophotometer in 1.5-mL quartz cuvettes with a 1-cm pathlength at 25°C and corrected for buffer absorption.

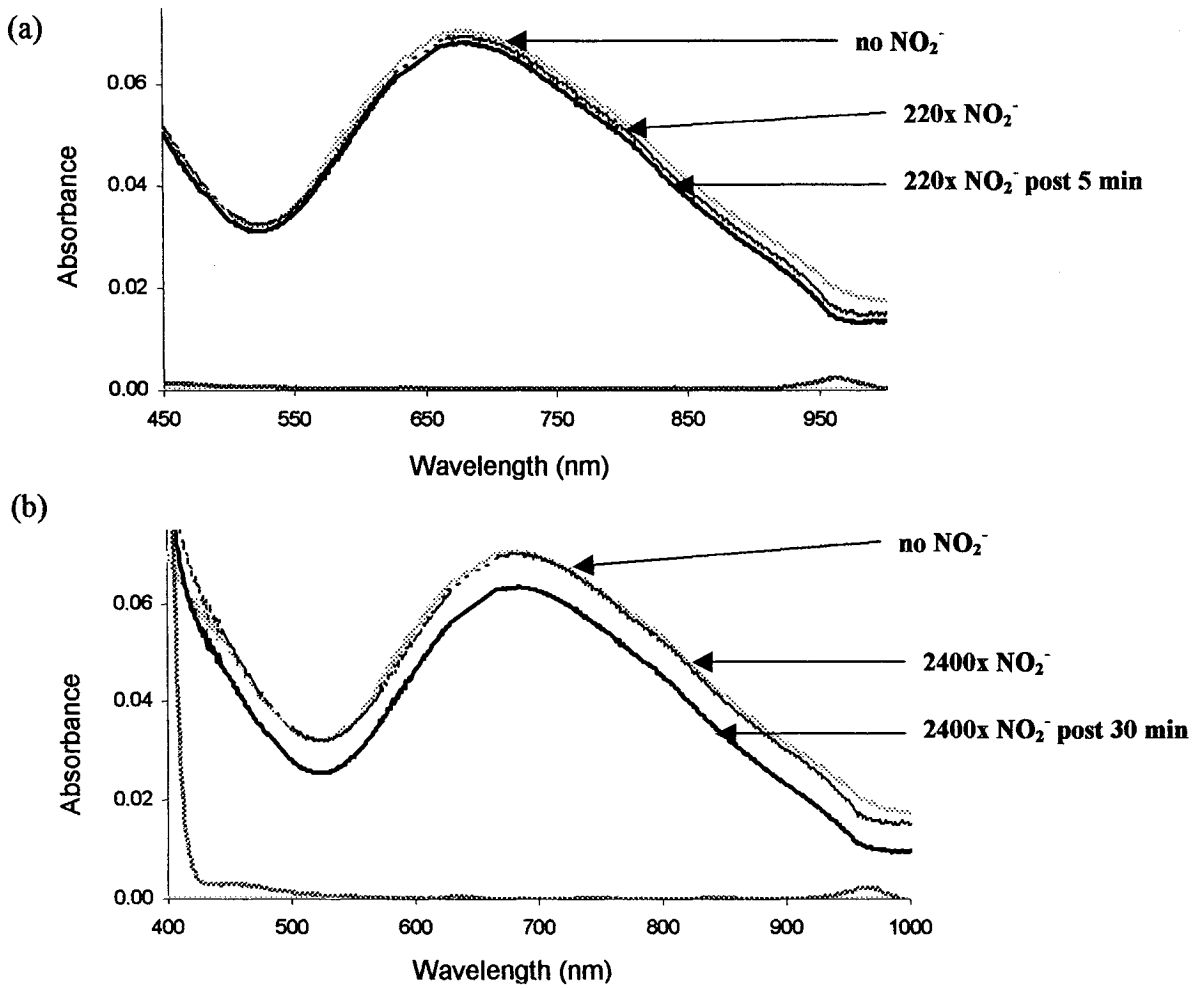

Figure 4.2 **d-d Absorption spectra of $Cu^{II}ZnSOD/NO_2^-$ incubates in 50 mM HEPES buffer (pH 7.4).** Spectra of (a) 230 μM $Cu^{II}ZnSOD$ monomer without (⋯⋯) and with 50 mM NO_2^- (1:220 $Cu:NO_2^-$ molar ratio) after 0 min (.....) and 5 min (—) incubation at room temperature, and (b) 208 μM $Cu^{II}ZnSOD$ monomer without (⋯⋯) and with 500 mM NO_2^- (1:2400 $Cu:NO_2^-$ molar ratio) after 0 min (——) and 30 min (—) incubation at room temperature. Spectra were recorded on an Agilent 8453 UV-vis spectrophotometer in 1.5-mL quartz cuvettes with a 1-cm pathlength at 25°C and corrected for buffer absorption (see Figure 4.5a). The spectra of NO_2^- containing samples were normalized to 233 μM $Cu^{II}ZnSOD$ monomer since the sample was diluted on NO_2^- addition.

Table 4.1 **Time dependence of loss of d-d absorption of $Cu^{II}ZnSOD$ on addition of NO_2^-**

	$Cu^{II}ZnSOD$	$Cu^{II}ZnSOD + NO_2^-$ (1:2400) [a, b]				
		0 min	5 min	10 min	20 min	30 min
A_{680}	0.071	0.072	0.070	0.068	0.065	0.063
ΔA_{680}	-	+0.001	-0.001	-0.002	-0.005	-0.007
% change [c]	-	+2%	-1%	-3%	-7%	-10%

[a] 208 μM CuZnSOD monomer was incubated with 500 mM NO_2^- (1:2400 Cu:NO_2^- molar ratio) in 50 mM HEPES buffer, pH 7.4, at 25°C.

[b] Concentration of CuZnSOD monomer calculated spectrophotometrically assuming ε_{680nm}= 300 $M^{-1}cm^{-1}$ per monomer (77).

[c] A_{680} for $Cu^{II}ZnSOD$ minus A_{680} for incubate at time t, divided by A_{680} for $Cu^{II}ZnSOD$ x 100%. Data from Figure 4.2b.

The observed bands in HEPES for 2 mM NO_2^- were at 220, 290 and 360 nm. However, the 220-nm absorption of the 20 mM and 100 mM NO_2^- samples saturated the detector, as did the 360-nm absorption in the 100 mM NO_2^- sample (Figure 4.4a).

Spectra obtained for 50 mM NO_2^- in Na*Pi* (Figure 4.4b) show similar bands at 230, 292 and 355 nm. The slight differences in peak maxima and intensities may be due to changes in the environment of NO_2^- resulting from the different buffers used, which have been reported to affect the optical properties of NO_2^- (79).

4.3.3 Absorption of $Cu^{II}ZnSOD$ incubates in the LTMCT Region

The 250 to 450 nm region of the spectra of $Cu^{II}ZnSOD/NO_2^-$ incubates with Cu to NO_2^- ratios of 1:10, 1:100 and 1:600 in 50 mM HEPES buffer, pH 7.4, was examined for evidence of ligand-to-metal charge-transfer (LTMCT) bands.

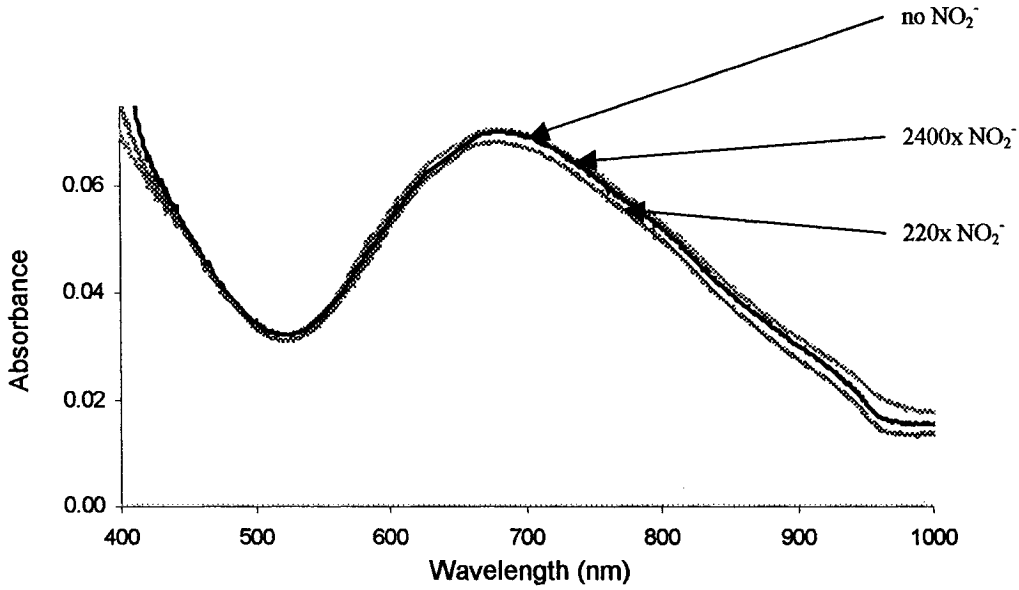

Figure 4.3 **d-d Absorption spectra of Cu^{II}ZnSOD/NO_2^- incubates in 50 mM HEPES buffer (pH 7.4).** Spectra of 233 μM Cu^{II}ZnSOD monomer without and with 50 mM or 500 mM NO_2^- (1:220 and 1:2400 Cu:NO_2^- molar ratios) after 5 min incubation at room temperature. Spectra were recorded on an Agilent 8453 UV-vis spectrophotometer in 1.5-mL quartz cuvettes with a 1-cm pathlength at 25°C and corrected for buffer absorption. The spectra of the NO_2^--containing sample were normalized to 233 μM Cu^{II}ZnSOD monomer since the protein was diluted to 208 μM on NO_2^- addition.

A LTMCT band is expected at ~ 350-420 nm on NO_2^- binding to Cu^{II} (76,80). Such a band is observed at 360 nm in the spectrum of CuZnSOD/NO_2^- containing 1:10 Cu:NO_2^- following correction for 2 mM NO_2^- (Figure 4.5a, inset). The LTMCT band is not observed in the spectrum of CuZnSOD/NO_2^- containing 1:100 Cu:NO_2^- (Figure 4.5b) due to the high absorbance of NO_2^- at 350 nm in this sample.

The absorbance of 100 mM NO_2^- in HEPES buffer (Figures 4.4a, 4.5c) was above the response limit of the instrument in the 1-cm cell used. Therefore, it was not possible to correct for NO_2^- absorbance in the Cu^{II}ZnSOD/NO_2^- incubates containing 100 mM NO_2^-.

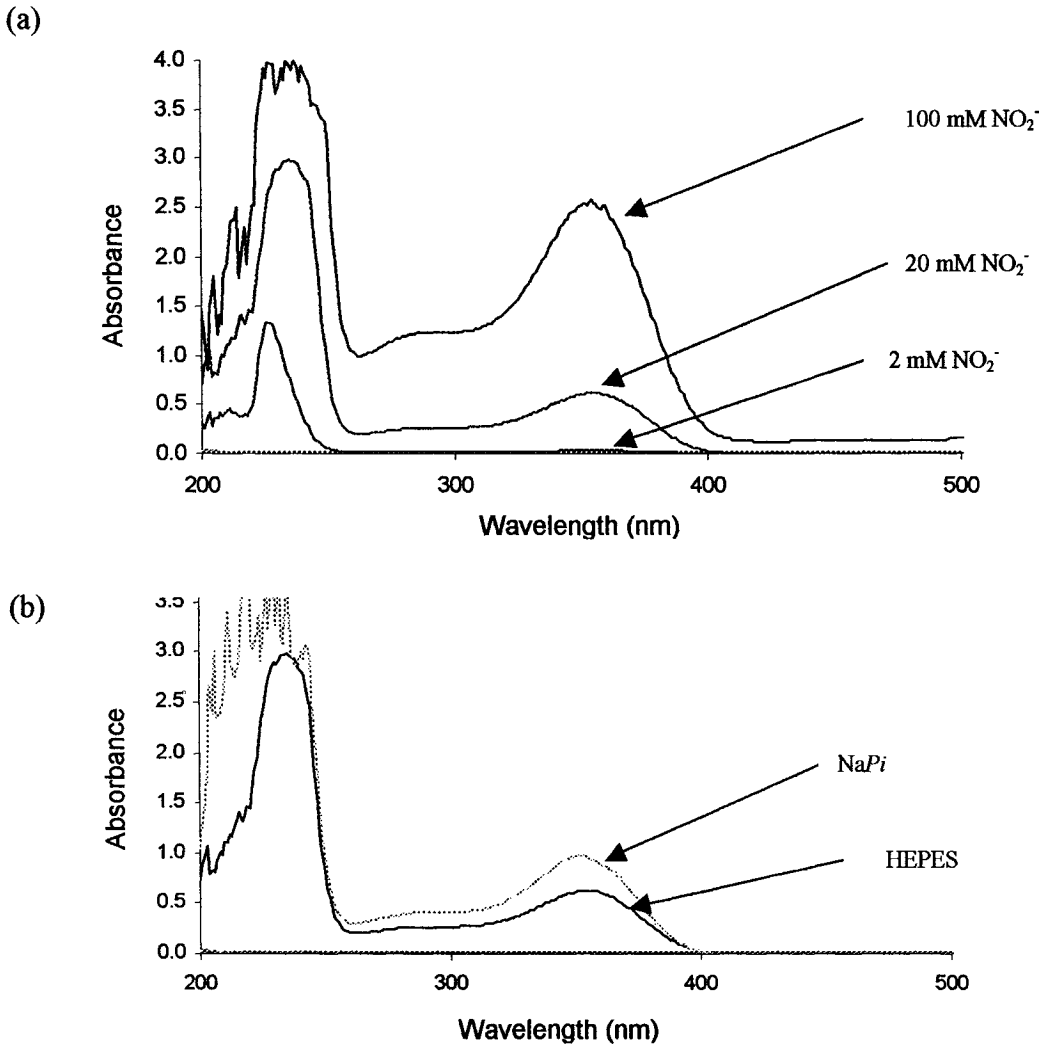

Figure 4.4 **Absorption spectra of NO_2^- in buffer.** Spectra of (a) 2 mM, 20 mM and 100 mM NO_2^- in 50 mM HEPES buffer, pH 7.4, and (b) 20 mM NO_2^- in HEPES buffer (——) and 50 mM NO_2^- in 100 mM sodium phosphate buffer, pH 7.2 (····). All spectra were recorded at 25°C on an Agilent 8453 UV-vis spectrophotometer in 1.5-mL quartz cuvettes with a 1-cm pathlength and corrected for buffer absorption.

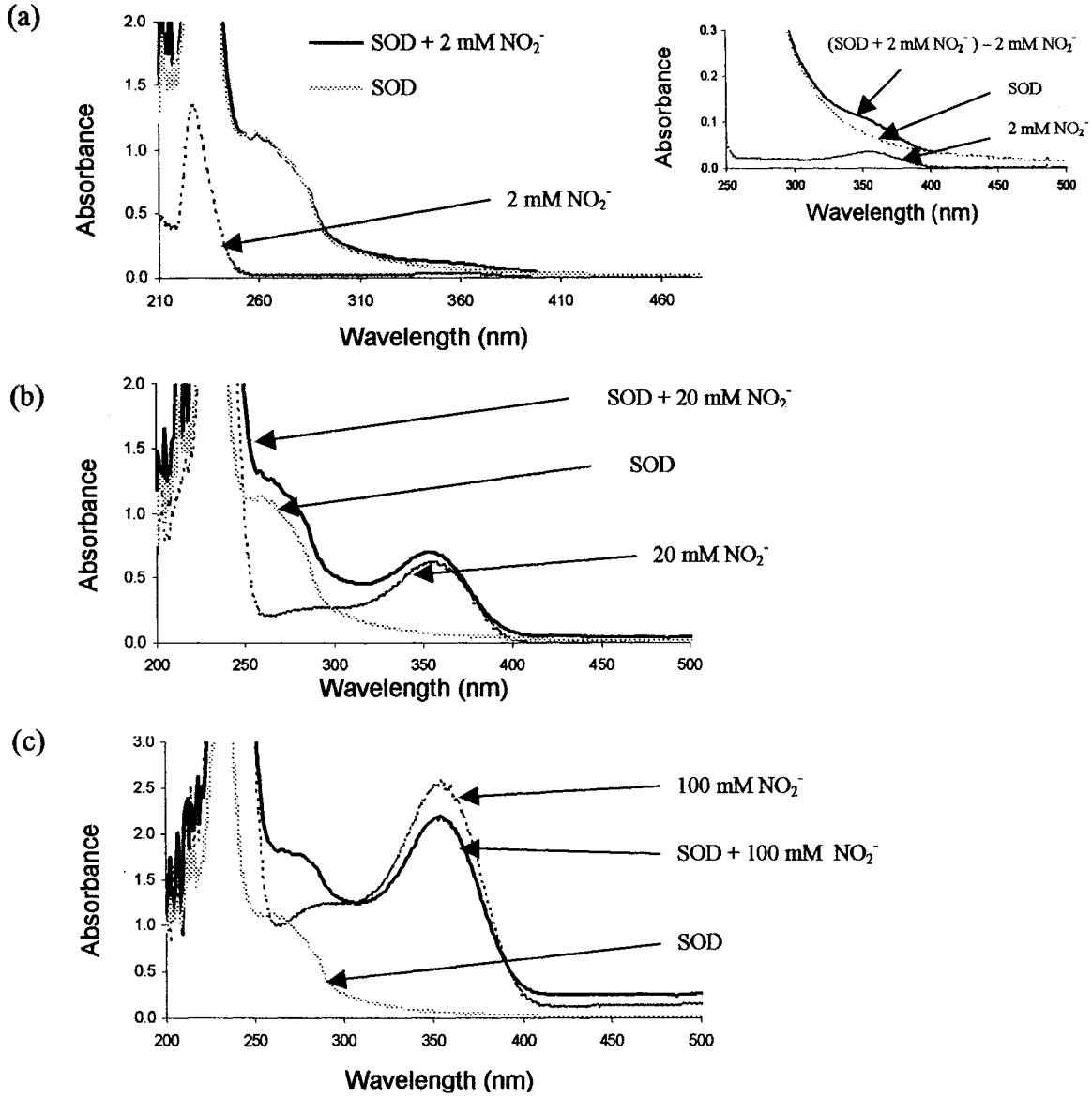

Figure 4.5 **Absorbance spectra in LTMCT region of $Cu^{II}ZnSOD/NO_2^-$ incubates in 50 mM HEPES buffer (pH 7.4) at room temperature.** (a) 200 μM $Cu^{II}ZnSOD$ monomer ± 2 mM NO_2^- after 5 min incubation, (b) 190 μM $Cu^{II}ZnSOD$ monomer ± 20 mM NO_2^- after 5 min incubation, and (c) 170 μM $Cu^{II}ZnSOD$ monomer ± 100 mM NO_2^- after 30 min incubation. Spectra were recorded at 25°C on an Agilent 8453 UV-vis spectrophotometer in 1.5-mL quartz cuvettes with a 1-cm pathlength and corrected for buffer absorption. The spectra of the NO_2^--containing samples were normalized to 200 μM $Cu^{II}ZnSOD$ monomer to correct for protein dilution on NO_2^- addition. Insert (a): difference spectrum of [(200 μM $Cu^{II}ZnSOD$ monomer + 2 mM NO_2^-) - 2 mM NO_2^-].

The observation of a possible LTMCT band at 360 nm ($\varepsilon = 0.5\ mM^{-1}cm^{-1}$) in the spectrum of the CuZnSOD/NO_2^- sample containing 1:10 Cu:NO_2^- (Figure 4.5a, insert) indicates that NO_2^- binding to Cu^{II} may be occurring at 2 mM NO_2^-.

4.4 DISCUSSION

4.4.1 Effects of added NO_2^- on the 680-nm d-d absorption of Cu^{II}ZnSOD

The scope of the experiments carried out here was to investigate whether CuZnSOD might catalyze NO_2^- reduction to NO. The decrease in absorbance of the 680-nm d-d band of Cu^{II}ZnSOD in the presence of NO_2^- over times greater than 5 min (Table 4.1) could be indicative of partial reduction of Cu^{II}ZnSOD with NO_2^- bound to Cu^I. Slow reduction of the copper centre would be consistent with electron donation from an amino acid residue in the Cu environment. Alternatively, NO_2^- binding to Cu^{II} could have perturbed the d-d absorption.

Typically, copper NiRs contain type 1 and type 2 Cu centers. The type 1 Cu centers mediate electron transfer, while the type 2 Cu centers are the active sites where NO_2^- binding and reduction occur (81). CuZnSOD has similar copper coordination as the type 2 Cu site of the NiR from *Alcaligenes xylosoxidans* (*Ax*NiR). In oxidized *Ax*NiR, three histidine ligands (1.95 ± 0.2 Å) and an O atom from water (1.98 ± 0.03 Å) are coordinated to the Cu 2 site (74). Upon reduction of *Ax*NiR, the water ligand is lost and the extended X-ray absorption fine structure (EXAFS) of the type 2 Cu^I center shows a strong resemblance to that of the Cu^I site of reduced CuZnSOD (82). Furthermore, *Ax*NiR was shown to possess SOD activity (74).

The perturbation of the 680-nm band in the presence of excess NO_2^- may be indicative of NO_2^- binding to Cu^{II}ZnSOD. In *Ax*NiR, NO_2^- coordinates to the oxidized

type 2 copper site *via* oxygen (83). Electron transfer from the type 1 Cu center reduces the active site with formation of Cu^{I}-NO^{+} following release of a water molecule (83). To establish if a Cu^{II}-NO_2^- complex forms in the Cu^{II}ZnSOD/NO_2^- incubates, the LTMCT region of their spectra was examined.

4.4.2 Absorption of Cu^{II}ZnSOD/NO_2^- incubates in the LTMCT region

No changes were observed in the LTMCT region for samples of NO_2^- and CuZnSOD in Na*Pi* buffer (data not shown). However, a possible LTMCT band at 360 nm was observed for the Cu^{II}ZnSOD/NO_2^- incubate with 2 mM NO_2^- (Cu/NO_2^- = 1:10) in HEPES (Figure 4.5a, insert), indicating that NO_2^- binding to Cu^{II} may be occurring since LTMCT from NO_2^- to Cu^{II}ZnSOD is expected. Binding *via* oxygen to the type 2 Cu^{II} center of *Ax*NiR is the first step in NO_2^- reduction to NO (82). Thus, if NO_2^- binding to Cu^{II} can be further demonstrated for CuZnSOD under different experimental conditions, this would provide evidence that the dismutase may also catalyze NO_2^- reduction. However, the reduction of NO_2^- by CuZnSOD in the presence of physiological reductants such as GSH or ascorbate should be examined directly.

5.0 SUMMARY AND SUGGESTIONS FOR FURTHER STUDY

In Chapter 2, a standard addition method was described for the determination of catalytically active CuZnSOD monomer in the presence of Hb. The basis of the assay is the determination of active CuZnSOD by measuring the decrease in pyrogallol oxidation. With standard addition, a calibration curve is obtained by adding known amounts of CuZnSOD to the sample and extrapolating to no CuZnSOD added to determine the amount of CuZnSOD originally present. It also was shown in Chapter 2 that removal of CuZnSOD from Sigma HbA, which is critical for direct determination of CuZnSOD monomer in Hb samples by the direct method, was not complete.

While the standard addition method of CuZnSOD analysis provided data with less error, there is still some variability in the method. Data with $r^2 < 0.9$ were rejected as the calibration curves were not considered linear (Appendix B). In future analyses it is recommended that assays be performed under controlled temperature conditions in order to decrease variability. Additionally, stirring during data collection should stabilize the rates of pyrogallol oxidation (48) and reduce the error in the slopes.

By standard addition, levels of CuZnSOD were shown to be higher in newborn than in adult RBC lysates prepared in a similar way. Metal ion analyses by ICP-MS previously carried out by our group also showed that Cu levels were higher in newborn *vs* adult RBC lysates (Table 2.3). Higher levels of CuZnSOD were found to correlate with higher levels of Hb-SNO in blood from preterm newborns. The parallel increase of CuZnSOD and Hb-SNO suggests that expression of CuZnSOD promotes Hb-SNO formation, consistent with the proposed role of CuZnSOD in the S-nitrosation of Hb. Since newborn blood contains > 80% HbF, it can be assumed that CuZnSOD catalyzes

NO transfer to Cysγ93 in a similar fashion to that described for Cysβ93 (11). Also, the fact that levels of Hb-SNO and CuZnSOD are higher following birth suggests that S-nitrosation of Hb becomes important as the infant circulation develops. This is in agreement with a report that Hb-SNO may be involved in the perinatal circulatory transition, with lower Hb-SNO levels detected in arterial cord blood samples from newborns who did not adjust normally to neonatal circulation (37).

In Chapter 3, it was shown that RSNO determination by means of the Saville assay is subject to many interferences. Interferences from reagent side reactions, such as those of $HgCl_2$ used for S-NO breakdown and of sulfamate used for the elimination of background nitrites, as well as interferences from matrix components (Hb, CuZnSOD and GSH), may lead to underestimated RSNO values (Tables 3.5 to 3.7). While methods (*e.g.*, photolysis-chemiluminescence, DAF-2 fluorescence assays, I_3-chemiluminescence) other than the Saville assay are used for RSNO determination, $HgCl_2$ is usually employed for S-NO breakdown (15,17,58). The published methods for Hb-SNO determination were performed on partially purified hemolysates (6,15,17,57) and therefore are susceptible to the interferences in RSNO determination identified here. In particular, while overestimation of RSNO levels can be prevented by using NEM to block free thiols (15), N-nitrosation of the primary amino side chains of lysine residues under acidic conditions will likely lead to RSNO underdetermination. An accurate method for the determination of Hb-SNO (especially at the submicromolar levels predicted *in vivo*) is yet to be found.

OxyHbF, oxyHbA and Sigma metHbA were found by the Saville assay to be S-nitrosated to the same extent by GSNO (Table 3.3). These results are in agreement with a previous study, which reported that HbF and HbA obtained from dialyzed fetal and adult

RBC supernatants scavenged NO at similar rates (39). Thus, the results suggest that HbA and HbF exhibit similar reactivity toward GSNO as a NO donor, and that differences in HbA-SNO and HbF-SNO levels in cells may arise from differences in the stabilities of their S-nitrosated forms.

The preferential S-nitrosation of γ_A *vs* γ_G suggested by mass spectral analysis (Figure 3.5) may have a biological significance. During fetal life γ_G makes up 70% of the γ globins, while during the postconceptional age switchover from HbF to HbA synthesis the two γ-chains are expressed equally (50). This may explain why there are higher levels of Hb-SNO as newborns age (42).

A decrease in absorbance of the 680-nm d-d band of Cu^{II}ZnSOD in the presence of NO_2^- was reported in Chapter 4. This suggests that reduction of Cu^{II}ZnSOD occurs in the presence of NO_2^-, or that Cu^{II}-NO_2^- binding is taking place. The presence of a possible LTMCT band at 360 nm in the spectrum of a Cu^{II}ZnSOD/NO_2^- incubate containing 2 mM NO_2^- provides evidence of NO_2^- binding to the active site Cu^{II}. Thus, NO_2^- could act as a NO pool if Cu^{II}ZnSOD catalyzes its reduction. Further elucidation of the mechanism of NO transfer in the vasculature needs to consider the possible roles of CuZnSOD in NO_x biochemistry.

A possible role for NO metabolites in the systemic and pulmonary adaptation of the newborn during the transition from fetal to neonatal life has been previously suggested (72). NO is used to improve oxygenation in premature and term newborns suffering from pulmonary hypertension (44,45). The results presented in Chapters 2 and 4, provide evidence that CuZnSOD may also play a role in the adaptation from fetal to

newborn circulation by promoting S-nitrosation of Hb and/or by catalyzing the reduction of NO_2^- to NO.

In the future, analysis of CuZnSOD in RBC lysates from infants at birth and up to 8 weeks should be undertaken and the results compared to Hb-SNO levels measured at Ste-Justine Hospital. While accurate determination of nanomolar levels of Hb-SNO is not yet possible, relative Hb-SNO concentrations still provide useful information. In addition, further elucidation of the mechanism of NO transfer in the vasculature taking into account a possible role for CuZnSOD in nitrite reduction is of interest.

6.0 APPENDIX A

Method of HbA preparation provided by Sigma

From Product Information Sheet (H7379), p 3 of 3

Hemoglobin is usually prepared by separating red blood corpuscles from the lighter plasma components by centrifugation. The plasma is siphoned off and ether is added to the corpuscle paste, causing the cells to burst. Another centrifugation removes the ruptured cell envelopes, and leaves a clear red solution of hemoglobin. References for methods of preparation of oxyhemoglobin (HbO_2) from horse, dog and human erythrocytes have been published (Merck Index, 12th Ed., S. Budavari, Ed., p. 794, # 4682 (1996)).

Note: HbA from Sigma is mainly in the met (Fe^{III}) form as determined by its Soret absorption (ε_{500nm} = 10 $mM^{-1}cm^{-1}$ per heme and ε_{630nm} = 4.4 $mM^{-1}cm^{-1}$ per heme).

7.0 APPENDIX B

Calibration curves obtained using the standard addition method for CuZnSOD monomer determination in samples containing 0.375 μM Hb tetramer

Sigma HbA analysis by standard addition

B.1

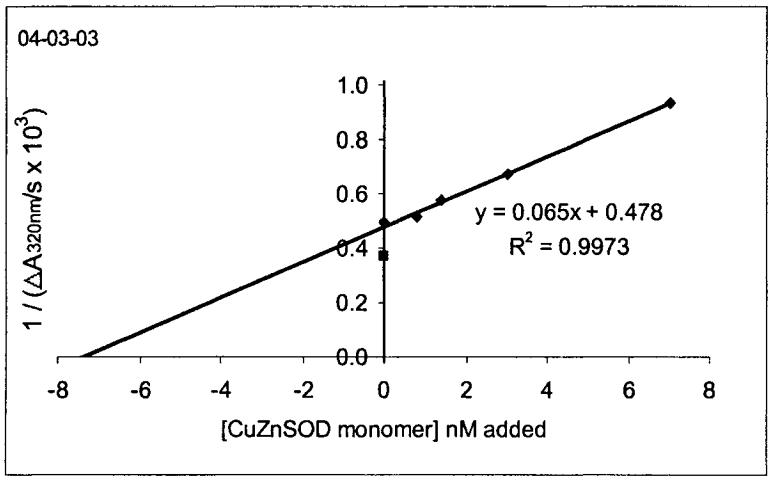

B.2

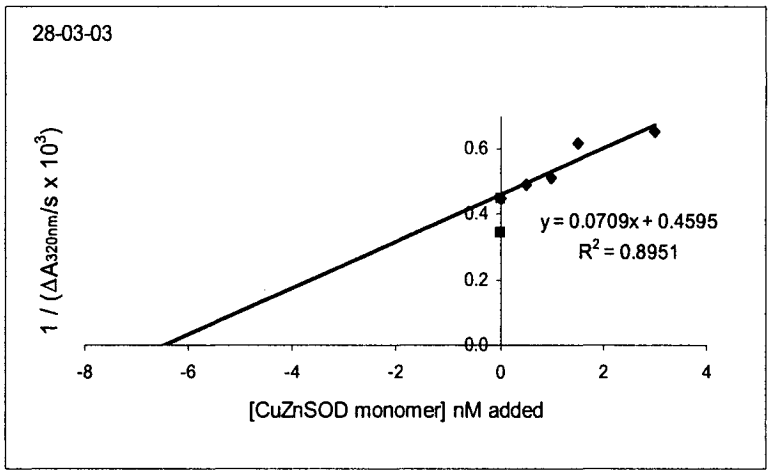

B.3

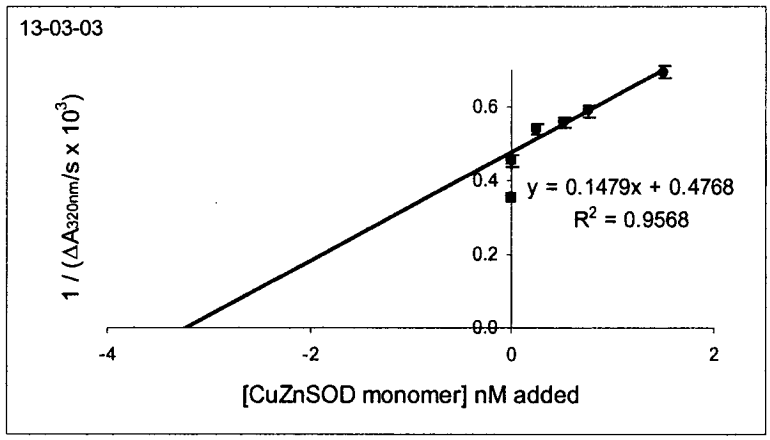

B.4

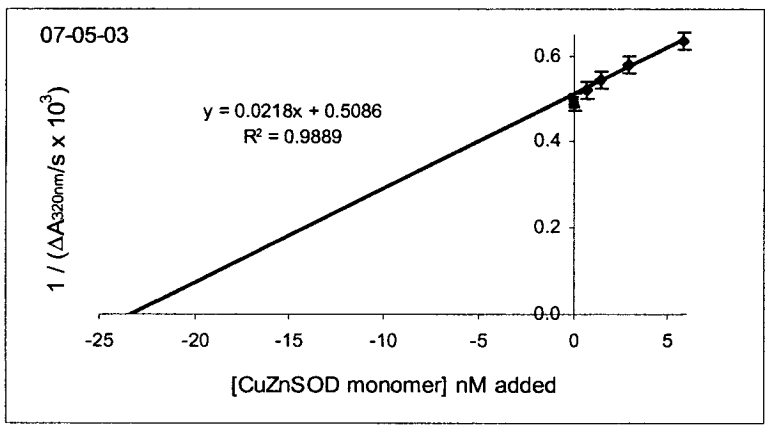

Figure	B.1[a]	B.2[a]	B.3[b]	B.4[b]
intercept	0.4780	0.4595	0.4768	0.5086
slope	0.0650	0.0709	0.1479	0.0218
linearity coefficient	1.00	0.90	0.96	0.99
1/(ΔA/s) in blank	0.37	0.35	0.35	0.49
[CuZnSOD monomer] (nM)	1.7	1.6	0.9	0.7

[a] Lot A Sigma HbA
[b] Lot B Sigma HbA

Observed data ($A_{320\ nm}$ *vs* time):

B1

Time (s)	Blank	0.375 μM Hb	+0.75 nM SOD	+ 1.5 nM SOD	+ 3.0 nM SOD	+7.0 nM SOD
1.4	0.02773	0.02034	0.01573	0.01969	0.01632	0.01539
17	0.06775	0.05175	0.11084	0.04790	0.03889	0.03163
32	0.10921	0.08291	0.11882	0.07364	0.06164	0.04798
47	0.15069	0.11367	0.13405	0.09947	0.08421	0.06384
62	0.19125	0.14405	0.15004	0.12575	0.10655	0.08014
ΔA/s	2.71	2.05	1.94	1.74	1.49	1.07
1/(ΔA/s)	0.37	0.49	0.52	0.57	0.67	0.94

B2

Time (s)	Blank	0.375 μM Hb	+ 0.5 nM SOD	+ 1.0 nM SOD	+ 1.5 nM SOD	+3.0 nM SOD
1.4	0.02264	0.02916	0.02622	0.02321	0.02006	0.02013
17	0.06640	0.06422	0.05882	0.05412	0.04575	0.04364
32	0.11102	0.09819	0.08946	0.08351	0.07001	0.06673
47	0.15481	0.13153	0.11921	0.11265	0.09451	0.09022
62	0.19747	0.16420	0.14929	0.14129	0.11872	0.11244
ΔA/s	2.90	2.23	2.03	1.95	1.63	1.53
1/(ΔA/s)	0.35	0.45	0.49	0.51	0.61	0.65

B3

Time (s)	Blank	0.375 μM Hb	+0.5 nM SOD	+1.0 nM SOD	+1.5 nM SOD	+3.0 nM SOD
1.4	0.03596	0.02603	0.02378	0.02079	0.02098	0.02095
17	0.07307	0.06023	0.05264	0.04905	0.04731	0.04329
32	0.11702	0.09453	0.08056	0.07622	0.07310	0.06501
47	0.16175	0.12804	0.10851	0.10329	0.09866	0.08691
62	0.20538	0.15932	0.13614	0.12946	0.12403	0.10828
ΔA/s	2.83	2.21	1.86	1.80	1.70	1.44
1/(ΔA/s)	0.35	0.45	0.54	0.56	0.59	0.69

B4

Time (s)	Blank	0.375 μM Hb	+0.75 nM SOD	+1.5 nM SOD	+3.0 nM SOD	+6.0 nM SOD
1.4	0.01615	0.01615	0.01648	0.01410	0.01109	0.01214
17	0.03487	0.03422	0.03389	0.02983	0.02587	0.02622
32	0.05441	0.05379	0.05252	0.04763	0.04252	0.04145
47	0.07434	0.07450	0.07196	0.06601	0.06021	0.05734
62	0.09390	0.09554	0.09166	0.08519	0.07788	0.07371
ΔA/s	1.93	2.03	1.93	1.84	1.73	1.58
1/(ΔA/s)	0.49	0.49	0.52	0.54	0.58	0.63

3xDEAE HbA analysis by standard addition

B.5

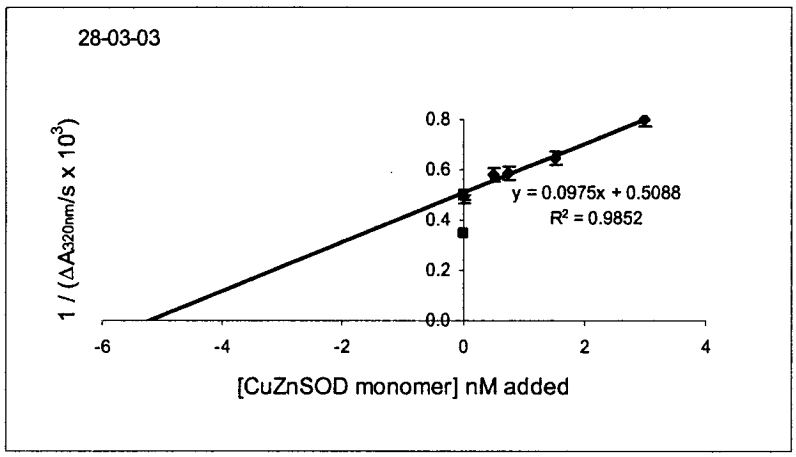

B.6

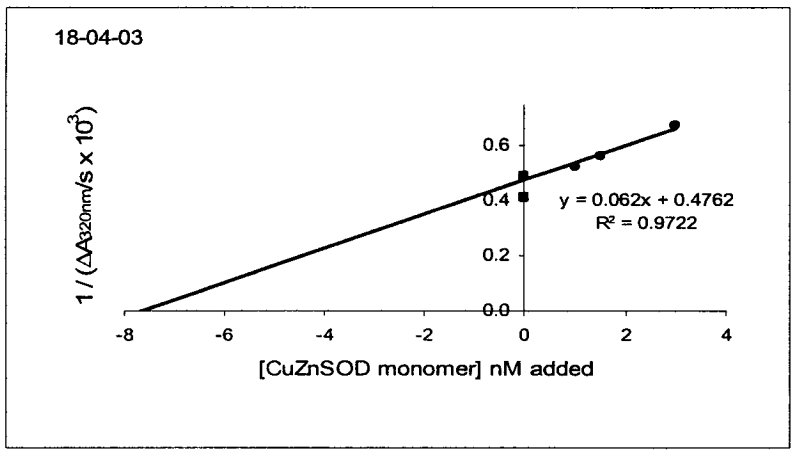

B.7

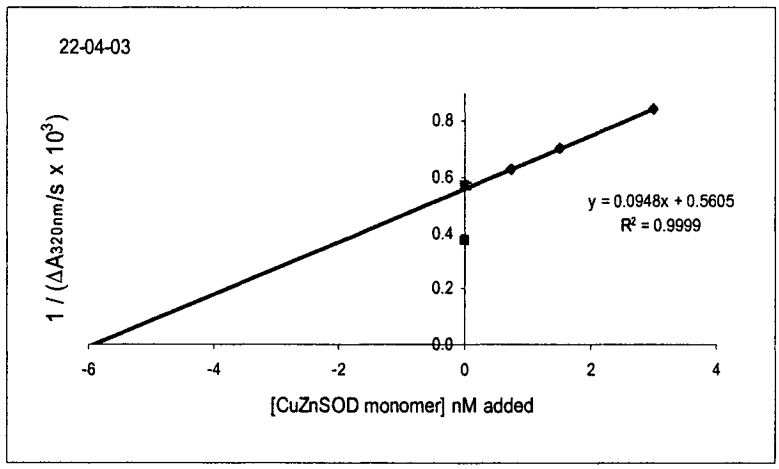

B.8

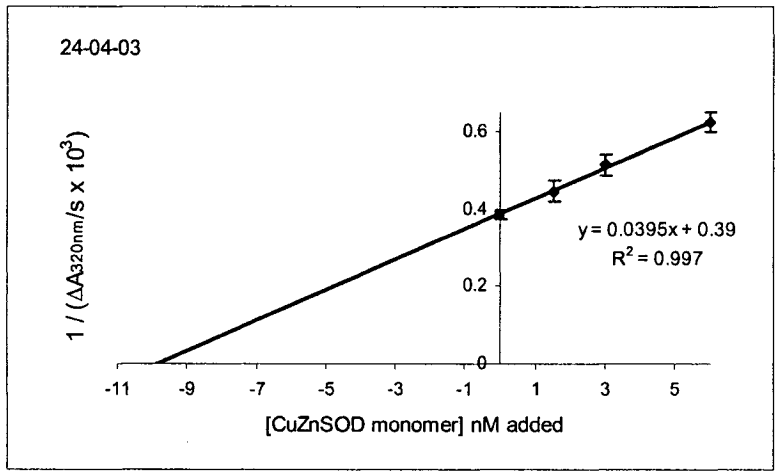

Figure	B.5[a]	B.6[a]	B.7[a]	B.8[b]
intercept	0.5088	0.4762	0.5805	0.3900
slope	0.0975	0.0620	0.0948	0.0395
linearity coefficient	0.99	0.97	1.00	1.00
1/(ΔA/s) in blank	0.35	0.41	0.38	0.38
[CuZnSOD monomer] (nM)	1.7	1.1	1.9	0.2

[a] 3xDEAE HbA prepared using lot A Sigma HbA
[b] 3xDEAE HbA prepared using lot B Sigma HbA

Observed data ($A_{320\ nm}$ *vs* time):

B5

Time (s)	Blank	0.375 μM Hb	+0.5 nM SOD	+0.7 nM SOD	+1.5 nM SOD	+3.0 nM SOD
1.4	0.02264	0.02817	0.02340	0.02683	0.01961	0.01567
17	0.06640	0.05976	0.05065	0.05358	0.04372	0.03457
32	0.11102	0.09022	0.07685	0.08005	0.06760	0.05328
47	0.15481	0.12079	0.10229	0.10523	0.08993	0.07231
62	0.19747	0.15116	0.12813	0.13057	0.11316	0.09122
ΔA/s	2.90	2.03	1.73	1.71	1.54	1.25
1/(ΔA/s)	0.35	0.49	0.58	0.58	0.65	0.80

B6

Time (s)	Blank	0.375 μM Hb	+1.0 nM SOD	+1.5 nM SOD	+3.0 nM SOD
1.4	0.01860	0.01886	0.01632	0.01715	0.01884
17	0.05357	0.04900	0.04436	0.04375	0.04085
32	0.09089	0.08007	0.07341	0.07048	0.06619
47	0.12830	0.11103	0.10240	0.09751	0.09127
62	0.16538	0.14230	0.13179	0.12469	0.11590
ΔA/s	2.44	2.04	1.91	1.78	1.49
1/(ΔA/s)	0.41	0.49	0.52	0.56	0.67

B7

Time (s)	Blank	0.375 μM Hb	+0.7 nM SOD	+1.5 nM SOD	+3.0 nM SOD
1.4	0.02100	0.01783	0.02058	0.01351	0.01271
17	0.05948	0.04316	0.04033	0.03503	0.03009
32	0.10044	0.06996	0.06510	0.05613	0.04814
47	0.14099	0.09715	0.09027	0.07756	0.06617
62	0.18064	0.12353	0.11572	0.09962	0.08422
ΔA/s	2.65	1.75	1.59	1.42	1.18
1/(ΔA/s)	0.38	0.57	0.63	0.70	0.84

B8

Time (s)	Blank	0.375 μM Hb	+1.5 nM SOD	+3.0 nM SOD	+6.0 nM SOD
1.4	0.02213	0.02230	0.01816	0.01888	0.01768
17	0.05992	0.05938	0.05180	0.03300	0.04234
32	0.09978	0.09930	0.08464	0.06200	0.06524
47	0.14010	0.13907	0.11963	0.09194	0.09001
62	0.17965	0.17917	0.15397	0.12151	0.11481
ΔA/s	2.61	2.60	2.24	1.95	1.60
1/(ΔA/s)	0.38	0.38	0.45	0.51	0.63

RBC lysate analysis by standard addition

B.9

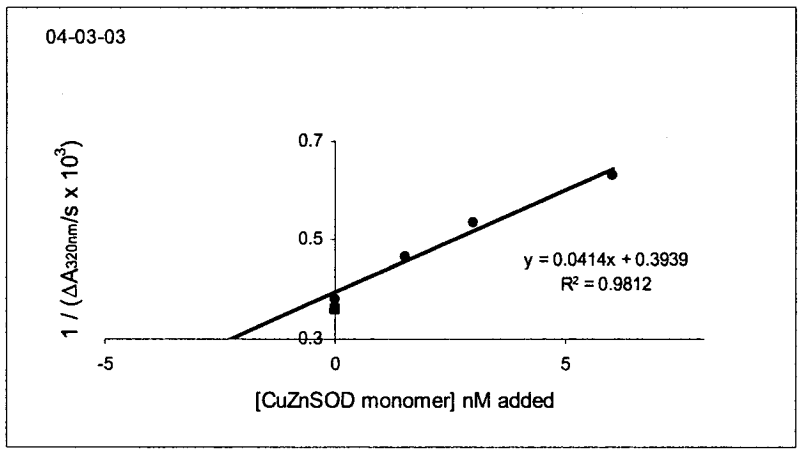

B.10

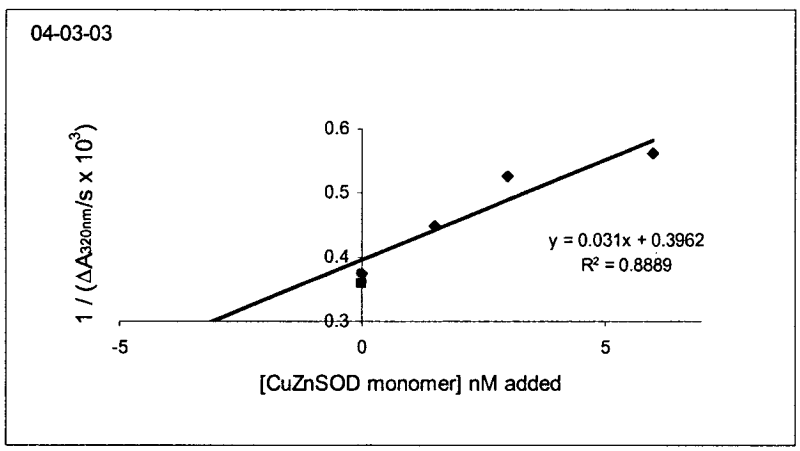

B.11

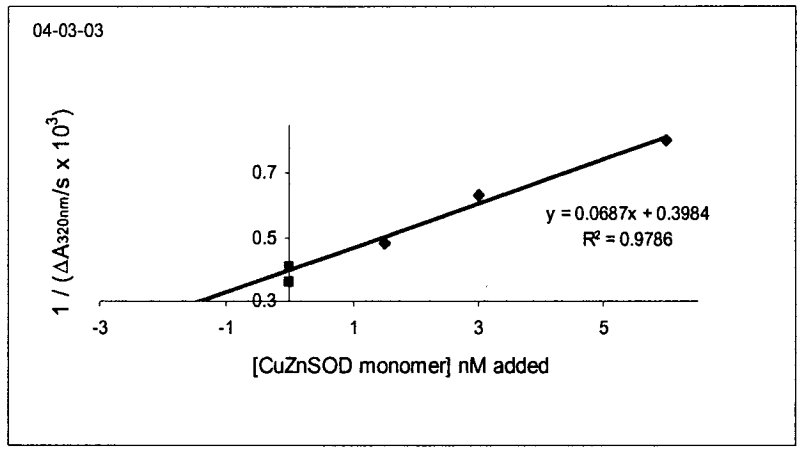

Figure	B.9 [a]	B.10 [b]	B.11
intercept	0.3939	0.3962	0.3984
slope	0.0414	0.0310	0.0687
linearity coefficient	0.99	0.93	0.98
1/(ΔA/s) in blank	0.36	0.36	0.36
[CuZnSOD monomer] (nM)	0.8	1.2	0.6

[a] RBC lysate from a preterm newborn from cord blood at birth.
[b] RBC lysate from a preterm newborn 3.5 days following birth.
[c] RBC lysate from a healthy adult male.
All blood samples were collected at Ste-Justine Hospital.

Observed data ($A_{320\ nm}$ *vs* time):

B9

Time (s)	Blank	0.375 μM Hb	+0.75 nM SOD	+ 1.5 nM SOD	+ 3.0 nM SOD
1.4	0.03009	0.03034	0.02628	0.02145	0.01904
17	0.07423	0.06884	0.05992	0.05049	0.04305
32	0.11710	0.11205	0.09193	0.07920	0.06664
47	0.15864	0.14953	0.12455	0.10744	0.09091
62	0.19884	0.18913	0.15690	0.13439	0.11476
ΔA/s	2.79	2.63	2.16	1.87	1.58
1/(ΔA/s)	0.36	0.38	0.46	0.54	0.63

B10

Time (s)	Blank	0.375 μM Hb	+0.75 nM SOD	+ 1.5 nM SOD	+ 3.0 nM SOD
1.4	0.03009	0.02915	0.02746	0.02180	0.02093
17	0.07423	0.07049	0.06350	0.05214	0.04911
32	0.11710	0.11241	0.09757	0.08137	0.07591
47	0.15864	0.15100	0.13005	0.10770	0.10229
62	0.19884	0.19122	0.16291	0.13728	0.12868
ΔA/s	2.79	2.68	2.23	1.90	1.78
1/(ΔA/s)	0.36	0.37	0.45	0.53	0.56

B11

Time (s)	Blank	0.375 μM Hb	+0.75 nM SOD	+ 1.5 nM SOD	+ 3.0 nM SOD
1.4	0.03009	0.02627	0.02312	0.02301	0.01621
17	0.07423	0.06410	0.05535	0.04754	0.03607
32	0.11710	0.10132	0.08664	0.07124	0.05595
47	0.15864	0.13813	0.11757	0.09491	0.07371
62	0.19884	0.17416	0.14825	0.11915	0.09166
ΔA/s	2.79	2.45	2.07	1.58	1.25
1/(ΔA/s)	0.36	0.41	0.48	0.63	0.80

8.0 APPENDIX C

Plots of A_{320nm} *vs* time used for the determination of relative SOD activities in newborn and adult RBC lysates from Ste-Justine Hospital

C1

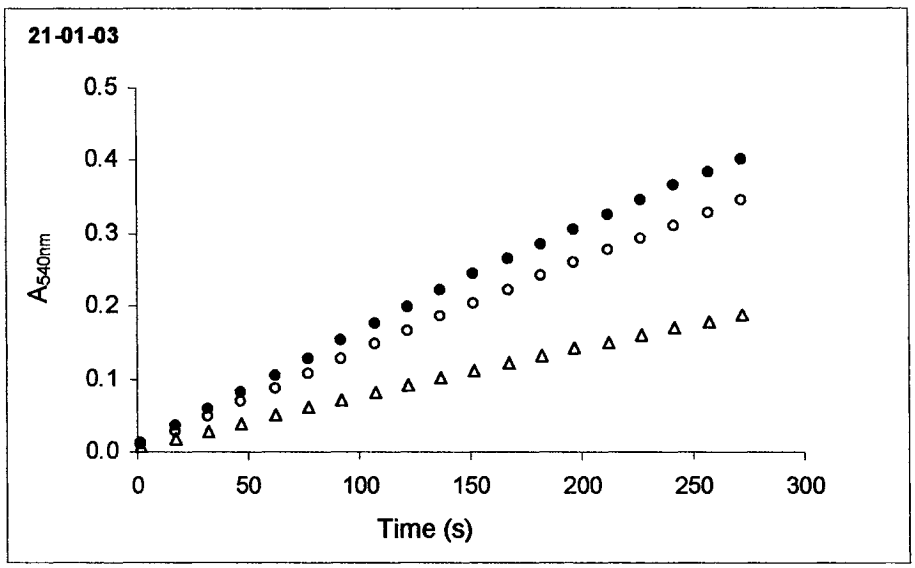

C2

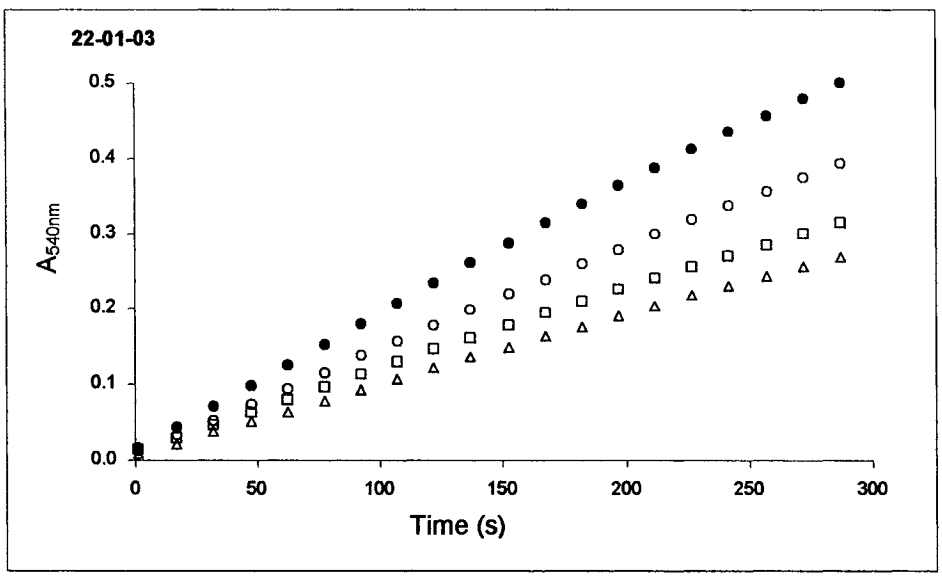

C3

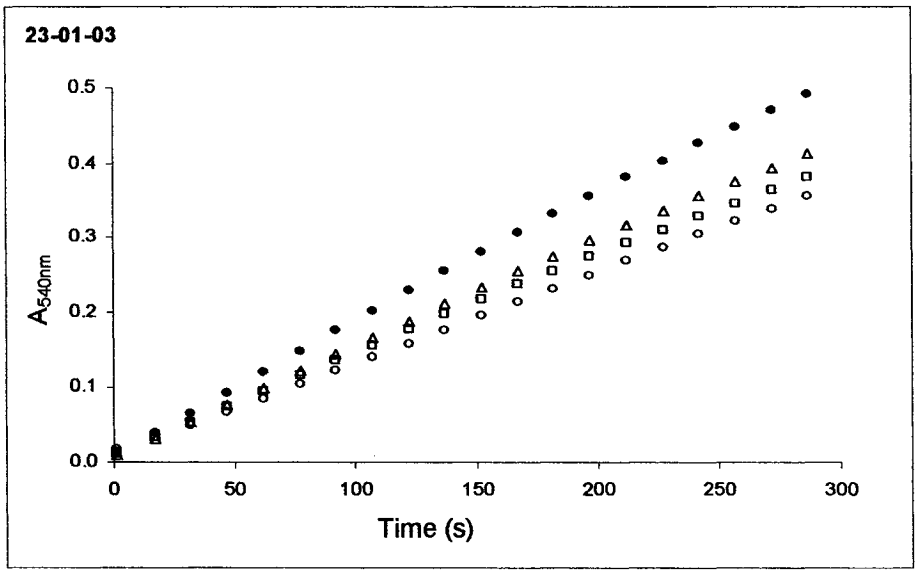

● 0.375 μM 3xDEAE-Hb tetramer

○ 0.375 μM 3xDEAE-Hb tetramer + 3.0 nM CuZnSOD monomer

△ 0.375 μM newborn RBC lysate

□ 0.375 μM adult RBC

Absorbances (A_{320nm}) were measured as described in Section 2.2.2.5.

BIBLIOGRAPHY

1. Fermi, G., Perutz, M.F., Shaanan, B., Fourme, R. *The structure of human deoxyhemoglobin at 1.74 A resolution.* J Mol Biol **1984**;175(2):159-174.

2. Antonini, E., Brunori, M. *Hemoglobin and myoglobin in their reactions with ligands.* In: Neuberger A, Tatum EL, editors. Frontiers of BIology. North-Holland Publishing Company: Amsterdam; **1971**. p 1, 13-54.

3. Jia, L., Bonaventura, C., Bonaventura, J., Stamler, J.S. *S-nitrosohemoglobin: a dynamic activity of blood involved in vascular control.* Nature **1996**;380:221-226.

4. Stamler, J.S., Jia, L., Eu, J.P., McMahon, T.J., Demchenko, I.T., Bonaventura, J., Gernert, K., Piantadosi, C.A. *Blood flow regulation by S-nitrosohemoglobin in the physiological oxygen gradient.* Science **1997**;276(5321):2034-2037.

5. Patel, R.P., Hogg, N., Spencer, N.Y., Kalyanaraman, B., Matalon, S., Darley-Usmar, M. *Biochemical characterisation of human S-nitrosohemoglobin - effects on oxygen binding and transnitrosation.* J Biol Chem **1999**;274(22):15487-15492.

6. Gladwin, M.T., Shelhamer, J.H., Schechter, A.N., Pease-Fye, M.E., Waclawiw, M.A., Panza, J.A., Ognibene, F.P., Cannon, R.O.I. *Role of circulating nitrite and S-nitrosohemoglobin in the regulation of regional blood flow in humans.* Proc Natl Acad Sci U S A **2000**;97(21):11482-11487.

7. McMahon, T.J., Stones, A.E., Bonaventura, J., Singel, D.J., Stamler, J.S. *Functional coupling of oxygen binding and vasoactivity in S-nitrosohemoglobin.* J Biol Chem **2000**;275(22):16739-16745.

8. Romeo, A.A., Filosa, A., Capobianco, J.A., English, A.M. *Metal chelators inhibit S-nitrosation of Cysβ93 in oxyhemoglobin.* J Am Chem Soc **2001**;123:1782-1783.

9. Romeo, A.A., Capobianco, J.A., English, A.M. *Heme nitrosylation of deoxyhemoglobin by S-nitrosoglutathione requires copper.* J Biol Chem **2002**;277(27):24135-24141.

10. Herold, S. *Interaction of nitrogen monoxide with hemoglobin and the artefactual production of S-nitroso-hemoglobin.* C R Biol **2003**;326:533-541.

11. Romeo, A.A., Capobianco, J.A., English, A.M. *Superoxide dismutase targets NO from GSNO to Cysβ93 of oxyhemoglobin in concentrated but not dilute solutions of the protein.* J Am Chem Soc **2003**;125:14370-14378.

12. Gladwin, M.T., Crawford, J.H., Patel, R.P. *The biochemistry of nitric oxide, nitrite and hemoglobin: role in blood flow regulation.* Free Radic Biol Med **2004**;36(6):707-717.

13. Amezcua, J.L., Palmer, R.M., de Souza, B.M., Moncada, S. *Nitric oxide synthesized from L-arginine regulates vascular tone in the coronary circulation of the rabbit.* Br J Pharmacol **1989**;97(4):1119-1124.

14. Ignarro, L.J., Buga, G.M., Wood, K.S., Byrns, R.E., Chaudhuri, G. *Endothelium-derived relaxing factor produced and released from artery and vein is nitric oxide.* Proc Natl Acad Sci U S A **1987**;84(24):9265-9269.

15. Gladwin, M.T., Wang, X., Reiter, C.D., Yang, B.K., Viva, E.X., Bonaventura, C., Schechter, A.N. *S-Nitrosohemoglobin is unstable in the reductive erythrocyte environment and lacks O_2/NO-linked allosteric function.* J Biol Chem **2002**;277(31):27818-27828.

16. Joshi, M.S., Ferguson, T.B., Han, T.H., Hyducke, D.R., Liao, J.C., Rassaf, T., Bryan, N., Feelisch, M., Lancaster, J.R.J. *Nitric oxide is consumed, rather than conserved, by reaction with oxyhemoglobin under physiological conditions.* Biochemistry **2002**;99(16):10341-10346.

17. McMahon, T.J., Moon, R.E., Luschinger, B.P., Carraway, M.S., Stone, A.E., Stolp, B.W., Gow, A.J., Pawloski, J.R., Watke, P., Singel, D.J., Piantadosi, C.A., Stamler, J.S. *Nitric oxide in the human respiratory cycle.* Nat Med **2002**;8(7):711-717.

18. Rassaf, T., Bryan, N.S., Maloney, R.E., Specian, V., Kelm, M., Kalyanaraman, B., Rodriguez, J., Feelisch, M. *NO adducts in mammalian red blood cells: too much or too little?* Nat Med **2003**;9(5):481-483.

19. Stamler, J.S., Hess, D.T., Singel, D.J. *reply to: No adducts in mammalian red blood cells; too much or too little?* Nat Med **2003**;9(5):483-484.

20. Cosby, K., Partovi, K.S., Crawford, J.H., Patel, R.P., Reiter, C.D., Martyr, S., Yang, B.K., Waclawiw, M.A., Zalos, G., Xu, X., Huang, K.T., Shields, H., Kim-Shapiro, D.B., Cannon, R.O.I., Gladwin, M.T. *Nitrite reduction to nitric oxide by deoxyhemoglobin vasodilates the human circulation.* Nat Med **2003**;9(12):1498-1505.

21. Schroeder, W.A., Shelton, J.R., Shelton, J.B., Cormick, J., Jones, R.T. *The amino acid sequence of the γ chain of human fetal hemoglobin.* Biochemistry **1963**;2(5):992-1008.

22. Stamatoyannopoulos, G., Nienhuis, A.W. *Hemoglobin Switching.* In: Stamatoyannopoulos G, Nienhuis AW, Majerus PW, Varmus H, editors. W.B. Saunders Co.: Philadelphia; **1994**. p 107-155.

23. Bard, H. *The postnatal decline of hemoglobin F synthesis in normal full-term infants.* J of Clin Invest **1975**;55(2):395-398.

24. Bard, H., Makowski, E.L., Meschia, G., Battaglia, F.C. *The relative rates of synthesis of hemoglobins A and F in immature red cells of newborn infants.* Pediatrics **1970**;45(5):766-772.

25. Bard, H. *Postnatal fetal and adult hemoglobin synthesis in early preterm newborn infants.* J Clin Invest **1973**;52(8):1789-1795.

26. Bauer, C., Ludwig, M., Ludwig, I., Bartels, H. *Factors governing the oxygen affinity of human adult and foetal blood.* Respir Physiol **1969**;7(3):271-277.

27. Tyuma, I., Shimizu, K. *Different response to organic phosphates of human fetal and adult hemoglobins.* Arch Biochem Biophys **1969**;129(1):404-405.

28. Voet, D., Voet, J.G. *Biochemistry.* John Wiley & Sons, Inc.; **1990**. p 212-215.

29. Bard, H., Peri, K.G., Gagnon, C. *The biological implications of a rare hemoglobin mutant that decreases oxygen affinity.* Pediatr Res **2001**;49(1):69-73.

30. Bard, H., Rosenberg, A., Huisman, T.H. *Hemoglobinopathies affecting maternal-fetal oxygen gradient during pregnancy; molecular, biochemical and clinical studies.* Am J Perinatol **1998**;15(6):389-393.

31. Myatt, L., Brewer, A., Brockman, D.E. *The action of nitric oxide in the perfused human fetal-placental circulation.* Am J Obstet Gynecol **1991**;164(2):687-692.

32. Myatt, L., Brewer, A.S., Langdon, G., Brockman, D.E. *Attenuation of the vasoconstrictor effects of thromboxane and endothelin by nitric oxide in the human fetal-placental circulation.* Am J Obstet Gynecol **1992**;166(1 Pt 1):224-230.

33. Mak, K.K., Gude, N.M., Walters, W.A., Boura, A.L. *Effets of vasoactive autacoids on the human umbilical-fetal placental vasculature.* Br J Obstet Gynaecol **1984**;91(2):99-106.

34. Conrad, K.P., Vill, M., McGuire, P.G., Dail, W.G., Davis, A.K. *Expression of nitric oxide synthase by syncytiotrophoblast in human placental villi.* FASEB J **1993**;7(13):1269-1276.

35. Myatt, L., Brockman, D.E., Eis, A.L., Pollock, J.S. *Immunohistochemical localization of nitric oxide synthase in the human placenta.* Placenta **1993**;14(5):487-495.

36. Funai, E.F., Davidson, A., Seligman, S.P., Finlay, T.H. *S-nitrosohemoglobin in the fetal circulation may represent a cycle for blood pressure regulation.* Biochem Biophys Res Commun **1997**;239(3):875-877.

37. Gaston, B., Fry, E., Sears, S., Heroman, W.M., Ignarro, L., Stamler, J.S. *Umbilical arterial S-nitrosothiols in stressed newborns: role in perinatal circulatory transition.* Biochem Biophys Res Commun **1998**;253:899-901.

38. Clementi, M.E., Orsini, F., Schinina, M.E., Noia, G., Giardina, B. *Effect of nitric oxide on the transport and release of oxygen in fetal blood.* Biochem Biophys Res Commun **2003**;302(3):515-519.

39. Calatayud, S., Beltran, B., Brines, J., Moncada, S., Esplughes, J.V. *Foetal erythrocytes exhibit an increased ability to scavenge for nitric oxide*. Eur J Pharmacol **1998**;347(2-3):363-366.

40. Nicolaides, K.H., Econimides, D.L., Soothill, P.W. *Blood gases, pH, and lactate in appropriate- and small-for-gestational-age fetuses*. Am J Obstet Gynecol **1989**;161(4):996-1001.

41. Chua, S., Yeong, S.M., Razvi, K., Arulkumaran, S. *Fetal oxygen saturation during labor*. Br J Obstet Gynaecol **1997**;104(9):1080-1083.

42. Bard, H., English, A.M., Bellemin, K., Gagnon, C. *Red blood cell nitric oxide during fetal development*. Biol Neonate **2004**;in press.

43. Beckman, J.S. *The double-edged role of nitric oxide in brain function and superoxide-mediated injury*. J Dev Physiol **1991**;5(1):53-59.

44. Wessel, D.L., Adatia, I., Van Marter, L.J., Thompson, J.E., Kane, J.W., Stark, A.R., Kourembanas, S. *Improved oxygenation in a randomized trial of inhaled nitric oxide for persistent pulomonary hypertension of the newborn*. Pediatrics **1997**;100(5):E7.

45. Da-Silva, S.S., Dellinger, R.P. *Inhaled nitric oxide: another weapon in our armamentarium in the battle against acute hypoxic respiratory failure in preterm infants*. Crit Care **2004**;8(2):77-78.

46. Singh, S.P., Wishnok, J.S., Keshive, M., Deen, W.M., Tannenbaum, S.R. *The chemistry of the S-nitrosoglutathione / glutathione system*. Proc Natl Acad Sci U S A **1996**;93(25):14428-14433.

47. Gartner, A., Weser, U. *Erythrocuprein (Cu_2Zn_2 superoxide dismutase) is the major copper protein of the red blood cell*. FEBS Lett **1983**;155(1):15-18.

48. Marklund, S., Marklund, G. *Involvement of superoxide anion radical in the autoxidation of pyrogallol and a convenient assay for superoxide dismutase*. Eur J Biochem **1974**;47(3):469-474.

49. *Human Hemoglobin: Product Information.* Sigma **1996**;Catalogue Number H7379(CAS NUMBER: 9008-02-0):11/15/96 MAC.

50. Bard, H., Wildness, J.A., Ziegler, E.E., Gagnon, C., Peri, K.G. *The proportions of G gamma- and A gamma-globins in the fetal hemoglobin synthesized in preterm and term infants.* Pediatr Res **1995**;37(3):361-364.

51. McCord, J.M., Fridovich, I. *Superoxide Dismutase.* JBC **1969**;244(22):6049-6055.

52. Williams, W.J., Beantler, E., Ersley, A.J., Rundles, R.W. *Hematology.* McGraw-Hill Book Company A Blakisten Publication: New York; **1972.** p 11.

53. Abbyad, P., Tromp, J., Lam, J., Salin, E. *Optimization of the technique of standard additions for inductively coupled mass spectrometry.* J Anal At Spectrom **2001**;16(5):464-469.

54. Turcotte, P. Enzyme inactivation by photoexcited titanium dioxide (TiO2) and prevention by encapsulation. Canadian Theses. Montreal; **2003.** p 94.

55. Hempe, J.M., Craver, R.D. *Separation of hemoglobin variants with similar charge by capillary isoelectric focusing: Value of isoelectric point for identification of common and uncommon hemoglobin variants.* Electrophoresis **2000**;21(4):743-748.

56. Marklund, S., Beckman, G. *A comparison between the common type and a rare generic variant of human cupro-zinc superoxide dismutase.* Eur J Biochem **1976**;65(2):412-422.

57. Datta, B., Tufnell-Barrett, T., Bleasdale, R.A., Jones, C.J., Beeton, I., Paul, V., Frenneaux, M., James, P. *Red blood cell nitric oxide as an endocrine vasoregulator: a potential role in congestive heart failure.* Circulation **2004**;109(11):1339-1342.

58. Stamler, J.S., Jaraki, O., Osborne, J., Simon, D.I., Keaney, J., Vita, J., Singel, D., Valeri, C.R., Loscalzo, J. *Nitric oxide circulates in mammalian plasma primarily as an S-nitroso adduct of serum albumin.* Proc Natl Acad Sci U S A **1992**;89:7674-7677.

59. Saville, B. *A scheme for the colorimetric determination of microgram amounts of thiols*. Analyst **1958**;83:670-672.

60. Zhang, Y.-Y., Xu, A.-M., Nomen, M., Walsh, M., Keaney, J.F.J., Loscalzo, J. *Nitrosation of tryptophan residue(s) in serum albumin and model dipeptides*. J Biol Chem **1996**;271(24):14271-14279.

61. Adachi, K., Kim, J., Asakura, T., Schwartz, E. *Characterization of two types of fetal hemoglobin: alpha 2G gamma 2 and alpha 2A gamma 2*. Blood **1990**;75(10):2070-2075.

62. Doyle, M.P., Pickering, R.A., De Weert, T.M., Hoekstra, J.W., Pater, D. *Kinetics and mechanism of the oxidation of human deoxyhemoglobin by nitrites*. J Biol Chem **1981**;256(23):12393-12398.

63. Solomons, G.T.W. *Fundamentals of Organic Chemistry*. John Wiley & Sons, Inc.; **1994**. pp 794-814.

64. Streitwieser, A., Heathcock, C.H., Kosower, E.M. *Introduction to Organic Chemistry*. Macmillan Publishing; **1992**. pp 753-756.

65. Moini, M., Demars, S.M., Huang, H. *Analysis of carbonic anhydrase in human red blood cells using capillary electrophoresis/ electrospray ionization-mass spectrometry*. Anal Chem **2002**;74(15):3772-3776.

66. Davies, C.A., Perrett, D., Zhang, Z., Nielsen, B.R., Blake, D.R., Winyard, P.G. *Simultaneous analysis of nitrite, nitrate and the nicotinamide nucleotides by capillary electrophoresis: Application to biochemical studies and human extracellular fluids*. Electrophoresis **1999**;20(10):2111-2117.

67. Knowles, R.G., Moncada, S. *Nitric oxide as a signal in blood vessels*. Trends Biochem Sci **1992**;17(10):399-402.

68. Averill, B.A. *Dissimilatory nitrite and nitric oxide reductases*. Chem Rev **1996**;96(7):2951-2964.

69. Millar, T.M., Stevens, C.R., Benjamin, N., Eisenthal, R., Harrison, R., Blake, D.R. *Xanthine oxidoreductase catalyses the reduction of nitrates and nitrite to nitric oxide under hypoxic conditions*. FEBS Lett **1998**;427(2):153-313.

70. Kleinbongard, P., Dejam, A., Lauer, T., Rassaf, T., Schindler, A., Picker, O., Scheeren, T., Godecke, A., Schrader, J., Schulz, R., Heusch, G., Schaub, G., Bryan, N.S., Feelisch, M., Kelm, M. *Plasma nitrite reflects constitutive nitric oxide synthase activity in mammals*. Free Radic Biol Med **2003**;35(7):790-796.

71. Endo, A., Ayusawa, M., Minato, M., Takada, M., Takahashi, S., Harada, K. *Endothelium derived relaxing and contracting factors during the early neonatal period*. Acta Paediatr **1997**;86(8):834-836.

72. Tsukahara, H., Sekine, K., Miura, M., Todoroki, Y., Ohshima, Y., Hiraoka, M., Hosokawa, K., Kotsuji, F., Mayumi, M. *Vasoactive and natriuretic mediators in umbilical cord blood: a report of our observation and review of the literature*. Early Hum Dev **2002**;69:57-64.

73. Endo, A., Shimada, M., Ayusawa, M., Minato, M., Takada, M., Takahashi, S., Harada, K., Masaoka, N., Sato, K. *Nitric oxide and endothelin 1 during postnatal life*. Biol Neonate **1996**;70(1):15-20.

74. Strange, R.W., M., L.M., E., D.F., H.L., A.Z., R., E.R., E., S.B., S., H.S. *Structural and Kinetic Evidence for an Ordered Mechanism of Copper Nitrite Reductase*. Journal of Molecular Biology **1999**;287(5):1001-1009.

75. Monzani, E., Koolhaas, A.G.J., Spandre, A., Leggieri, E., Casella, L., Gullotti, M., Nardin, G., Randaccio, L., Fotani, M., Zanello, P., Reedijk, J. *Binding of nitrite and its reductive activation to nitric oxide at biometric copper centers*. Journal of Biological Inorganic Chemistry **2000**;5(2):251-261.

76. Monzani, E., Koolhaas, A.G.J., Spandre, A., Leggieri, E., Casella, L., Gullotti, M., Nardin, G., Randaccio, L., Fotani, M., Zanello, P., Reedijk, J. *Binding of nitrite and its reductive activation to nitric oxide at biometric copper centers*. J Biol Inorg Chem **2000**;5(2):251-261.

77. Rotilio, G., Agro, A.F., Calabrese, L., Bossa, F., Guerrieri, P., Mondovi, B. *Studies of the metal sites of copper proteins, ligands of copper in hemocuprein.* Biochemistry **1971**;10(4):616-621.

78. Mota de Freitas, D., Valentine, J.S. *Phosphate Is an Inhibitor of Copper-Zinc Superoxide Dismutase.* Biochemistry **1984**;23(9):2079-2082.

79. Sidman, J.W. *Electronic and vibrational states of the nitrite ion.* J Am Chem Soc **1957**;79:2669-2675.

80. Casella, L., Carugo, O., Gullotti, M., Doldi, S., Frassoni, M. *Synthesis, Structure, and Reactivity of Model Complexes of Copper Nitrite Reductase.* Inorganic Chemistry **1996**;35:1101-1113.

81. Howes, B.D., Abraham, Z.H.L., Lowe, D.J., Bruser, T., Eady, R.R., Smith, B.E. *EPR and electron nuclear double resonance (ENDOR) studies show nitrite binding to the type 2 copper centers of the dissimilatory nitrite reducatse of Alcaligenes xylosoxidans (NCIMB 11015).* Biochemistry **1994**;33:3171-3177.

82. Strange, R.W., Loretta, M.M., Dodd, F.E., Abraham, Z.H.L., Eady, R.R., Smith, B.E., Hasnain, S.S. *Structural and kinetic evidence for an ordered mechanism of copper nitrite reductase.* J Mol Biol **1999**;287(5):1001-1009.

83. Tocheva, E.I., Rosell, F.I., Mauk, A.G., Murphy, M.E.P. *Side-on copper-nitrosyl coordination by nitrite reductase.* Science **2004**;304(5672):867-870.